BESIII Analysis Memo

BAM-250

version 26

Cross section measurement of $e^+e^- \to K^+K^-$ in energy region $2.0 - 3.08$ GeV

Dong Liu, Chi Wang, Zhen Gao, Wenbiao Yan, Guangshun Huang

October 28, 2017

University of Science and Technology of China

Abstract

The cross section of the process $e^+e^- \to K^+K^-$ is studied with 651 pb^{-1} of data collected with Beijing Spectrometer(BESIII) at $\sqrt{s} = 2.0 - 3.08$ GeV with higher precision than previous experiments whose line shape clarifies a structure near 2.2 GeV which can be described with a resonance with mass $2245.6 \pm 8.3 \pm 11.4$ MeV/c^2 and width $136.3 \pm 11.8 \pm 10.7$ MeV . The kaon form factor is extracted with $\sigma(e^+e^- \to K^+K^-)$ and compared with theory prediction.

Contents

1 Introduction

Hadronic process contributes an important part to vacuum polarization(VP) [1] with a size of 700×10^{-10} [2]. Light quarks (u, d) contribute the main part ($> 90\%$) while strange quark also play an important role ($\sim 7\%$) with leading contribution from the sum of the K^+K^- and $K^0\bar{K}^0$ channels [2], as shown in Fig. 1, though contribution from BESIII energy region 2 - 4.6 GeV is not clear. Therefore, there is necessity to measure the cross section of $e^+e^- \to K^+K^-$. Besides, the cross section of $e^+e^- \to K^+K^-$ and the form factor of $K^\pm$ can reveal the properties of ρ, ω, ϕ and their excited states, e.g. the state $\phi(2170)$ which is expected to decay to kaon pairs in some model [3], as well as test some QCD predictions such as the asymptotic behavior of the form factor, $F_K = 16\pi\alpha_s(s)\frac{f_K^2}{s}$ [4]. The understanding of nuclear and hypernuclear forces also need good knowledge of timelike form factors [5].

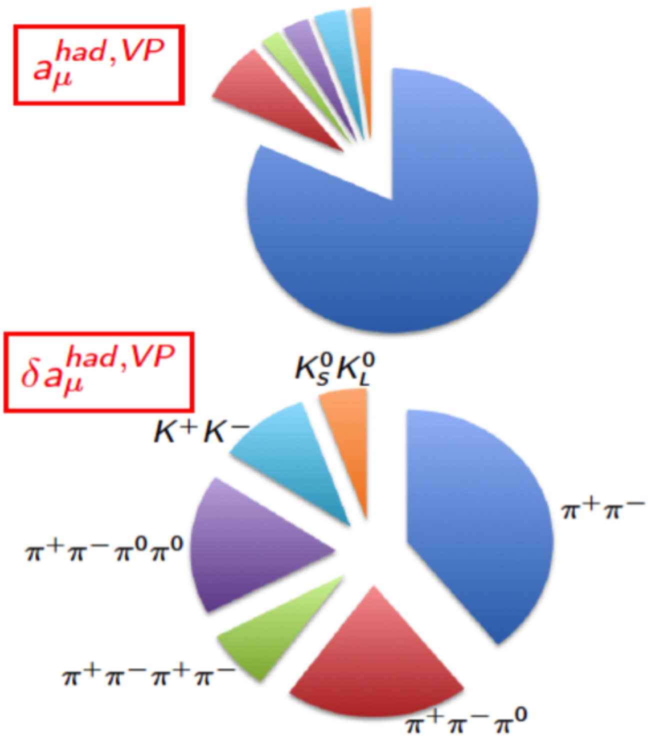

Figure 1: Contributions to VP from hadronic processes.

The cross section of $e^+e^- \to K^+K^-$ and form factor of kaon has been measured by many experiments [6], such as DM2 [7], CMD-2 [8], BABAR [9,10]. In energy region near $\phi(1020)$ resonance, the precision of the cross section measurement is very high, but much poorer when energy is higher than 2 GeV, except results at a few points [11,12]. Recently, BABAR experiment uses initial-state radiation method to study the process and provides result in a wide energy range from threshold of K^+K^- to 8 GeV [9, 10] which shows complicate structure between 1.8 and 2.4 GeV. Our data taken in energy region from 2 to 3.08 GeV has higher statistics than previous experiments which can help to improve the precision of cross section measurement clarify the structure near 2.2 GeV.

2 Detector

Beijing Electron-Positron Collider (BEPCII) [13] is a double-ring e^+e^- collider designed to provide a peak luminosity of 10^{33} cm^{-2}s^{-1} at $\sqrt{s}$ = 3770 MeV. BESIII [13] detector has a geometrical acceptance of 93% of the full solid angle and has four main components: (1) A small-cell, helium-based (60% He, 40% C_3H_8) main drift chamber (MDC) with 43 layers providing an average single-hit resolution of 135 μm, and charged-particle momentum resolution in a 1 T magnetic field of 0.5% at 1 GeV/c. (2) An electromagnetic calorimeter (EMC) consisting of 6240 CsI(Tl) crystals in cylindrical structure has one barrel and two endcaps. The energy resolution at 1.0 GeV/c is 2.5% (5%) in the barrel (endcaps), and the position resolution is 6 mm (9 mm) in the barrel (endcaps). (3) Particle Identification is provided by a time-of-flight system constructed of 5-cm-thick plastic scintillators, with 176 detectors of 2.4 m length in two layers in the barrel and 96 fan-shaped detectors in the endcaps. The barrel (endcaps) time resolution of 80 ps (110 ps) provides $2\sigma K/\pi$ separation for momenta up to $\sim$ 1.0 GeV/c. (4) The muon system (MUC) consists of 1000 m^2 of Resistive Plate Chambers (RPCs) in nine barrel and eight endcap layers and provides 2 cm position resolution.

3 Data sample and Monte Carlo simulation

3.1 Data samples

The data used in this analysis are taken at 22 energy points ranging from 2 to 3.08 GeV with total integrated luminosity 651 pb^{-1} which is reconstructed and analyzed with BESIII Offline Software System (BOSS) [14] version 6.6.5.p01.The detail of experimental data are listed in Tab. 1.

Table 1: Information of experimental data

E_{cm} (GeV)	runNo	$\mathcal{L}$ (pb^{-1})	E_{cm} (GeV)	runNo	$\mathcal{L}$ (pb^{-1})
2	41729-41909	10.074	2.5	40771-40776	1.098
2.05	41911-41958	3.343	2.6444	40128-40296	33.722
2.1	41588-41727	12.167	2.6464	40300-40435	34.003
2.125	42004-43253	108.49	2.7	40436-40439	1.034
2.15	41533-41570	2.841	2.8	40440-40443	1.008
2.175	41416-41532	10.625	2.9	39775-40069	105.253
2.2	40989-41121	13.699	2.95	39619-39650	15.942
2.2324	41122-41239	11.856	2.981	39651-39679	16.071
2.3094	41240-41411	21.089	3	39680-39710	15.881
2.3864	40806-40951	22.549	3.02	39711-39738	17.290
2.396	40459-40769	66.869	3.08	39355-39618	126.185

3.2 Monte Carlo simulation

Monte Carlo (MC) samples simulated with the full detector are used to study the selection criteria, efficiency and background. The simulation program provides an event generator, contains the detector geometry description and simulates the detector response and signal digitization. The detector geometry, material description and the transportation of the decay particles through the detector including interactions are handled by GEANT4 [15].

Different processes are generated with different models at each energy point, 1 M Bhabha, 1 M di-gamma and 500 K di-mu events with BABAYAGA [16], 500 K hadronic events with LUARLW [17], 500 K two-photon events, 1 M exclusive K^+K^- events with CONEXC [18].

The line shape of signal process $e^+e^- \to K^+K^-$ used as input in CONEXC generator is obtained as follows:

- Step 1: BaBar's result is used as initial line shape of cross sections to generate MC samples and calculate $1+\delta$. Then selection criteria are applied to both data and MC to get N_{obs} and ϵ. With these values the Born cross sections at 22 energy points are calculated.
- Step 2: The cross sections obtained from previous step and BaBar result are fitted with continuous and smooth function, which is then used as input line shape to generate MC, and measure the Born cross sections again.
- Step 3: Step 2 is repeated until difference of cross sections between last two iterations is less than 0.5%, which is regarded as converged since the typical systematic uncertainty at each energy point is more than 1.5%.

4 Event selection

Cross section of $e^+e^- \to K^+K^-$ is measured with final $K^\pm$ which is usually identified in particle identification(PID) system with the dE/dx and Time of Flight (TOF) information. In BESIII detector, PID can separate $e^\pm$, $\mu^\pm$, $\pi^\pm$, $K^\pm$ and $p(\bar{p})$ well at low momentum but not so good at high momentum which covering the momentum of $K^\pm$ from the precess in the energy region to be studied. On the other hand, the introduction of PID system will bring additional uncertainty in the cross section measurement. The control of uncertainty is significant in a precise measurement so that PID system is avoided to be used.

$e^+e^- \to K^+K^-$ is a two-body process with specific momentum in final states when the center-of-mass energy is a certain value. For two-body process, the momenta of final tracks are determined by its center-of-mass energy and the mass of final particles. Thus, two-kaon process should be separated from other two-body processes with momentum which is confirmed by Ref [21] and Monte Carlo study in energy region $2.0-3.08$ GeV. Fig. 2 shows the comparison of the momentum of $K^\pm$ from $e^+e^- \to K^+K^-$ with other 2-body processes and $3\sigma K/\mu$ separation for $\sqrt{s}$ up to 3.1 GeV. Further event selection criteria are needed to suppress background.

4.1 Good charged tracks selection

For the process $e^+e^- \to K^+K^-$, there are 2 charged tracks in final state so that charged particles are required with one positive and one negetive tracks located in specific space in the detector. To veto cosmic ray and other background, charged tracks must locate within $V_r = \sqrt{V_x^2+V_y^2} < 1.0$ cm and $|V_z| < 10.0$ cm, where V_x, V_y and V_z are

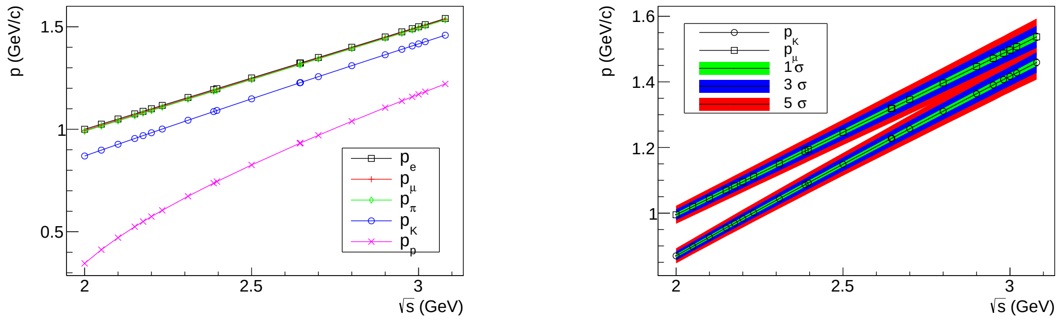

a) momentum of different 2-prong processes at different center of mass energy

b) momentum separation of $K^{\pm}$ and $\mu^{\pm}$ at different center of mass energy

Figure 2: Momentum comparison of different 2-prong precess

the x, y, z coordinates of the point of closest approach to the run dependent interaction point respectively. The polar angle of each track should lie in region $|\cos\theta| < 0.93$ due to acceptance of BESIII detector.

4.2 Bhabha suppression

QED processes like Bhabha and di-mu have large cross section and can pollute interest signal. The tracks of Bhabha events are mainly in the forward directions of $e^{\pm}$ beams and hit the endcap of the detector, as shown in Fig. 3 and 4. Thus polar angle can be used to veto them with requirement: $\cos\theta_{+} < 0.8$ for positive tracks and $\cos\theta_{-} > -0.8$ for negative tracks.

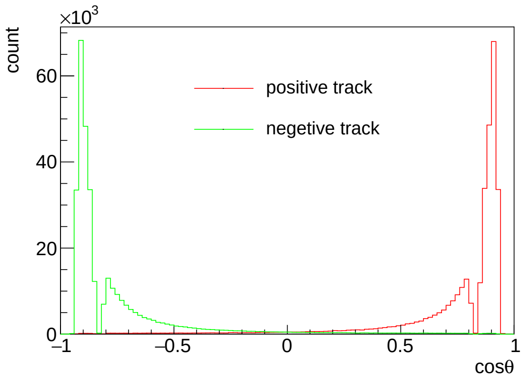

Figure 3: Polar angle distribution of tracking from Bhabha MC at 2.0 GeV. Red line is positive tracks. Green line is negetive tracks.

After rejecting forward tracks, there are still lots of Bhabha events. Further study shows the ratio of energy deposit in EMC to the momentum of the track (E/p) can be used to separate $K^{\pm}$ and $e^{\pm}$. Plots in Fig. 5 are the E/p spectra of $e^{\pm}$ and $K^{\pm}$ showing that most E/p of $e^{\pm}$ accumulate at 1, while the E/p of $K^{\pm}$ are far away from 1, indicating E/p can be used to veto Bhabha events. The cut value is optimized via maximizing signal to noise ratio.

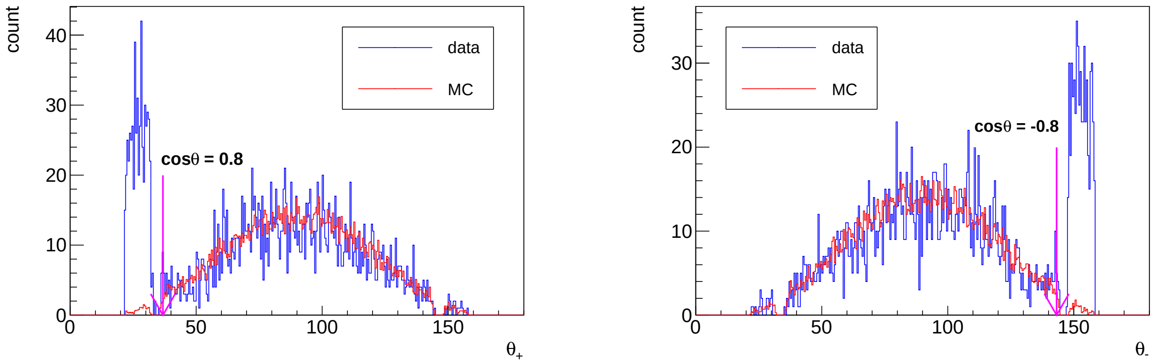

a) polar angle of positive charged track b) polar angle of negative charged track

Figure 4: Polar angle distribution of tracks at 2.0 GeV. Red line is from K^+K^- MC. Blue line is from data. For data, the events are after all events selection criteria except rejecting forward tracks.

$$FOM = N_S/\sqrt{N_{S+B}} \tag{1}$$

where N_S is the number of signals, N_{S+B} is the number of both signal and background. Here, we only consider events in 3σ region of signals. The uncertainty of FOM is estimated with

$$\delta_{FOM} = \sqrt{\frac{N_1'}{N_2}(fN_{01} - N_1') + \frac{N_1'^2}{4N_{02}N_2^3}(N_{02} - N_2)} \tag{2}$$

where N_{01} is the number of generated signal MC, and event selection reduce it to N_1. Considering the different luminosity of data and MC, we donate $N_1' = fN_1 = N_s$. Total number of signal and background is N_{02}, after selection it is N_2, $N_2 = N_{S+B}$.

Fig. 6 shows the cut value optimized with signal to noise ratio at 2 GeV. There is trend that the cut value decreases as energy goes up, though the value may fluctuate due to statistical uncertainty, and can be described with a second polynomial function to determine optimized cut values.

4.3 Multi-body processes suppression

For pure K^+K^- events, the two tracks should be back to back, the relative angle between 2 tracks should be near 180° in the center of mass system (c.m.) of initial electron and positron, which is quite different when comparing with multi-prong events. Therefore, the angle of one track with respect to another track in e^+e^- c.m. is required to be larger than 179° to veto background according to MC as shown in Fig. 7.

4.4 Cosmic-ray suppression

The cosmic-ray muon has a broad momentum range, and could be reconstructed as 2 back-to-back tracks, but it has a striking character that the two tracks have different time of flight, so that it can be identified from collision event, which on the other hand has tracks with approximately same flight time. For cosmic rays, typical time difference,

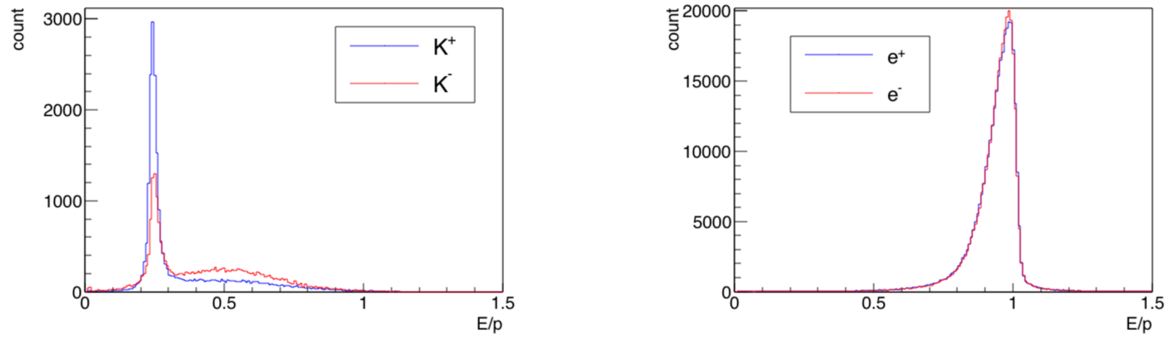

a) E/p of $K^{\pm}$. b) E/p of $e^{\pm}$

Figure 5: E/p of kaon and electron at 2.0 GeV. For electron, it is near 1. For Kaon, it is far away from 1.

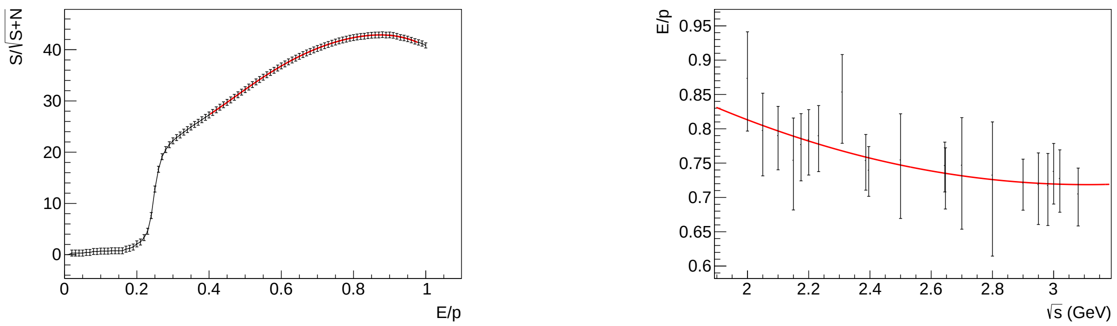

a) E/p optimization at 2.0 GeV. b) Optimized E/p cut at different energy points.

Figure 6: E/p cut value optimization. The cut value may fluctuate due to statistical uncertainty. A 2nd polynomial function is used to fit the cut values from optimization. E/p cut values are set to values on the function

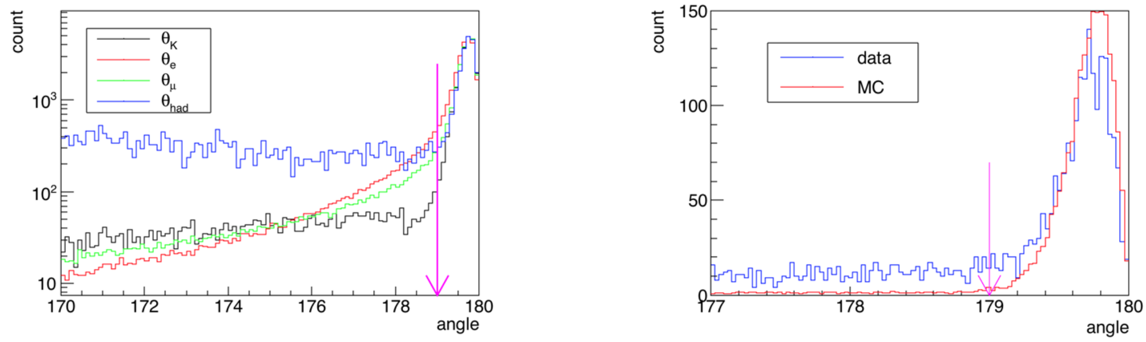

a) relative polar angle between 2 tracks for different process. b) relative polar angle of K^+ and K^- for experimental data and MC.

Figure 7: Angle between 2 tracks. a) Angle between two tracks for different process, black line is KK MC, red line is Bhabha MC, green line is di-mu MC, blue line is hadronic MC. b) Comparison of MC and data. Note: when comparing angle, tracks have been boost to center of mass system.

i.e. δTOF = TOF1 − TOF2 is the difference of flight time between positive and negetive tracks, is about 6 ns, so a requirement of $|\delta\text{TOF}| < 3$ ns is applied, as shown in Fig. 8.

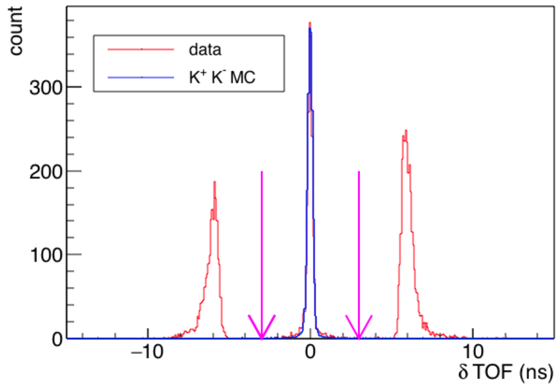

Figure 8: The distribution of TOF difference of 2 tracks for data and K^+K^- MC

5 Background analysis

Background is analyzed in 3 sigma region under the peak of kaon in momentum spectra with MC simulation which shows di-mu process is the main part, as shown in Tab. 2 and Fig. 9. The momentum spectra of muon from di-mu MC are scaled to data according to their luminosity. Table 3 shows the number of di-mu background estimated from different methods with consistent values and implies that we can use MC shape of di-mu process to describe background. Background from bhabha, di-gamma contribute very few and no event survives from MC after imposing selection criteria in signal region. Contributions from hadrons are flat and negligible in signal region. Fig. 9 shows that background increase as energy goes up which can be predicted from Fig. 2 that the momenta of kaon and muon get closer and the resolution become worse as energy goes up. Background of the analysis is subtracted with a suitable function to describe it in the fit of momentum spectra.

6 Cross section and form factor

6.1 Efficiency and correction factor

Cross section calculated with Eq. 12 involves the number of candidates, luminosity, detection efficiency and correction factor due to ISR and VP. The detection efficiency and correction factor are obtained from MC of the process $e^+e^- \to K^+K^-(\gamma)$ generated with CONEXC generator at each energy point. Detection efficiency (ϵ) is determined with the ratio of survived MC events (N_{remain}) after event selection as applied on experimental data and total generated events (N_{gen}), $\epsilon = N_{remain}/N_{gen}$. To obtain a reliable correction factor $(1+\delta)$ which is provided in generator, the cross section measured by BABAR experiment, as shown in Fig. 10, and in this work are combined to put into the generator with iterative procedure as described in the section of MC samples.

Table 2: Background from QED and hadrons.

E_{cm}(GeV)	di-mu		bhabha		di-gamma		twophoton		hadrons	
	$n_{\mathcal{L}}$	N_f	$n_{\mathcal{L}}$	N_f	$n_{.\mathcal{L}}$	N_f	$n_{\mathcal{L}}$	N_f	$n_{\mathcal{L}}$	N_f
2.0	2.22	20	0.49	0	1.14	0	34.04	0	0.89	0
2.05	7.02	18	0.17	0	3.59	0	98.59	0	2.74	1
2.1	2.01	30	0.05	0	1.03	0	26.01	0	0.87	1
2.15	9.06	24	0.22	0	4.66	0	107.58	2	3.39	1
2.175	2.48	30	0.06	0	1.27	0	28.25	0	0.92	0
2.2	1.97	48	0.05	0	1.01	0	21.51	0	0.88	1
2.2324	2.34	40	0.06	0	1.20	0	24.39	0	0.85	0
2.3094	1.40	48	0.38	0	0.94	0	13.06	0	0.90	0
2.3864	1.40	56	0.03	0	0.94	0	11.71	0	0.91	1
2.396	1.02	151	0.01	0	0.98	0	3.92	0	0.95	0
2.5	31.63	68	0.77	0	16.27	0	225.99	0	11.00	0
2.6444	1.15	127	0.03	0	0.94	0	6.85	0	0.92	0
2.6464	1.14	114	0.03	0	0.94	0	6.79	0	0.93	0
2.7	39.01	132	0.96	0	20.07	0	218.21	1	14.07	0
2.8	42.89	174	1.05	0	22.20	0	215.01	0	16.35	0
2.9	1.00	496	0.01	0	0.98	0	1.98	0	0.97	2
2.95	3.01	262	0.07	0	1.55	0	12.88	0	1.13	1
2.981	3.05	266	0.07	0	1.58	0	12.60	0	1.15	0
3.0	3.13	281	0.08	0	1.61	0	12.68	0	1.19	0
3.02	2.91	289	0.07	0	1.51	0	11.54	0	1.09	1
3.08	0.96	829	0.01	0	0.92	0	1.56	0	0.91	1

$n_{\mathcal{L}}$ is relative size of MC when regarding the size of data as 1.
N_f is the number of event after event selection in 3 sigma region of the momentum of kaon.

Table 3: The number of di-mu background estimated from different ways. "all" means the numbers are obtained from full fit range and "signal region" means the numbers estimated in 3 sigma region of signal. It should be noticed that background is only analyzed in signal region which is only part of the fit value shown in Fig. 12.

E_{cm}(GeV)	$N_{\mu\mu}$ from MC	$N_{\mu\mu}$ from MC shape fit		$N_{\mu\mu}$ from CB+G fit	
		all	signal region	all	signal region
2.0	9	125	15	121	7
2.05	3	57	6	57	6
2.1	15	154	20	146	13
2.15	3	34	3	34	3
2.175	12	128	12	136	19
2.2	24	195	27	188	18
2.2324	17	165	18	167	21
2.3094	34	383	37	395	53
2.3864	40	470	41	478	56
2.396	148	1344	132	1324	129
2.5	2	22	2	26	6
2.6444	110	1109	108	1102	93
2.6464	100	1131	102	1125	102
2.7	3	53	5	53	4
2.8	4	41	4	43	6
2.9	496	5650	549	5563	442
2.95	87	913	89	901	73
2.981	87	978	94	970	86
3.0	90	986	96	981	88
3.02	99	1197	115	1193	105
3.08	864	8806	893	8849	931

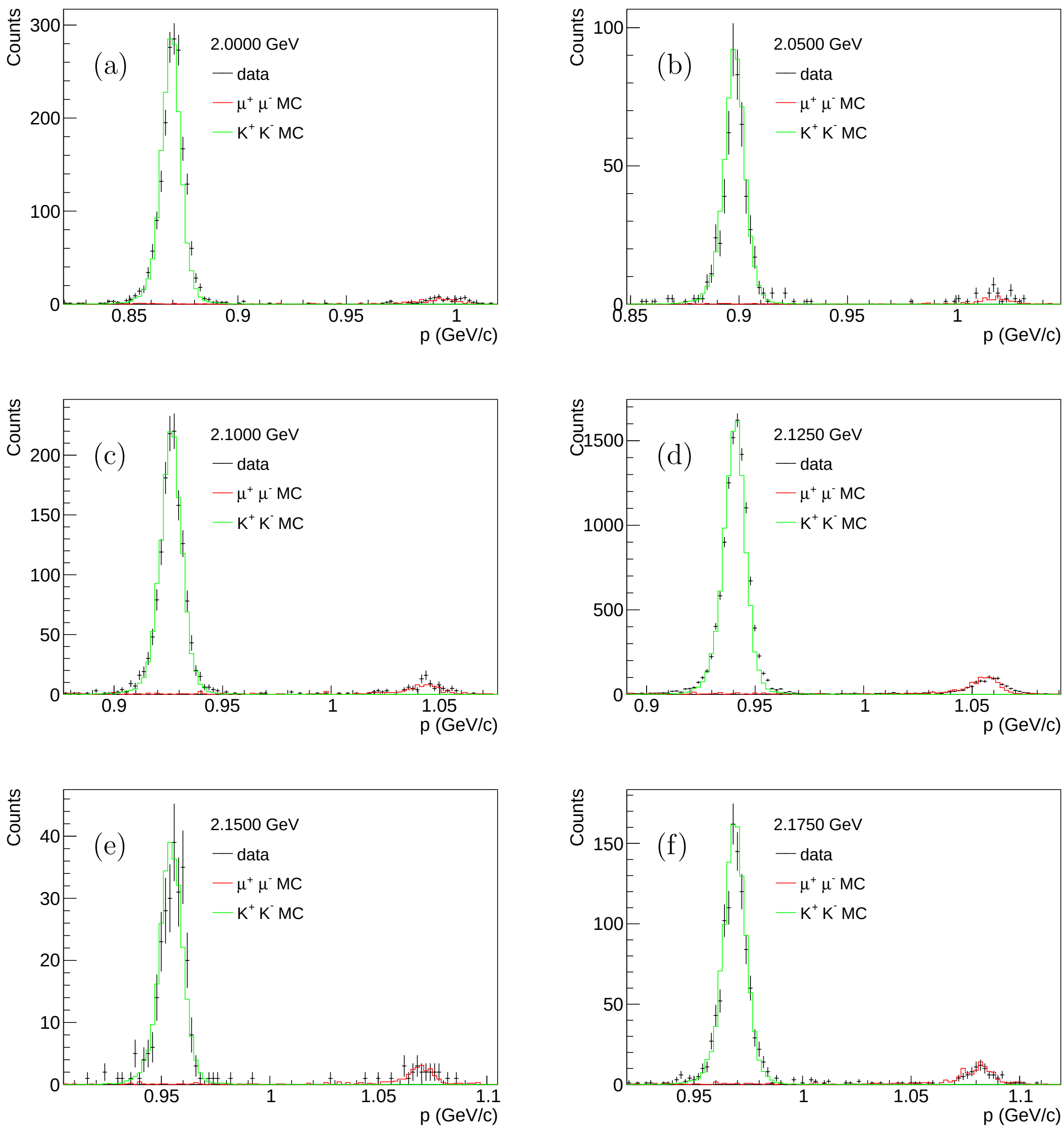

Figure 9: momentum spectra of data and di-mu MC at 22 energy points. dots are from data. Red lines are from di-mu MC which are scaled to data according to luminosity. Green line are from K^+K^-MC which are scale to data according to the peak value.

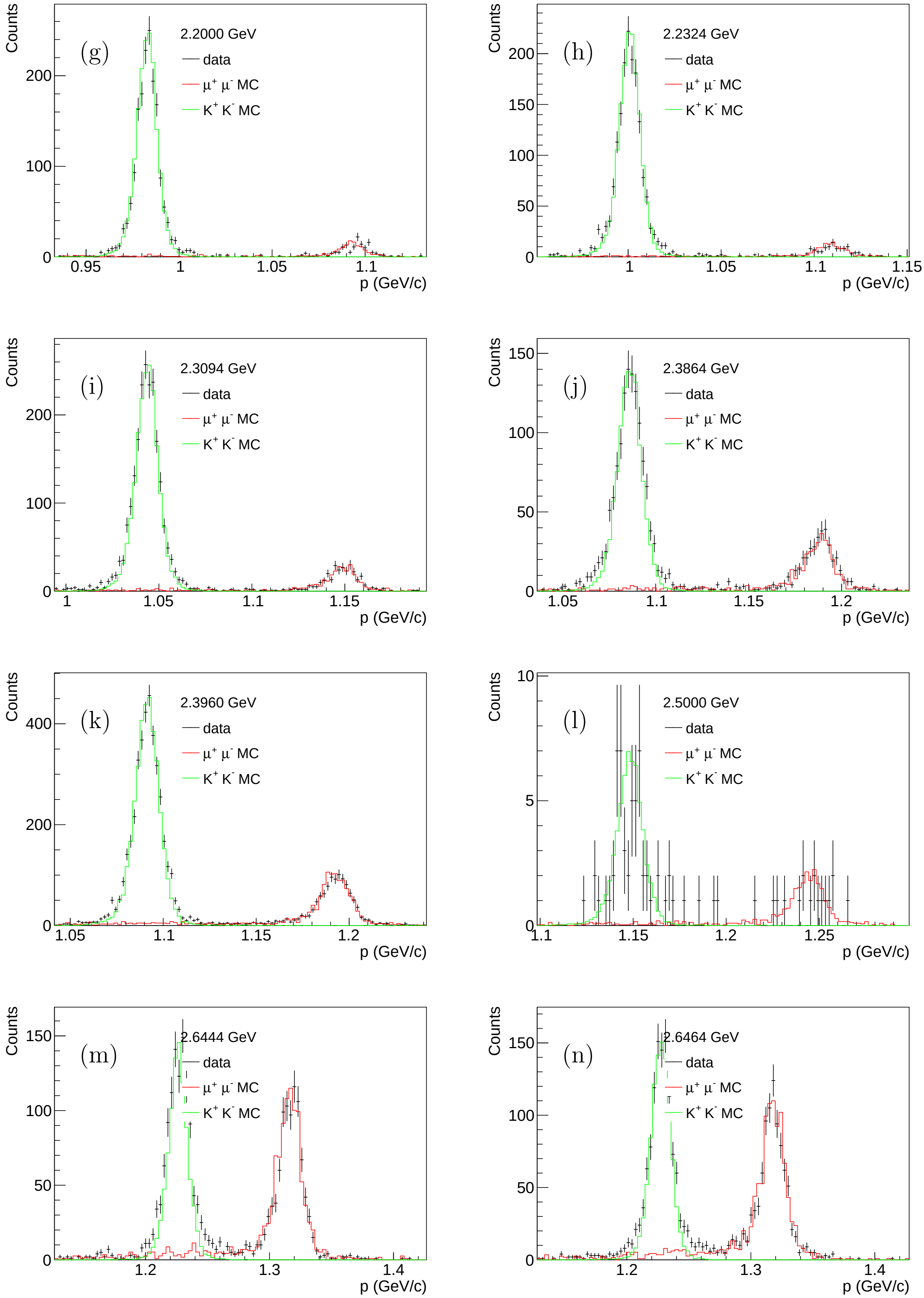

Continuation of Figure 9

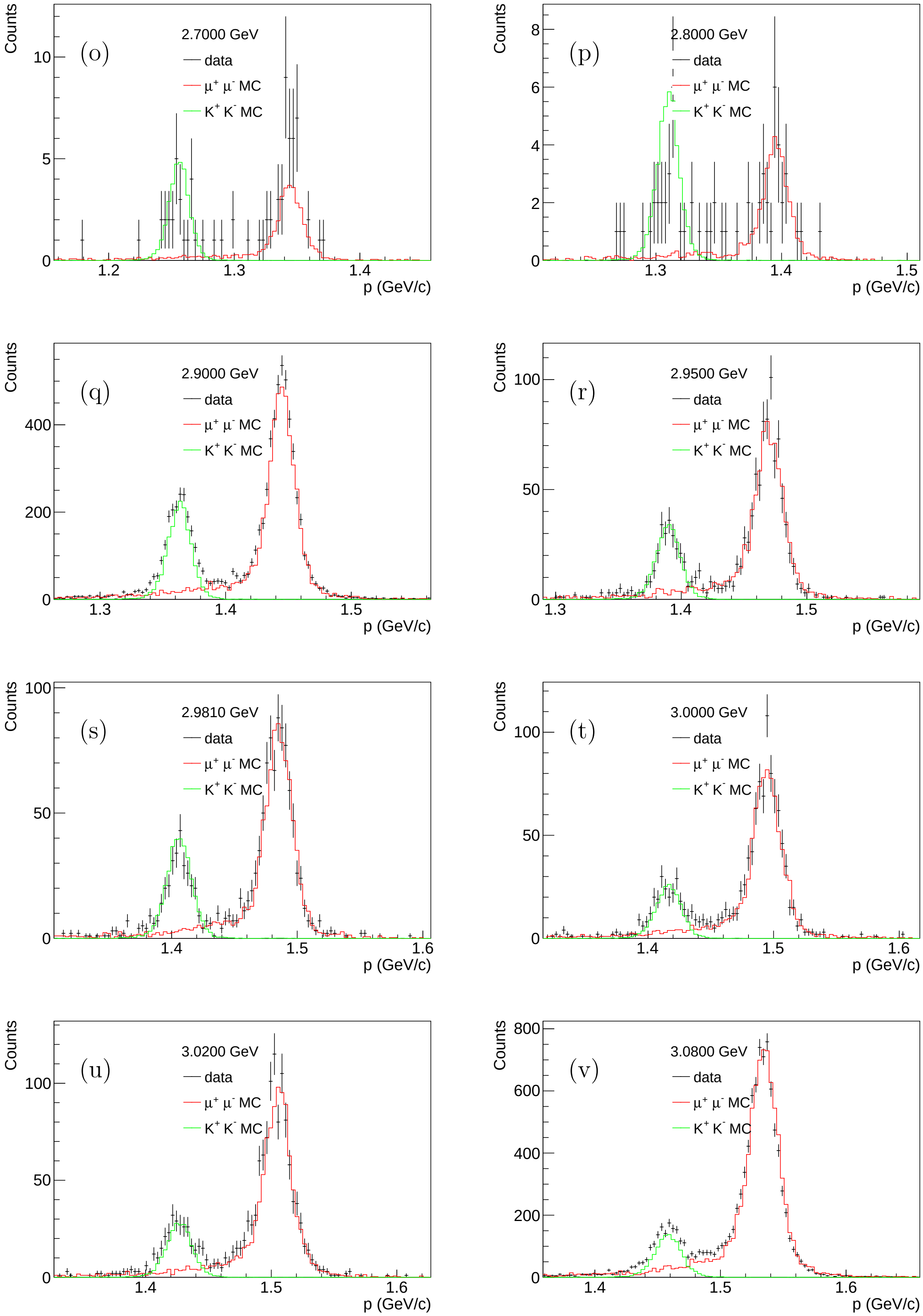

Continuation of Figure 9

In the generator, the cross section for ISR process ($\sigma_{e^+e^-\to\gamma X_i}$) is determined with the relation:

$$\sigma_{e^+e^-\to\gamma X_i} = \int dm \frac{2m}{s} W(s,x) \frac{\sigma_0(m)}{[1-\Pi(m)]^2} \tag{3}$$

where m is the invariant mass of final states with $m = s(1-x)$, and $x \equiv 2E_\gamma/\sqrt{s} = 1 - m^2/s$, $\Pi(m)$ is the vacuum polarization, which includes contributions from lepton and quarks, and $W(s,x)$ is radiator function.

$$W(s,x) = \Delta \cdot \beta x^{\beta-1} - \frac{\beta}{2}(2-x) + \frac{\beta^2}{8}\{(2-x)[3\text{ln}(1-x) - 4\text{ln}x] - 4\frac{\text{ln}(1-x)}{x} - 6 + x\} \tag{4}$$

where

$$\begin{aligned}
L &= 2\text{ln}\frac{\sqrt{s}}{m_e} \\
\Delta &= 1 + \frac{\alpha}{\pi}(\frac{3}{2}L + \frac{1}{3}\pi^2 + (\frac{\alpha}{\pi})^2\delta_2) \\
\delta_2 &= (\frac{9}{8} - 2\xi_2)L^2 - (\frac{45}{16} - \frac{11}{2}\xi_2 - 3\xi_3)L - \frac{6}{5}\xi_2^2 - \frac{9}{2}\xi_3 - 6\xi_2\text{ln}2 + \frac{3}{8}\xi_2 + \frac{57}{12} \\
\beta &= \frac{2\alpha}{\pi}(L-1), \xi_2 = 1.64493407, \xi_3 = 1.2020569
\end{aligned} \tag{5}$$

For the ISR photon angular distribution, we use the formula:

$$\frac{d\sigma_{e^+e^-\to\gamma X_i}}{dm d\text{cos}\theta_\gamma} = \frac{2m}{s} W(s,x,\theta_\gamma)\sigma_0(m) \tag{6}$$

where

$$W(s,x,\theta_\gamma) = \frac{\alpha}{\pi x}(\frac{2-2x+x^2}{\text{sin}^2\theta_\gamma} - \frac{x^2}{2}) \tag{7}$$

The Born cross sections are taken from experiments. The generator provides the ISR(f_{ISR}) and vacuum polarization(f_{vacuum}) factor, they are calculated by the definition

$$1 + \delta = f_{ISR} f_{vacuum} = \frac{\sigma_{e^+e^-\to\gamma X_i}(s)}{\sigma_{Born}(s)} \tag{8}$$

The values are listed in Tab 5.

6.2 Signal extraction

After imposing event selection criteria, there are events accumulating at expect momentum which calculated with Eq. 9 in two-dimensional momentum spectrum, as shown in Fig. 11.

$$p_{exp} = \sqrt{(E_{cm}/2)^2 - m_K^2} \tag{9}$$

where p_{exp} is the theoretical momentum of kaon in e^+e^- c.m.; E_{cm} is the collision energy; m_K is the mass of charged kaon.

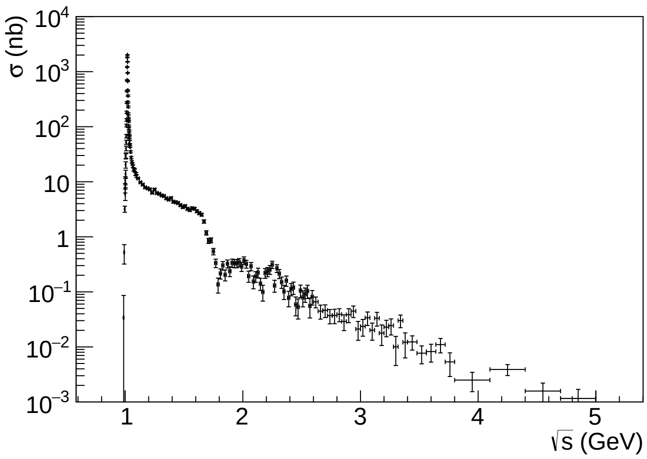

Figure 10: Cross section of $e^+e^- \to K^+K^-$ measured by BABAR [9]

The number of candidates is obtained via fitting the momentum spectrum of one track while momentum of another track is required to be within $(p_{exp} - 3\sigma_p, p_{exp} + 3\sigma_p)$, where σ_p is the momentum resolution determined with MC. In the fit, the signal is described with MC shape from K^+K^- MC convoluted with a Gaussian function and background is described with MC shape from di-mu MC convoluted with another Gaussian function, as shown in Fig. 13. From the momentum spectra, as energy goes higher the background is more in signal region which can also be known from the Fig. 2.

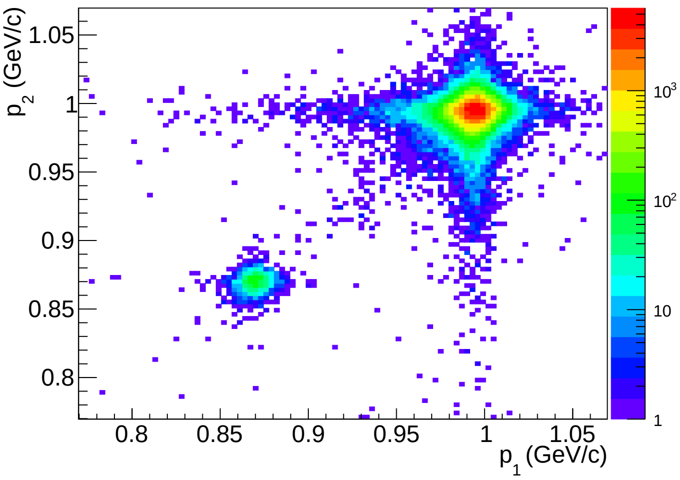

Figure 11: 2-dimensional momentum distribution after event selection at 2.0 GeV, $p_{exp} \approx$ 0.87 GeV/c

6.3 Subtraction contribution from J/ψ

At energies near J/ψ resonance, the contribution from $J/\psi \to K^+K^-$ is not negligible, both the directly resonance decay and the interference between resonance and continuum. BESIII has a set of data samples taken near J/ψ resonance which have been used to study the strong phase of J/ψ by Zhenxing and Francesca [19, 20]. Taking the convenience from the phase study, we can estimate the contribution of J/ψ in K^+K^- channel. The line shape of the ratio of the number of detected events and luminosity is fitted with following formula [20]:

$$\sigma(E_{cm}) = |D\frac{S \cdot e^{i\phi} + E}{M_{J/\psi} - E_{cm} - i\Gamma_{J/\psi}/2} - C|^2. \tag{10}$$

where S and E are strong and electromagnetic part, respectively. The sign of E and C keeps the same.

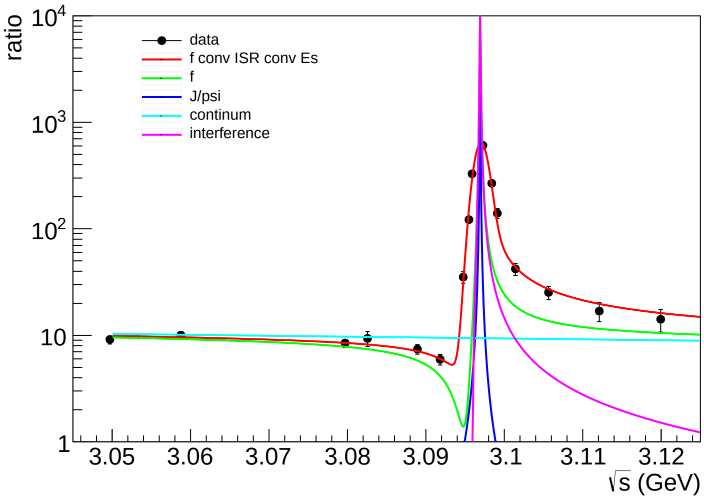

Figure 12: Line shape of $N/\mathcal{L}$. The function used to fit the line shape is Eq. 10 convoluted with energy spread and ISR with strong phase fixed to $-91°$ [20] and other parameters left free.

The continuum part can be separated from the formula, which can be used to estimate the difference of pure continuum process and the total cross section. The relative difference is estimated:

$$\Delta(\sigma) = \frac{\sigma_{con}(E_{cm}) - \sigma(E_{cm})}{\sigma(E_{cm})}, \qquad \sigma_{con} = |C|^2. \tag{11}$$

With the J/ψ scan data, it is found J/ψ resonance only influences the cross section measurement at a few points above 3 GeV through the interference between resonance and continuum while it is negligible below 3 GeV. Therefore we only correct the cross sections measured above 3 GeV. In the strong phase measurement, there are two solutions for the phase angle with quite large uncertainties. To check the influence from different strong phase angle, we fix phase angle to several values, as shown in Table 4. From the table shows that the differences are very small and we taken the case $\phi = -91°$ to correct the cross sections while the largest difference among them is taken as systematic uncertainty.

Based on Table 4, the born cross sections above 3 GeV are corrected as $\sigma_{con} = \sigma(1 - \Delta(\sigma))$.

E_{cm} (GeV/c)	$\Delta(\sigma)(\phi=-91°)$	$\Delta(\sigma)(\phi=-80°)$	$\Delta(\sigma)(\phi=-100°)$	$\Delta(\sigma)(\phi=91°)$
3.0	-3.6 ± 0.5 %	-3.6%	-3.6%	-3.8%
3.02	-4.7 ± 0.8 %	-4.7%	-4.6%	-4.9%
3.08	-25.0 ± 5.5 %	-25.6%	-25.2%	-26.9%

Table 4: contribution of J/ψ resonance in the cross section measurement of K^+K^- channel with ϕ fixed to different values.

6.4 Cross section of $e^+e^- \to K^+K^-$

Cross section can be calculated with Eq. 12.

$$\sigma^0 = \frac{N_{obs}}{\mathcal{L}\cdot\epsilon\cdot(1+\delta)} \tag{12}$$

where σ^0 is the bare cross section of $e^+e^- \to K^+K^-$; N_{obs} is the number of fitted yield; $\mathcal{L}$ is the integrated luminosity; $(1+\delta)$ is the correction factor due to ISR and VP. The signal part of momentum spectrum is fitted with MC shape of K^+K^- convoluted with Gaussian function and background part, which is mainly comes from di-mu process due to ISR and other effect, is described with MC shape of di-mu process convoluted with another Gaussian function as shown in Fig. 13. Cross section are calculated with Eq. 12 and summarized in Tab. 5. Fig. 14 shows the measured cross section are consistent with the results from BABAR experiment but with much smaller uncertainties. The line shape of the cross section is fitted with Eq. 13.

$$\sigma = |A_K|^2 \tag{13}$$

$$\begin{aligned} A_K = \quad & c_\phi BW_\phi + c_{\phi'} BW_{\phi'} + c_{\phi''} BW_{\phi''} \\ & + c_\rho BW_\rho + c_{\rho'} BW_{\rho'} + c_{\rho''} BW_{\rho''} + c_{\rho'''} BW_{\rho'''} \\ & + c_\omega BW_\omega + c_{\omega'} BW_{\omega'} + c_{\omega''} BW_{\omega''} + c_{\omega'''} BW_{\omega'''} \\ & + c_{con}\cdot s^{-\alpha}\cdot e^{i\cdot\theta} \end{aligned} \tag{14}$$

where c's are coefficients; BW's are Breit-Wigner functions of resonances, including $\phi(\phi(1020))$, ϕ' ($\phi(1680)$), ρ ($\rho(770)$), ρ' ($\rho(1450)$), ρ'' ($\rho(1700)$), ω ($\omega(782)$), ω' ($\omega(1420)$), ω ($\omega(1650)$) and other resonances whose parameters are to be determined; $s^{-\alpha}$ is used to describe continuous process; θ is the relative phase between resonances and continuous process. Parameters of resonances below 2.0 GeV are determined from BABAR data while parameters between 2.0 and 3.08 GeV are determined from both BABAR and BESIII data. The fit clarifies the structure near 2.2 GeV with $m = 2245.6 \pm 8.3$ MeV/c^2 and $\Gamma = 136.3 \pm 11.8$ MeV . Here, Breit-Wigner parameters is used to describe the resonance. Actually, pole position is another way to describe it, which corresponds to the pole in the complex s-plane and takes the form $\sqrt{s_p} = m_p - i\Gamma_p/2$. In our case, the relation between Breit-Wigner parameters and the pole position is $m_p = \sqrt{m_{BW}^2 - \Gamma_{BW}^2/4}$, $\Gamma_p = \Gamma_{BW}$. Therefore, the pole of the resonance is $\sqrt{s} = 2244.6(8.3) - i68.2(5.8)$ MeV, where the number in brackets are uncertainties.

The statistical significance of the structure is estimated by comparing the change of $\Delta\chi^2 = 555$ with and without the component in the fit, and taking the number of degree of freedom (Δndf = 3) into account, which is 23σ.

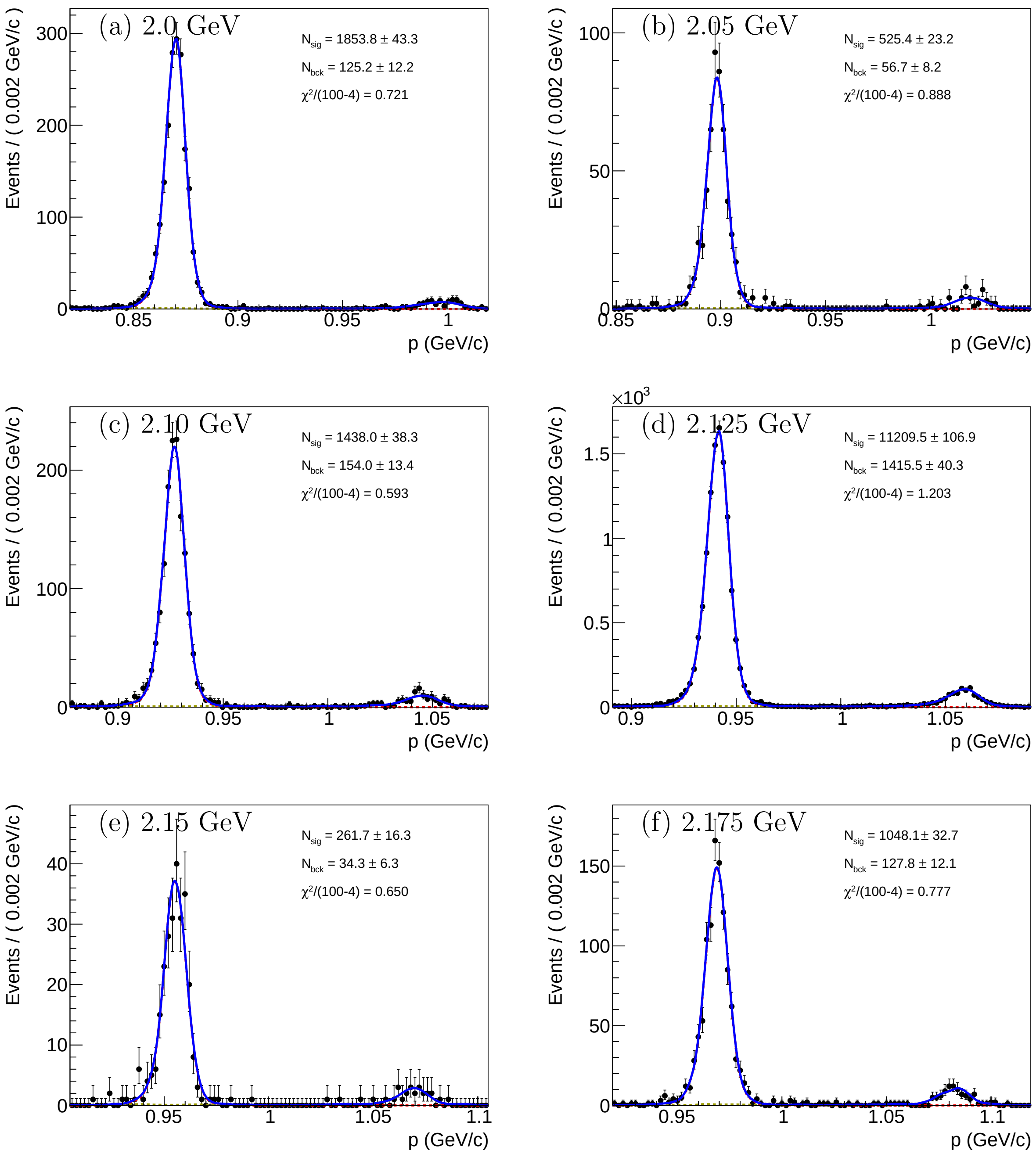

Figure 13: momentum spectra at 22 R scan energy points. Signal is described with MC shape of K^+K^- convoluted with a Gaussian function (red line). Background is described with MC shape of $\mu^+\mu^-$ convoluted with another Gaussian function (green line).

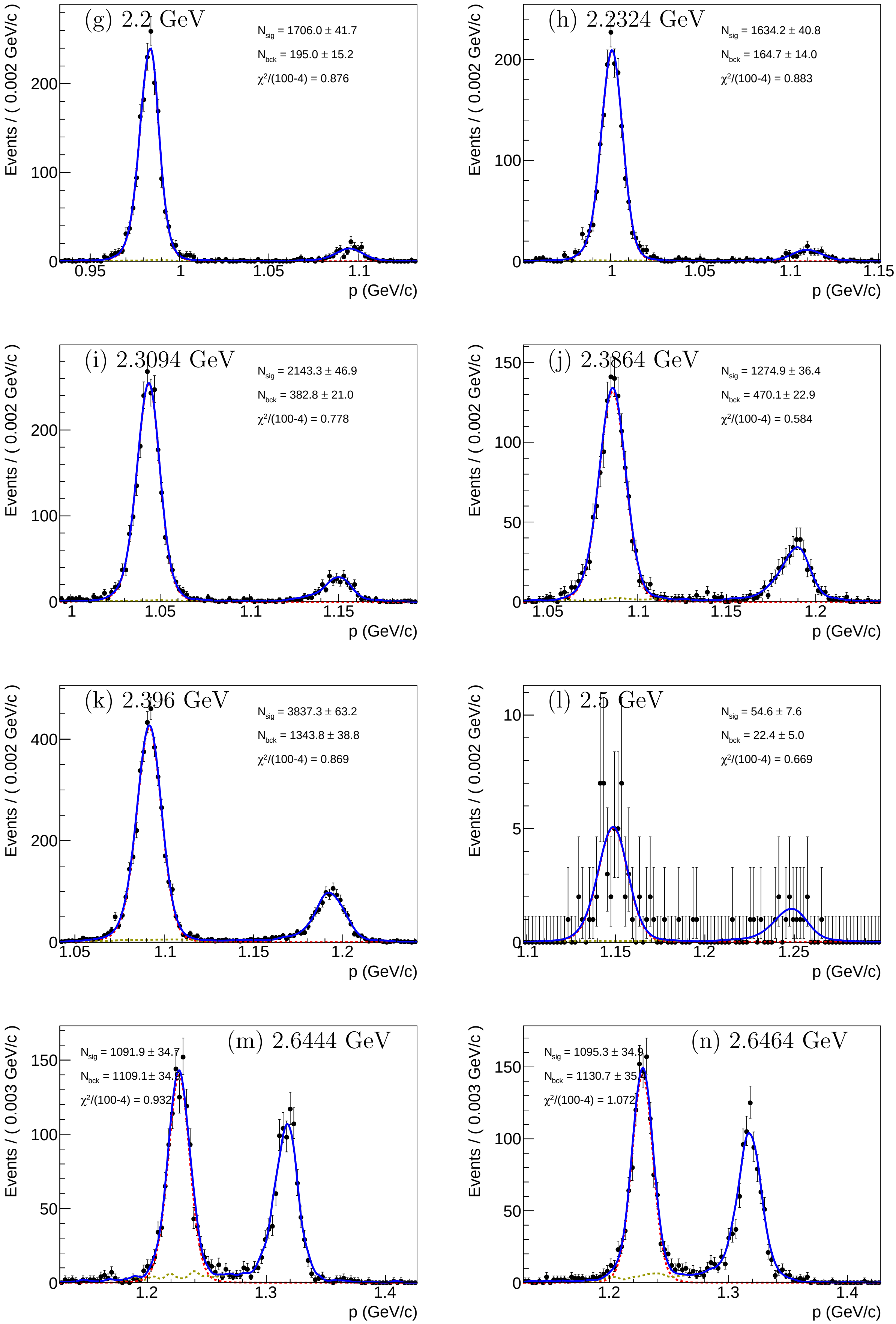

Continuation of Figure 13.

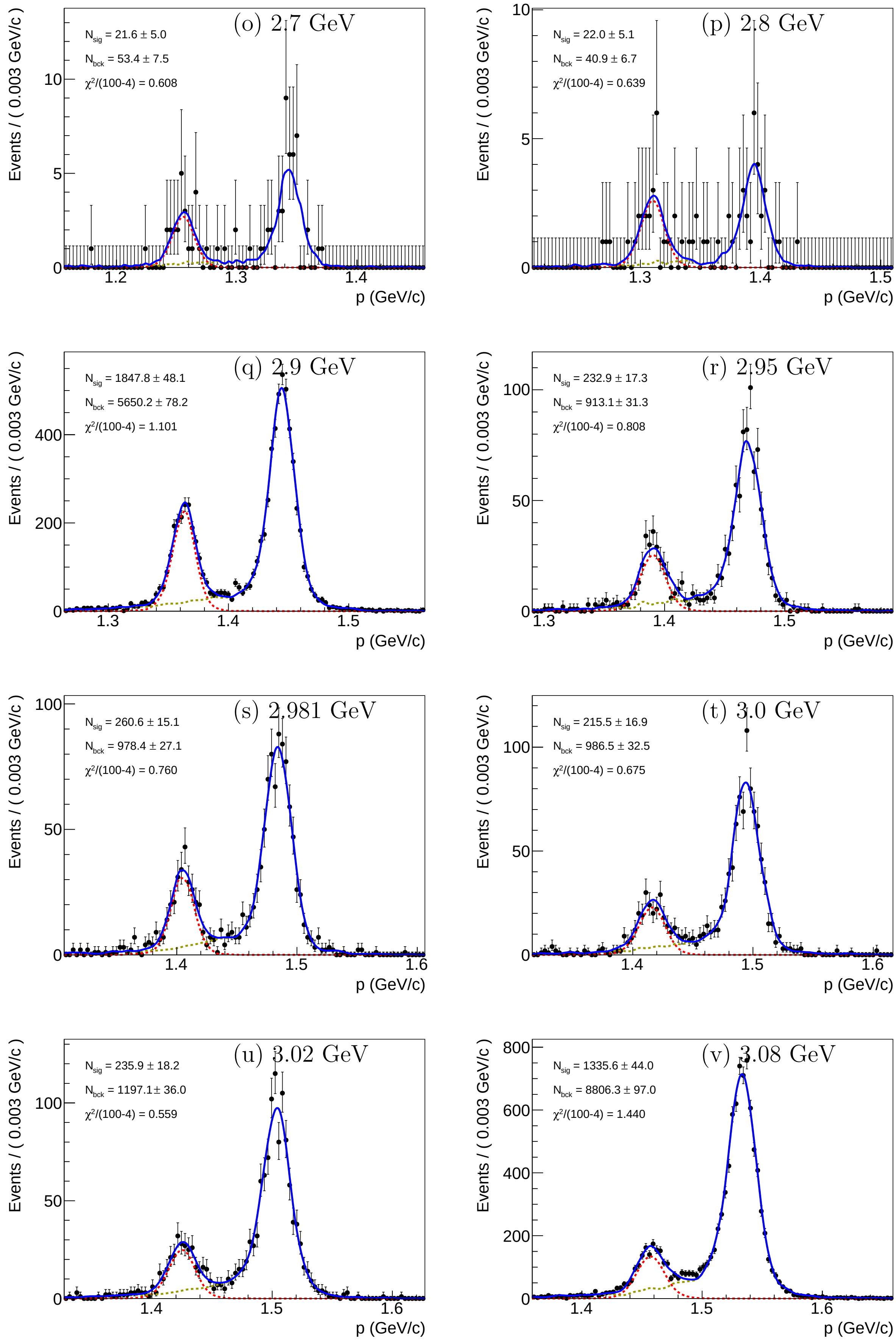

Continuation of Figure 13.

6.5 Form factor

Form factor of charged kaon can be extracted from cross section with Eq. 15.

$$|F_K|^2(s) = \frac{3s}{\pi\alpha(0)^2\beta_K^3}\frac{\sigma_{KK}(s)}{C_{FS}} \tag{15}$$

where

$$\sigma_{KK}(s) = \sigma^0_{KK}(s)\left(\frac{\alpha(s)}{\alpha(0)}\right)^2 \tag{16}$$

is the dressed cross section, deduced from the bare cross section σ^0_{KK}, $\beta_K = \sqrt{1-4m_K^2/s}$ is the kaon velocity, and $C_{FS} = 1 + \frac{\alpha}{\pi}\eta_K(s)$ is the final-state correction [9].

QCD prediction for helicity zero meson is inversely proportional to s, $F_K = 16\pi\alpha_s(s)\frac{f_K^2}{s}$ [4]. A fit is performed with the function $A\alpha_s^2(s)/s^n$ when $\sqrt{s} > 2.38$GeV, as shown in Fig. 15. A and n are left free in the fit and $n = 1.94 \pm 0.09$ is obtained which is in agreement with QCD prediction $n = 2$. The detail of the fit procedure can refer to Appendix. A. The fit is not performed at lower ranger because there are resonances which can not described by the function at lower range. To describe structure in energy region below 2.38 GeV, a model [9, 24] based on a sum of resonances can be used to fit the form factors. The form factor can be expressed as

$$\begin{aligned} F_K = \quad & (a_\phi BW_\phi + a_{\phi'}BW_{\phi'} + a_{\phi''}BW_{\phi''})/3 \\ & +(a_\rho BW_\rho + a_{\rho'}BW_{\rho'} + a_{\rho''}BW_{\rho''} + a_{\rho'''}BW_{\rho'''})/2 \\ & +(a_\omega BW_\omega + a_{\omega'}BW_{\omega'} + a_{\omega''}BW_{\omega''} + a_{\omega'''}BW_{\omega'''})/6 \end{aligned} \tag{17}$$

with constraints

$$\begin{aligned} a_\phi + a_{\phi'} + a_{\phi''} &= 1, \\ a_\rho + a_{\rho'} + a_{\rho''} + a_{\rho'''} &= 1, \\ a_\omega + a_{\omega'} + a_{\omega''} + a_{\omega'''} &= 1 \end{aligned} \tag{18}$$

All the a_r amplitudes are assumed to be real. The resonance shapes are described by Breit-Wigner expressions,

$$BW(s, m, \Gamma) = \frac{m^2}{m^2 - s - i\sqrt{s}\Gamma(s)} \tag{19}$$

where the width is, in general, energy dependent. For the ρ, the dependence is given by

$$\Gamma_\rho(s) = \Gamma_\rho \frac{s}{m_\rho^2}\left(\frac{\beta(s, m_\pi)}{\beta(m_\rho^2, m_\pi)}\right)^3 \tag{20}$$

with $\beta(s, m) = \sqrt{1 - 4m^2/s}$. For the ϕ, there are separate contributions from different decay modes (with branching fractions $\mathcal{B}$), approximated as

$$
\begin{aligned}
\Gamma_\phi(s) =&\Gamma_\phi\Big[\mathcal{B}(\phi\to K^+K^-)\frac{\Gamma_{\phi\to K^+K^-}(s,m_\phi,\Gamma_\phi)}{\Gamma_{\phi\to K^+K^-}(m_\phi^2,m_\phi,\Gamma_\phi)}\\
&+\mathcal{B}(\phi\to K^0\bar{K}^0)\frac{\Gamma_{\phi\to K^0\bar{K}^0}(s,m_\phi,\Gamma_\phi)}{\Gamma_{\phi\to K^0\bar{K}^0}(m_\phi^2,m_\phi,\Gamma_\phi)}\\
&+1-\mathcal{B}(\phi\to K^+K^-)-\mathcal{B}(\phi\to K^0\bar{K}^0)\Big]
\end{aligned}
\tag{21}
$$

where $\Gamma_{\phi\to K\bar{K}}(s,m_\phi,\Gamma_\phi)$ is given in Eq. 20 with suitable replacement. A fixed width is used for resonances other than ϕ and ρ.

Mass and width of (ϕ, ϕ'), (ρ, ρ', ρ'') and (ω, ω', ω'') are set to value in PDG while mass and width of ϕ'', ρ''' and ω''' are free in the fit. The number of energy point is not large enough to perform a well fit for resonances, the result from BABAR experiment is included in the fit. The fit result is shown in Fig. 16.

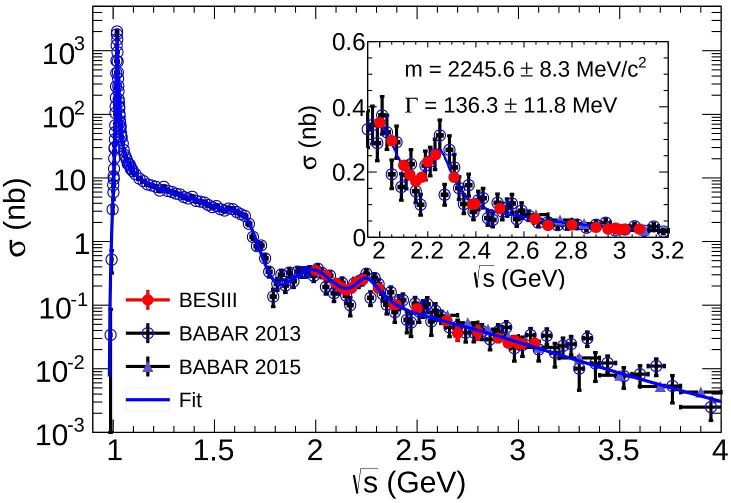

Figure 14: Cross section of $e^+e^-\to K^+K^-$.

7 Systematic uncertainty

Several aspects can contribute systematic uncertainty to the cross section measurement including all components in Eq. 12, the procedure to obtain N_{obs}, $\mathcal{L}$, ϵ, $(1+\delta)$ and some other sources. They are summarized in Tab. 7. All of them are discussed in details in subsections.

7.1 Luminosity

The integrated luminosity is measured using bhabha events, with an uncertainty about 1% [22, 23].

7.2 MC efficiency and ISR/VP correction factor

ϵ and $(1+\delta)$ are determined with MC simulation whose statistics introduces an uncertainty as described with Eq. 22 and the uncertainty of correction factor for ISR and

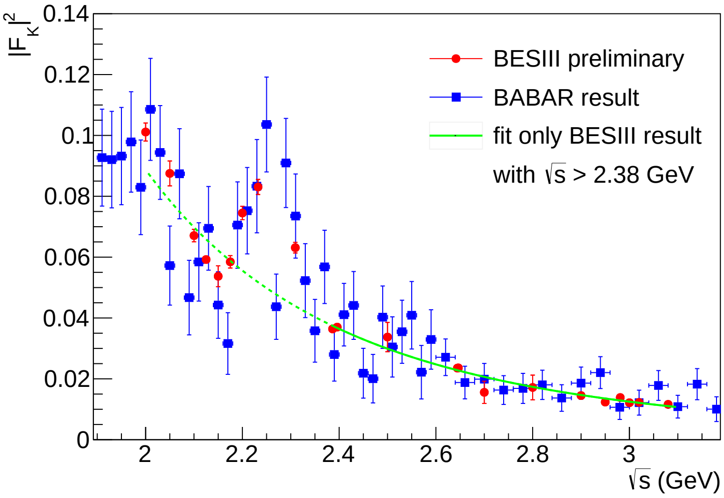

Figure 15: $|F_K|^2$ of $e^+e^- \to K^+K^-$. Red dots are results in this work. Green line is the fit result at $\sqrt{s} > 2.38$ GeV which extrapolating to lower range.

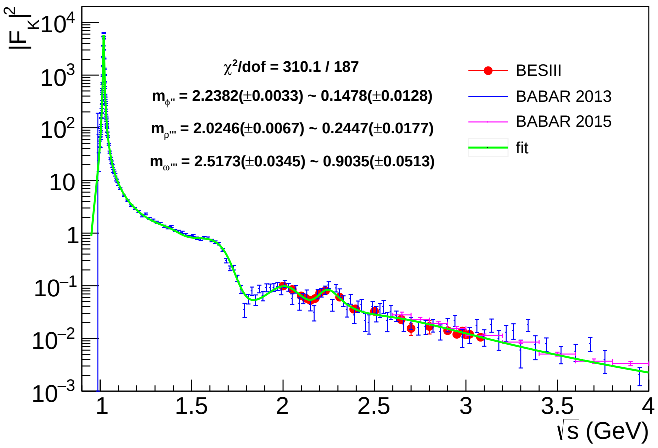

Figure 16: $|F_K|^2$ of $e^+e^- \to K^+K^-$. Blue and pink dots with error bar are the result of BABAR. Red dots are results in this work. Green line is the fit function. The legend shows the mass, first value with uncertainty in bracket, and width, second value with uncertainty in bracket.

Table 5: Summary of cross section of K^+K^-.

E_{cm} (GeV)	ϵ	$(1+\delta)$	$\mathcal{L}$ (pb^{-1})	N_{sig}	σ (pb)
2.0	0.1927	2.717	$10.074 \pm 0.005 \pm 0.073$	1853.8 ± 43.3	$351.5 \pm 8.2 \pm 6.4$
2.05	0.1853	2.864	$3.343 \pm 0.003 \pm 0.024$	525.4 ± 23.2	$296.1 \pm 13.1 \pm 4.7$
2.1	0.1591	3.368	$12.167 \pm 0.006 \pm 0.077$	1438.0 ± 38.3	$220.6 \pm 5.9 \pm 3.2$
2.125	0.1453	3.704	$^{*}108.49 \pm 0.02 \pm 0.92$	11209.5 ± 106.9	$192.0 \pm 1.8 \pm 2.9$
2.15	0.1346	3.987	$2.841 \pm 0.003 \pm 0.022$	261.7 ± 16.3	$171.7 \pm 10.7 \pm 2.7$
2.175	0.1521	3.521	$10.625 \pm 0.006 \pm 0.069$	1048.1 ± 32.7	$184.2 \pm 5.7 \pm 3.0$
2.2	0.1802	2.986	$13.699 \pm 0.007 \pm 0.108$	1706.0 ± 41.7	$231.4 \pm 5.7 \pm 4.0$
2.2324	0.2011	2.707	$11.856 \pm 0.007 \pm 0.077$	1634.2 ± 40.8	$253.2 \pm 6.3 \pm 4.2$
2.3094	0.1697	3.255	$21.089 \pm 0.009 \pm 0.156$	2143.3 ± 46.9	$184.0 \pm 4.0 \pm 3.1$
2.3864	0.1222	4.557	$22.549 \pm 0.010 \pm 0.192$	1274.9 ± 36.4	$101.5 \pm 2.9 \pm 2.1$
2.396	0.1189	4.702	$66.869 \pm 0.017 \pm 0.461$	3837.3 ± 63.2	$102.6 \pm 1.7 \pm 2.2$
2.5	0.1005	5.616	$1.098 \pm 0.002 \pm 0.009$	54.6 ± 7.6	$88.1 \pm 12.2 \pm 2.8$
2.6444	0.0909	6.289	$33.722 \pm 0.013 \pm 0.223$	1091.9 ± 34.7	$56.6 \pm 1.8 \pm 2.1$
2.6464	0.0902	6.300	$34.003 \pm 0.013 \pm 0.262$	1095.3 ± 34.9	$56.7 \pm 1.8 \pm 1.6$
2.7	0.0873	6.580	$1.034 \pm 0.002 \pm 0.008$	21.6 ± 5.0	$36.3 \pm 8.4 \pm 1.2$
2.8	0.0804	7.159	$1.008 \pm 0.002 \pm 0.007$	22.1 ± 5.1	$37.9 \pm 8.8 \pm 1.6$
2.9	0.0738	7.837	$105.253 \pm 0.025 \pm 0.905$	1847.8 ± 48.1	$30.4 \pm 0.8 \pm 1.4$
2.95	0.0702	8.217	$15.942 \pm 0.010 \pm 0.108$	232.9 ± 17.3	$25.3 \pm 1.9 \pm 1.3$
2.981	0.0683	8.466	$16.071 \pm 0.010 \pm 0.108$	260.6 ± 15.1	$28.0 \pm 1.6 \pm 1.6$
3.0	0.0667	8.622	$15.881 \pm 0.010 \pm 0.137$	215.5 ± 16.9	$24.4 \pm 1.8 \pm 1.5$
3.02	0.0656	8.791	$17.290 \pm 0.011 \pm 0.121$	235.9 ± 18.2	$24.8 \pm 1.8 \pm 1.5$
3.08	0.0564	9.266	$126.185 \pm 0.029 \pm 0.959$	1335.6 ± 44.0	$25.3 \pm 0.7 \pm 2.2$

ϵ is the selection efficiency.
$(1+\delta)$ is the correction factor, a combination of ISR and VP correction.
$\mathcal{L}$ is the luminosity measuared with bhabha and di-gamma events. [22]
N_{sig} is the number of events obtained from experimental data.
σ is the cross section. 1st uncertainty is statistical uncertainty and 2nd one is systematic uncertainty.
* Luminosity refer to BAM218 [23] at 2.125 GeV.

Table 6: Form factor of charged kaon

E_{cm} (GeV)	$\lvert F_K\rvert^2$	E_{cm} (GeV)	$\lvert F_K\rvert^2$
2.0	$0.1021 \pm 0.0024 \pm 0.0018$	2.5	$0.0341 \pm 0.0047 \pm 0.0011$
2.05	$0.0878 \pm 0.0039 \pm 0.0013$	2.6444	$0.0237 \pm 0.0008 \pm 0.0009$
2.1	$0.0666 \pm 0.0018 \pm 0.0009$	2.6464	$0.0240 \pm 0.0008 \pm 0.0006$
2.125	$0.0593 \pm 0.0006 \pm 0.0009$	2.7	$0.0158 \pm 0.0037 \pm 0.0005$
2.15	$0.0539 \pm 0.0034 \pm 0.0008$	2.8	$0.0173 \pm 0.0040 \pm 0.0007$
2.175	$0.0590 \pm 0.0018 \pm 0.0009$	2.9	$0.0145 \pm 0.0004 \pm 0.0007$
2.2	$0.0744 \pm 0.0018 \pm 0.0013$	2.95	$0.0125 \pm 0.0009 \pm 0.0006$
2.2324	$0.0843 \pm 0.0021 \pm 0.0013$	2.981	$0.0139 \pm 0.0008 \pm 0.0008$
2.3094	$0.0635 \pm 0.0014 \pm 0.0010$	3.0	$0.0122 \pm 0.0009 \pm 0.0007$
2.3864	$0.0367 \pm 0.0010 \pm 0.0007$	3.02	$0.0124 \pm 0.0009 \pm 0.0008$
2.396	$0.0371 \pm 0.0006 \pm 0.0008$	3.08	$0.0118 \pm 0.0003 \pm 0.0010$

VP can be estimated with last two different input line shapes in the iterative procedure.

$$\Delta_{MC} = \frac{1}{\sqrt{N_{gen}}} \cdot \sqrt{\frac{1-\epsilon}{\epsilon}} \tag{22}$$

where N_{gen} is the number of event generated in simulation. ϵ is the event selection efficiency.

7.3 Kaon tracking efficiency

Systematic uncertainty due to the procedure of obtaining N_{obs} includes the reconstruction of charge tracks and event selection criteria. $K^{\pm}$ are reconstructed in MDC which may be different for data and MC. The process of $e^+e^- \to K^+K^-\pi^+\pi^-$ is chosen as the control sample to study the reconstruction efficiency (tracking efficiency) with method described in Ref. [25]. The comparison of data and MC is shown in Fig. 17 and shows average difference is $(1.0 \pm 0.2)\%$ for K^+, and $(0.7 \pm 0.3)\%$ for K^-. Tracking uncertainty is estimated as:

$$\begin{aligned} \Delta_{track\pm} &= \frac{\int f_{\pm}(p_t) \cdot \omega \cdot \Delta\epsilon \mathrm{d}p_t}{\int f_{\pm}(p_t) \cdot \omega \mathrm{d}p_t} \\ \omega &= \frac{1}{\sigma^2_{\Delta\epsilon}} \\ \Delta_{track} &= \Delta_{track+} + \Delta_{track-} \end{aligned} \tag{23}$$

where $\Delta_{track\pm}$ is systematic uncertainty from tracking efficiency of kaon; $f_{\pm}(p_t)$ is the transverse momentum distribution function of K^+ and K^-; $\Delta\epsilon$ is the difference of tracking efficiency between data and MC. $\sigma_{\Delta\epsilon}$ is the uncertainty of $\Delta\epsilon$. Considering $\sigma_{\Delta\epsilon}$ is different at different p_t, a weighting factor ω is added to the calculation of systematic uncertainty from tracking.

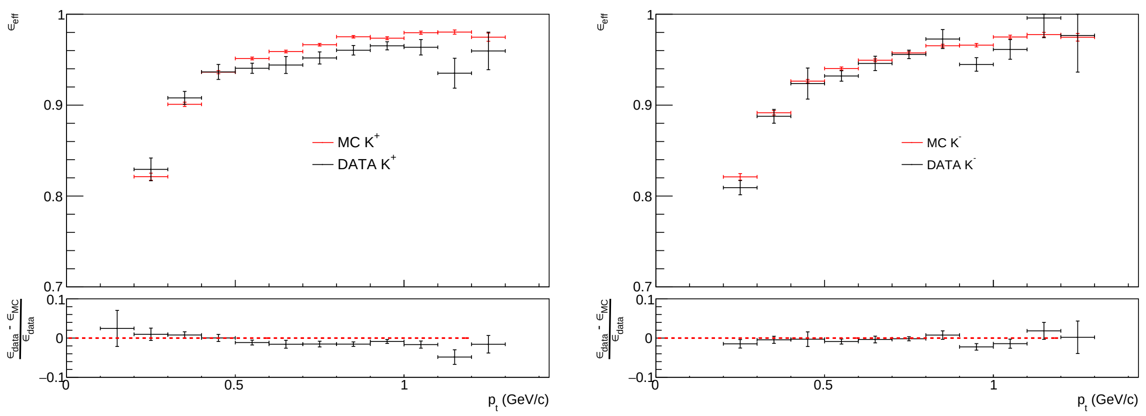

a) tracking efficiency of K^+ b) tracking efficiency of K^-

Figure 17: Comparison of tracking efficiency of kaon between data and MC

7.4 Event selection

7.4.1 Open angle

Fig. 18 shows the open angle of 2 charged tracks for data and K^+K^- MC. Events are selected with criteria in Sec. 4 execpt the open angle requirement. The spectra of MC are scaled to data according to the numbers of events. From the figure, the open angle cut at 179° is enough for all energy points. It should be noticed that dimu process are required with momentum of one track should be less than $p_{exp} + 3\sigma$, most muons are vetoed, the open angle of remaining muons are not back to back.

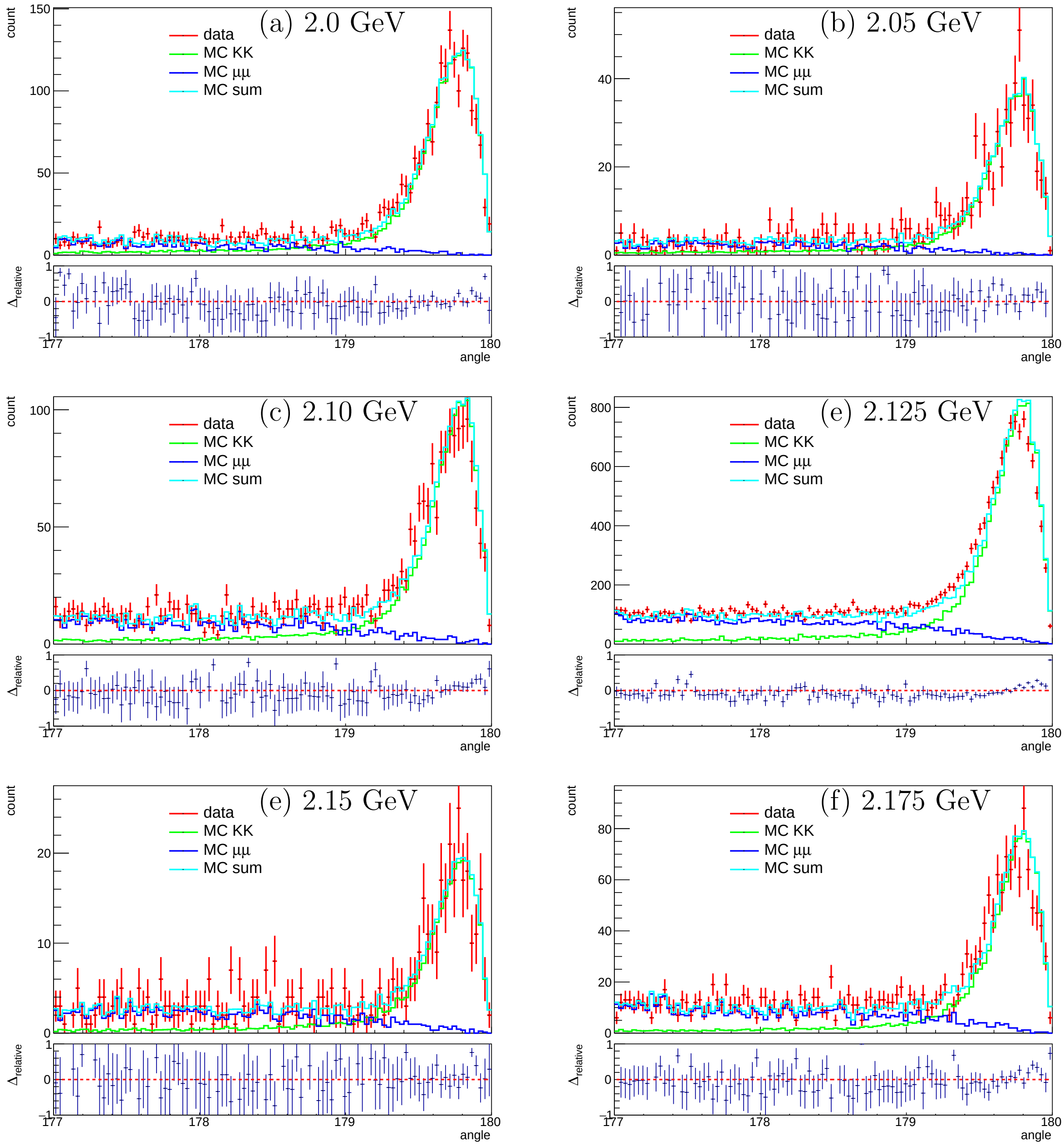

Figure 18: Open angle of 2 charged tracks at 22 R scan energy points. The sum of MC is the sum of K^+K^- MC and di-mu MC. The relative differences between the sum of MC and data are shown.

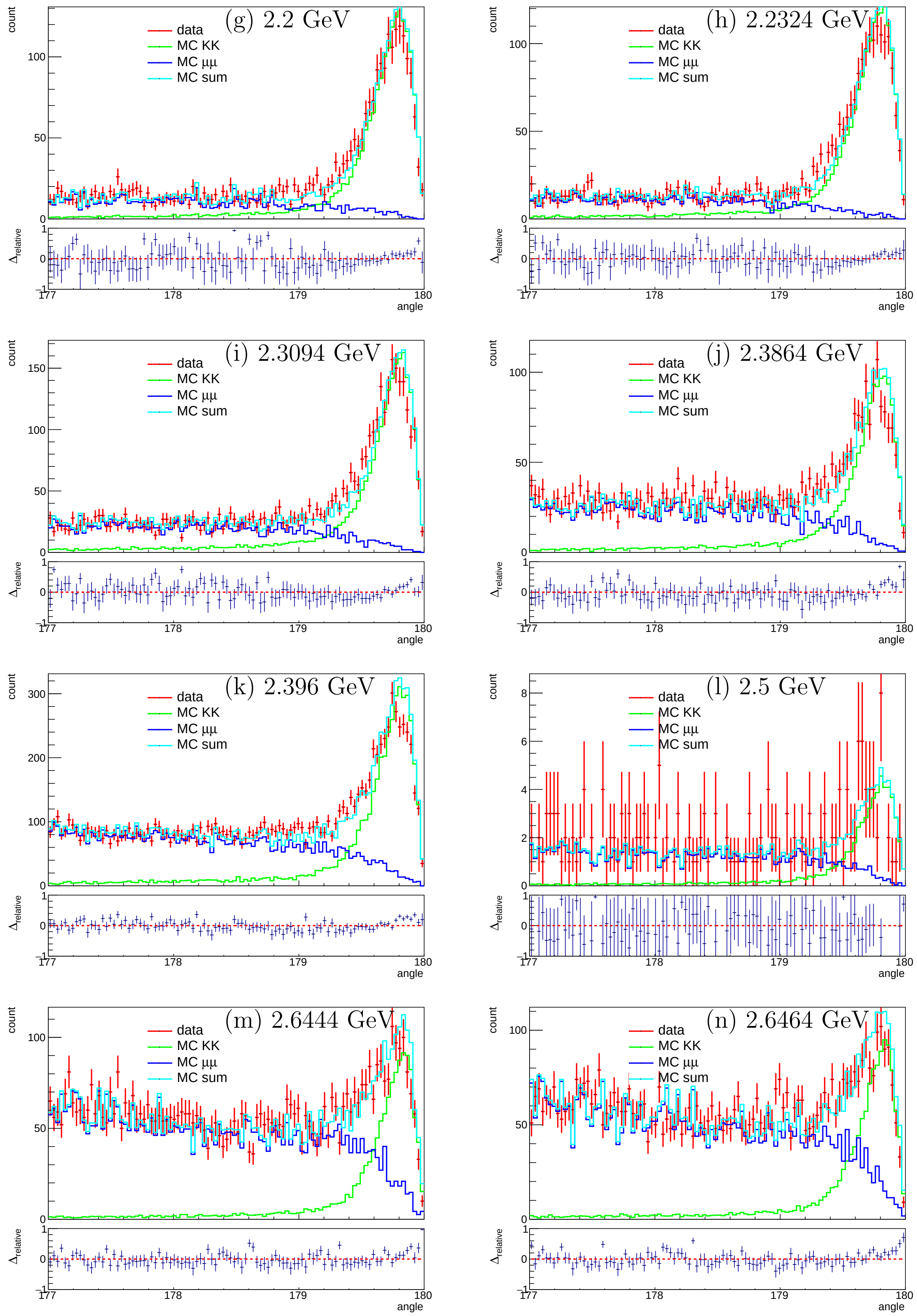

Continuation of Figure 18.

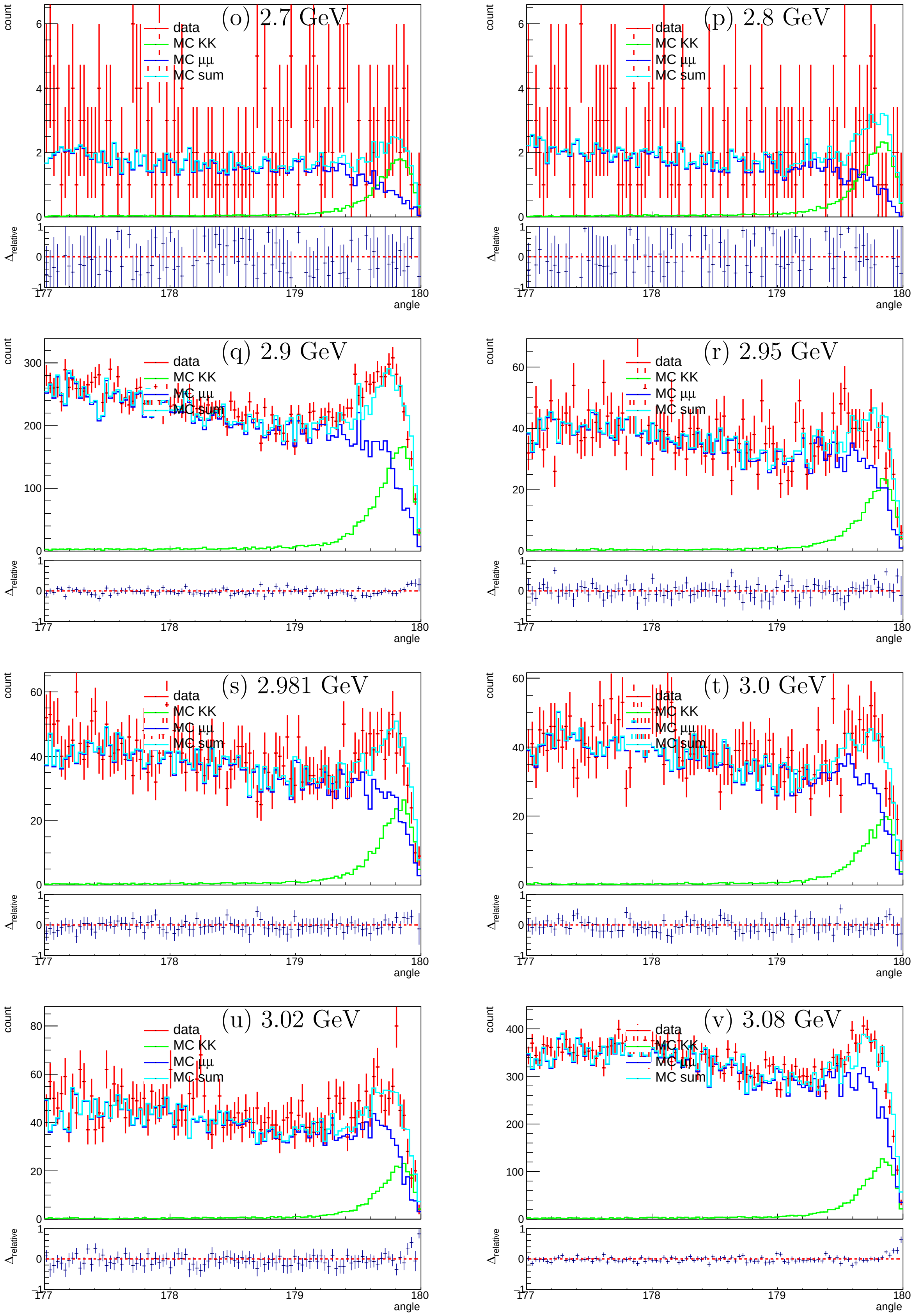

Continuation of Figure 18.

From the comparison of data and MC, there are some discrepancy between data and MC, thus the uncertainty is estimated by smearing open angle distribution of MC to data and comparing the changes of event selection efficiency.

7.4.2 Other cuts

For other cuts, the uncertaintys are similar with the open angle which is estimated by smearing the distribution of MC to that of data and taking the changes of efficiency as uncertainty.

7.5 Signal extraction

7.5.1 Momentum requirement

The signal number is obtained via requiring momentum of one kaon in signal region and fitting the momentum spectrum of another kaon. The kaon is tagged when its momentum is less than $p_{exp} + 3 \cdot \delta_p$ in which δp is obtained with MC. Mean value and resolution of momentum of kaon can also be obtained from experimental data which may be slightly different from MC. Fig. 9 shows the comparison of MC and data which are comparable. The uncertainty from the difference of p_{exp} and δ_p is estimated via replacing the kaon tagging criterion determined from MC with criterion determined from experimental data and comparing the obtained cross section.

7.5.2 fit range

The fit of momentum spectra are performed in specific ranges and uncertainty from which is estimated by changing the the fit range about 1 sigma of momentum distribution of kaon.

7.5.3 Signal and background shape

The signal and background are described Monte Carlo shape convoluted with Gaussian function. The shapes used to describe signal and background are not perfect. To describe uncertainty from signal and background shapes, we use Crystal-ball plus Gaussian functions to do the fit. For signal shape, the differences of final results from fit with functions and with MC shapes are taken as systematic uncertainty. For background shape, we also do a fit with pure MC shape (without convolution with Gaussian function). The largest difference among three background shapes is taken as systematic uncertainty. Due to the low statistics at some energies. there are jumps for uncertainties of some nearby points. To solve this problem we use uncertainties at some large statistical energies as standards, and estimated uncertainties of other energy points with linear interpolation. The standard points are taken at 2.125, 2.6444, 2.6464, 3.08 GeV. For 2.6444 and 2.6464 GeV, since they are quite close, the larger uncertainty is used.

7.6 Uncertainty of structure near 2.2 GeV

From the line shape of $\sigma(K^+K^-)$, the structure near 2.2 GeV is very clear, denoted as R. The mass and width of R is fitted with a formula based on Breit-Wigner function of many resonances. For a wide resonance, the vertex function should be considered. For example, if the J^P is 1^-, there is an additional factor p_K^2. And a phase space factor p/s can

Table 7: Systematic uncertainty (%) of cross section of K^+K^-.

E_{cm} (GeV)	2	2.05	2.1	2.125	2.15	2.175	2.2	2.2324	2.3094	2.3864	2.396
Δ_{MC}	0.2	0.2	0.2	0.2	0.3	0.2	0.2	0.2	0.2	0.3	0.3
$\Delta_{1+\delta}$	0.2	0.1	0.3	0.3	0.5	0.3	0.3	0.5	0.2	0.4	0.4
$\Delta_{\mathcal{L}}$	0.9	0.9	0.9	0.8	0.9	0.9	0.9	0.9	0.9	0.9	0.9
Δ_{tag}	0.7	0.0	0.2	0.0	0.0	0.3	0.4	0.1	0.0	0.2	0.3
$\Delta_{E/p}$	0.6	0.7	0.5	0.6	0.6	0.6	0.6	0.5	0.6	0.4	0.4
Δ_{angle}	0.8	0.7	0.8	0.7	0.7	0.7	0.8	0.8	0.7	0.9	1.0
Δ_{TOF}	< 0.1	< 0.1	< 0.1	< 0.1	< 0.1	< 0.1	< 0.1	< 0.1	< 0.1	< 0.1	< 0.1
Δ_{track}	0.9	0.2	0.1	0.5	0.5	0.6	0.6	0.5	0.1	0.7	0.8
Δ_{range}	0.0	0.7	0.1	0.3	0.1	0.1	0.5	0.2	0.6	0.5	0.4
$\Delta_{sigshape}$	0.2	0.2	0.2	0.2	0.3	0.4	0.4	0.5	0.7	1.0	1.0
$\Delta_{bckshape}$	0.4	0.4	0.4	0.4	0.4	0.4	0.4	0.4	0.5	0.5	0.6
sum	1.8	1.6	1.5	1.5	1.5	1.6	1.7	1.6	1.7	2.0	2.1
E_{cm} (GeV)	2.5	2.6444	2.6464	2.7	2.8	2.9	2.95	2.981	3	3.02	3.08
Δ_{MC}	0.3	0.3	0.3	0.3	0.3	0.4	0.4	0.4	0.4	0.4	0.4
$\Delta_{1+\delta}$	0.2	0.3	0.3	0.3	0.3	0.3	0.3	0.3	0.3	0.3	0.3
$\Delta_{\mathcal{L}}$	0.9	0.9	0.9	0.9	0.9	0.9	0.9	0.9	0.9	0.9	0.9
Δ_{tag}	1.4	0.4	0.5	0.5	0.5	0.1	0.1	0.5	1.6	1.1	1.1
$\Delta_{E/p}$	0.6	0.6	0.6	0.4	0.7	0.4	0.4	0.5	0.4	0.5	0.4
Δ_{angle}	0.8	0.9	0.8	0.9	1.3	0.8	0.9	1.2	0.9	0.9	1.0
Δ_{TOF}	< 0.1	< 0.1	< 0.1	< 0.1	< 0.1	< 0.1	< 0.1	< 0.1	< 0.1	< 0.1	< 0.1
Δ_{track}	2.1	1.1	1.2	1.5	1.4	1.0	1.3	1.6	1.7	1.7	1.9
Δ_{range}	0.3	2.7	0.8	1.0	1.0	1.1	0.3	0.2	0.7	0.7	0.8
$\Delta_{sigshape}$	1.3	1.7	1.7	2.0	2.5	3.0	3.3	3.4	3.5	3.6	3.9
$\Delta_{bckshape}$	0.6	0.7	0.8	1.2	2.1	3.0	3.5	3.8	3.9	4.1	4.6
sum	3.2	3.8	2.8	3.3	4.1	4.7	5.2	5.6	6.0	6.1	8.8

Δ_{MC} is the uncertainty from MC statistics
$\Delta_{1+\delta}$ is the uncertainty from correction factor.
$\Delta_{\mathcal{L}}$ is the uncertainty from measurement of luminosity.
Δ_{tag} is the uncertainty from signal extracting method.
$\Delta_{E/p}$ is the uncertainty from E/p cut.
Δ_{angle} is the uncertainty from the cut of the angle between 2 tracks.
Δ_{TOF} is the uncertainty from TOF cut.
Δ_{track} is the uncertainty from tracking efficiency.
Δ_{range} is the uncertainty from fitting range of momentum spectra.
$\Delta_{sigshape}$ is the uncertainty from the signal shape used in fitting.
$\Delta_{bckshape}$ is the uncertainty from the background shape used in fitting.

also be considered which modify the Breit-Wigner function to be $BW = \frac{p^2}{m^2-s-i\sqrt{s}\Gamma(s)} \cdot \frac{p}{s}$ and a fit has been performed as shown in Fig. 19, mass 2239.4 ± 2.4 MeV/c^2 and width 137.2 ± 11.6 MeV. The related uncertainties are $\Delta m = 6.2$ MeV/c^2 and $\Delta\Gamma = 0.9$ MeV.

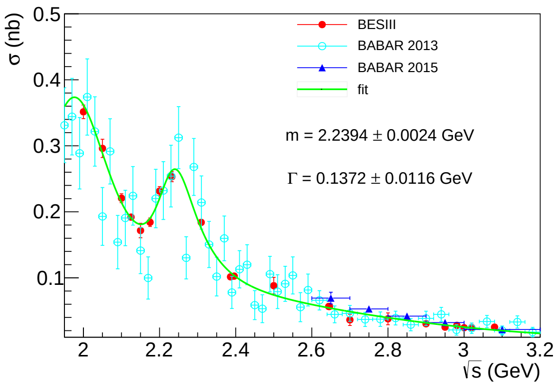

Figure 19: Line shape of $\sigma_{K^+K^-}$ with different formula of Breit-Wigner function. $BW = \frac{p^2}{m^2-s-i\sqrt{s}\Gamma(s)} \cdot \frac{p}{s}$.

In the fitting, we have cited parameters of several resonances from PDG to describe background. There are uncertainties on the parameters which may introduce uncertainty to the parameters of the resonance around 2230 MeV. The systematics is estimated by sampling the PDG quoted parameters with Gaussian functions whose mean values and errors are the PDG provided values and their uncertainties. We sample the parameters and do the fitting for 1000 times. The widths of the distributions of the fitting results are taken as the systematics which are shown in Fig. 20, which are $\Delta m = 8.8$ MeV/c^2 and $\Delta\Gamma = 9.2$ MeV.

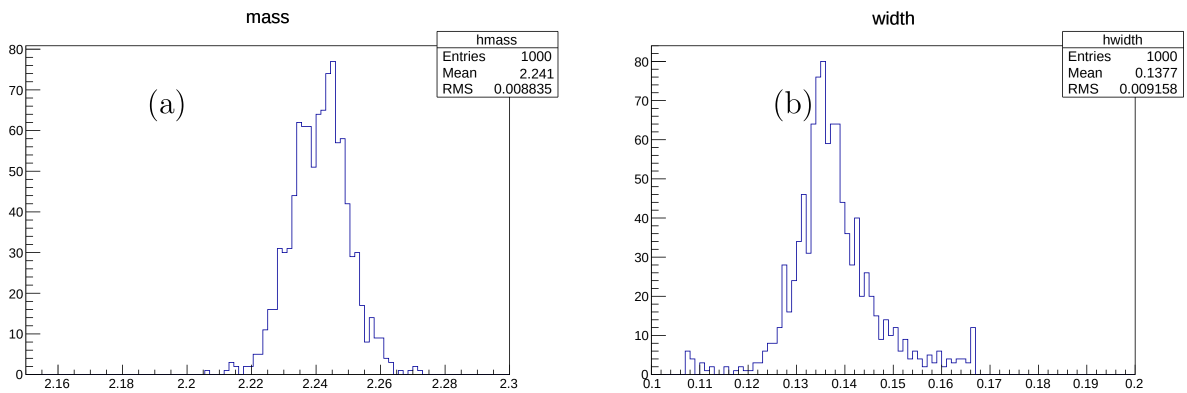

Figure 20: Distributions of fit results when sampling PDG quoted parameters. (a) and (b) are the distributions of the mass and width of the resonance around 2.23 GeV in the fit, respectively.

We have treated the width of R as fixed. Since the width is not narrow, the width may be energy dependent. The different parameterization of width may introduce uncertainties. The width can be parameterized as

$$\Gamma_R(s) = \Gamma \frac{s}{m_R^2} \left(\frac{\beta(s, m_K)}{\beta(m_R^2, m_K)} \right)^3 . \quad (24)$$

Using the energy-dependent width, the fitting result of parameters of R are $m = 2252.2 \pm 7.2$ MeV$/c^2$ and $\Gamma = 130.9 \pm 5.0$ MeV as shown in Fig. 21. The related uncertainties are $\Delta m = 3.6$ MeV$/c^2$ and $\Delta\Gamma = 5.4$ MeV.

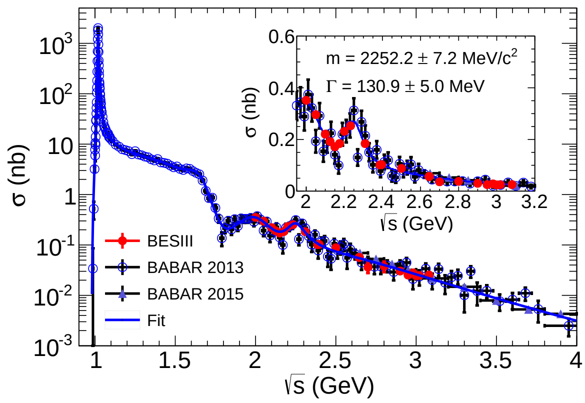

Figure 21: Line shape of $\sigma_{K^+K^-}$ fitted using Breit-Wigner function with energy-dependent width.

Uncertainties from other sources, like energy calibration and energy spread, are negligible in the measurement of parameters of the structure. The total systematics are estimated by the root mean square values from each source, which are $\Delta m = 11.4$ MeV$/c^2$ and $\Delta\Gamma = 10.7$ MeV, respectively.

8 Conclusion

The cross section of the process $e^+e^- \to K^+K^-$ and form factor of charged kaon are measured in energy region between 2.0 to 3.08 GeV with much better accuracy than previous experiment and showing a structure near 2.2 GeV. The selection criteria with E/p, relative polar angle, TOF and momentum requirement can well separate signal from background when $\sqrt{s} < 2.5$ GeV$/c$ and suppress background heavily at higher energy. A simple fit of the from factor, which extracted from cross section, with a function $A\alpha(s)/s^n$ in energy region higher than 2.38 GeV confirms the QCD prediction for the relation of s and $|F_K|$ while a model based on a sum of resonances can describe the structure in energy region below 2.4 GeV showing a resonance with mass $2245.6 \pm 8.3 \pm 11.4$ MeV$/c^2$ and width $136.3 \pm 11.8 \pm 10.7$ MeV can describe the structure at 2.2 GeV. The result can help to improve the accuracy of $(g-2)_\mu$ measurement, the understanding of nature of kaon and property of resonances between 2.0 to 3.08 GeV.

References

[1] H. Burkhardt *et al.*, Z. Phys. C—Particles and Fields, **43**, 407 (1989).

[2] B. Chakraborty *et al.*, (HPQCD collaboration), Phys. Rev. D **89**, 114501 (2014).

[3] S Coito *et al.*, Phys. Rev. D **80**, 094011(2009).

[4] G.P. Lepage and S.J. Brodsky, Phys. Lett. B **87**, 359 (1979).

[5] K.S. Kamal *et al.*, Phys. Rev. L **110**, 022002 (2013).

[6] M.R. Whalley, J. Phys. G: Nucl. Part. Phys. **29**, A1 (2003).

[7] D. Bisello *et al.*, (DM2 Collaboration), Z. Phys. C **39**, 13 (1988).

[8] R.R. Akhmetshin *et al.*, (CMD-2 Collaboration), Phys. Lett. B **669**, 217 (2008).

[9] J.P. Lees *et al.*, (BABAR Collaboration), Phys. Rev. D **88**, 032013 (2013).

[10] J.P. Lees *et al.*, (BABAR Collaboration), Phys. Rev. D **92**, 072008 (2015).

[11] M. Bernardini *et al.*, Phys. Lett. B **46**, 261 (1973).

[12] T.K. Pedlar *et al.*, (CLEO Collaboration), Phys. Rev. Lett. **95** 26803 (2005).

[13] M. Ablikim *et al.*, (BESIII Collaboration), Nucl. Instrum. Meth. A **614**, 345 (2010).

[14] W.D. Li *et al.*, Proceeding of CHEP06, Mumbai, India, 2006.

[15] S. Agostinelli *et al.* (GEANT4 Collaboration), Nucl. Instrum. Meth. A **506**, 250 (2003).

[16] G. Balossini *et al.*, Nucl. Phys. B **785**, 227 (2006).

[17] B. Andersson and H. Hu, hep-ph/9810285.

[18] R.G. Ping, Chin Phys. C, **38**(8), 083001 (2014).

[19] Z.X. Chen. BAM-153.

[20] Francesca. Tau and QCD group meeting.

[21] Z. Gao *et al.*, BAM-157.

[22] Zhang Bingxin's report on BESIII collaboration meeting, June 16, 2015.

[23] J.Q. Zhang *et al.*, BAM-218.

[24] C. Bruch *et al.*, Eur. Phys. J. C **39**, 41(2005).

[25] W.L. Yuan *et al.*, arXiv: 1507.03453 [hep-ex].

A Check pQCD prediction for $|F_K|^2$

The perturbative QCD prediction for form factor of kaon $|F_K|^2$ is $F_K = 16\pi\alpha_s(s)\frac{f_K^2}{s}$ [4]. The checking of this formula involves $|F_K|^2$ at several energy points which are obtained with the same procedure. Therefore, part of uncertainties of these values are correlated and need to be considered in fitting of the data. Firstly, the formula is simplified as $|F_K|^2 = A\alpha_s^2(s)/s^n$, where $\alpha_s \propto \frac{1}{ln(s/\Lambda^2)}$ with 100 MeV $< \Lambda c <$ 500 MeV ($\Lambda c = 300$ MeV is chosen here). The best value of A and n is obtained by minimizing the χ^2-function which defined as follows:

$$\chi^2 = \boldsymbol{\Delta X^T M^{-1} \Delta X} \tag{25}$$

where $\boldsymbol{\Delta X}$ is the difference between measured values and values calculated with pQCD prediction; $\boldsymbol{M}$ is the covariance matrix. Now, the main issue is to obtain the covariance matrix.

The uncertainty of measured value includes statistical and systematical components. Statistical uncertainties are not correlated while systematical ones are not the case. Tab. 7 shows systematical uncertainties from different sources at different energy points. Here, it is assumed that uncertainties from MC statistics, $1+\delta$, luminosity measurement and tracking efficiency are correlated while other systematical uncertainties are individual for each energy.

$$\boldsymbol{M}_{i,j} = \sum_k x_i \cdot \epsilon_{i,j,k} \cdot x_j \cdot \epsilon_{j,i,k}, \quad i \neq j \tag{26}$$

where x_i is the measured value at energy point i; $\epsilon_{i,j,k} = \epsilon_{j,i,k}$ is the common relative systematic uncertainty of x_i and x_j from correlated source k and choose the minimum value of the uncertainty at energy i, j of the same source since correlated relative uncertainty cannot larger than any measurements total relative uncertainty. The uncorrelated uncertainty should be added when $i = j$.

With the covariance matrix, the parameter in the pQCD prediction can be optimized with MINUIT package. And it gives $n = 2.03 \pm 0.18$ and $A = 23.4 \pm 9.2$. When the correlation of uncertainty between energy points is ignored, the result is $n = 2.02 \pm 0.19$ and $A = 23.2 \pm 9.4$ which is almost the same with the correlated case. Here there is hypothsis $\Lambda c = 300$ MeV, the value of Λc can also be chosen to other values. When $\Lambda c = 100$ MeV, $n = 2.17 \pm 0.19$ and $A = 70.7 \pm 27.7$. When $\Lambda c = 500$ MeV, $n = 1.89 \pm 0.19$ and $A = 10.6 \pm 4.2$. The value of n are consistent in all cases.

B Tracking efficiency of $K^{\pm}$

B.1 Data set

The tracking efficiency of $K^{\pm}$ for data taken in 2015 is study with process $e^+e^- \to K^+K^-\pi^+\pi^+$. To cover the momentum range of the data set and reduce statistic uncertainty, the data at 3.08 GeV and 2.9 GeV are used. The MC sample used here is $e^+e^- \to K^+K^-\pi^+\pi^+(\gamma)$ generated with CONEXC at 3.08 GeV.

B.2 Event selection

The event selection criteria are as follows:

- Good charged tracks: Each charged track is required to originate from the iteraction point (IP), with $V_r = \sqrt{V_x^2 + V_y^2} < 1$cm, $|V_z| < 10$cm. Here V_x, V_y and V_z are the x, y and z coordinates of the point of the closest approach to the run-dependent IP respectively. The polar angle of each track is required to be within region: $|cos\theta| < 0.93$. In general, the number of good charged tracks should be 3 or 4.
- particle identification (PID): There should be at least 1 track identified as π^+ and 1 track identified as π^- which will ultilize PID algorithm to statisfy: $Prob_\pi > Prob_K$ and $Prob_\pi > Prob_p$, here $Prob_{\pi,K,p}$ is the probibility of one track to be identified as pion, kaon or proton. Meanwhile, there should be at least one track to be identified as K^+ or K^-, $Prob_K > Prob_\pi$ and $Prob_K > Prob_p$.
- neutral tracks: A good neutral track is required to deposite energy more than 25 MeV in EMC. And the relative angle and between the shower in EMC and a good charged track statisfying $\theta > 20°$ and $\phi > 20°$. As there is no neutral track in the process, the number of neutral tracks should be zero.

After selection, hadronic MC shows the purity of control sample is more than 95 %. The main components of hadronic MC is listed in Tab. 8

B.3 Efficiency

The tracking efficiency ϵ is defined as the following formula:

$$\epsilon = \frac{n}{N} \tag{27}$$

where n represents the number of events having four good charged tracks and at least three tracks are π^+, π^-, $K^{+/-}$. N represents the number of events with three or four good charged tracks and at least three tracks are π^+, π^-, $K^{+/-}$. Here if $K^{+/-}$ is K^+ then the efficiency if for K^- and the required sign of K should be the same, vice versa.

The difference between data and MC in tracking efficiency $\Delta\epsilon$ is defined as:

$$\Delta\epsilon = 1 - \epsilon^{MC}/\epsilon^{data} \tag{28}$$

Considering that n is a subset of N. The uncertainty on the tracking efficiency for data is :

$$\sigma_{\epsilon^{data}} = \frac{1}{N}\sqrt{(1 - 2\epsilon^{data})\sigma_n^2 + \epsilon^{data^2}\sigma_N^2} \tag{29}$$

Table 8: Hadonic MC components after event section for $K^+K^-\pi^+\pi^-$ control sample. The purity of signal $K^+K^-\pi^+\pi^-(\gamma)$ is more than 95 %.

No.	decay chain	final states	nEvt	nTot
0	$e^+e^- \to K^+K^-\pi^+\pi^-$	$\pi^-K^-\pi^+K^+$	4237	4237
1	$e^+e^- \to K^*K^-\pi^+, K^* \to K^+\pi^-$	$\pi^-K^-\pi^+K^+$	1946	6183
2	$e^+e^- \to K^+K^-\rho^0, \rho^0 \to \pi^+\pi^-$	$\pi^-K^-\pi^+K^+$	565	6748
3	$e^+e^- \to K_2^{*0}K^-\pi^+, K_2^{*0} \to K^+\pi^-$	$\pi^-K^-\pi^+K^+$	371	7119
4	$e^+e^- \to \gamma^*\gamma, \gamma^* \to K^+K^-\pi^+\pi^-$	$\pi^-K^-\pi^+\gamma K^+$	191	7310
5	$e^+e^- \to \phi\pi^-\pi^+, \phi \to K^+K^-$	$\pi^-K^-\pi^+K^+$	88	7398
6	$e^+e^- \to \gamma^*\gamma, \gamma^* \to K^*K^-\pi^+, K^* \to K^+\pi^-$	$\pi^-K^-\pi^+\gamma K^+$	84	7482
7	$e^+e^- \to \gamma^*\gamma, \gamma^* \to K_0^0\bar{K}_0^{*0}, K_0^0 \to K^+\pi^-, \bar{K}_0^{*0} \to K^-\pi^+$	$\pi^-K^-\pi^+\gamma K^+$	67	7549
8	$e^+e^- \to \gamma^*\gamma, \gamma^* \to \pi^-\pi^+K^-K^+$	$\pi^-K^-\pi^+\gamma K^+$	66	7615
9	$e^+e^- \to \gamma^*\gamma, \gamma^* \to K^+K^-$	$K^-\gamma K^+$	60	7675
10	$e^+e^- \to \gamma^*\gamma, \gamma^* \to f_0(1710)K^+K^-, f_0(1710) \to \pi^+\pi^-$	$\pi^-K^-\pi^+\gamma K^+$	53	7728
11	$e^+e^- \to K^+K^-\pi^+\pi^-\pi^0$	$\pi^-K^-\pi^0\pi^+K^+$	43	7771
12	$e^+e^- \to \gamma^*\gamma, \gamma^* \to K_SK^-\pi^+, K_S \to \pi^+\pi^-$	$\pi^-K^-\pi^+\pi^+\gamma$	27	7798
13	$e^+e^- \to \gamma^*\gamma, \gamma^* \to K^+K^-\rho^0, \rho^0 \to \pi^+\pi^-$	$\pi^-K^-\pi^+\gamma K^+$	23	7821
14	$e^+e^- \to \omega K^+K^-, \omega \to \pi^-\pi^+$	$\pi^-K^-\pi^+K^+$	22	7843
15	$e^+e^- \to \gamma^*\gamma, \gamma^* \to K_2^{*0}K^-\pi^+, K_2^{*0} \to K^+\pi^-$	$\pi^-K^-\pi^+\gamma K^+$	17	7860
16	$e^+e^- \to \phi\gamma, \phi \to K^+K^-$	$K^-\gamma K^+$	13	7873
17	$e^+e^- \to \pi^+\pi^-\pi^+\pi^-\pi^+\pi^-$	$\pi^-\pi^-\pi^-\pi^+\pi^+\pi^+$	11	7884
18	$e^+e^- \to K^*K^-\pi^+, K^* \to K^0\pi^0, K_S \to \pi^+\pi^-$	$\pi^-K^-\pi^0\pi^+\pi^+$	10	7894
19	$e^+e^- \to K^{*+}K^-\pi^0, K^{*+} \to K^0\pi^+, K_S \to \pi^+\pi^-$	$\pi^-K^-\pi^0\pi^+\pi^+$	9	7903
20	$e^+e^- \to \gamma^*\gamma, \gamma^* \to K^0\pi^+K^-, K_S \to \pi^+\pi^-$	$\pi^-K^-\pi^+\pi^+\gamma$	9	7912
21	$e^+e^- \to \gamma^*\gamma, \gamma^* \to K_2^{*0}\bar{K}_0^{*0}, K_2^{*0} \to K^+\pi^-, \bar{K}_0^{*0} \to K^-\pi^+$	$\pi^-K^-\pi^+\gamma K^+$	8	7920
22	$e^+e^- \to \gamma^*\gamma, \gamma^* \to K_0^0K_2^{*0}, K_0^0 \to K^+\pi^-, K_2^{*0} \to K^-\pi^+$	$\pi^-K^-\pi^+\gamma K^+$	8	7928
23	$e^+e^- \to K_SK^-\pi^+, K_S \to \pi^+\pi^-$	$\pi^-K^-\pi^+\pi^+$	6	7934
24	$e^+e^- \to \gamma^*\gamma, \gamma^* \to K_S\bar{K}^*, K_S \to \pi^+\pi^-, \bar{K}^* \to K^-\pi^+$	$\pi^-K^-\pi^+\pi^+\gamma$	6	7940

where the σ_n and σ_N are the statistical uncertainties of n and N.

The uncertainty on the tracking efficiency of MC is

$$\sigma_{\epsilon^{MC}} = \sqrt{\frac{\epsilon^{MC}(1-\epsilon^{MC})}{N}} \tag{30}$$

The uncertainty of $\Delta\epsilon$ is estimated with error propagation formula.

B.4 Data and MC Analysis

After performing the selection requirements, the number of events is extracted from recoil invariant mass $RM(\pi^+\pi^-K^-)$ spectrum for the efficiency of K^+. For K^-, it is similar. From the spectrum, there is clear K peak. and the numbers of signals from data are fitted with MC shape convoluted with a Gaussian both for n and N, while n and N of MC are counted from RM spectra of MC sample. Fig. 22 shows the $RM(\pi^+\pi^-K^-)$ spectra of MC and data with expected K^+ track tranverse momentum p_t in specific range. Similarly, Fig. 23 shows the result of K^-.

The difference between data and MC in different transverse momentum ranges is shown in Fig. 24. For K^+, the average difference between data and MC is $1.0 \pm 0.2\%$, and for K^- is $0.7 \pm 0.3\%$. The difference in difference polar angle ranges is shown in Fig. 25. The average difference for K^+ is $0.9 \pm 0.3\%$ and for K^- is $0.1 \pm 0.2\%$.

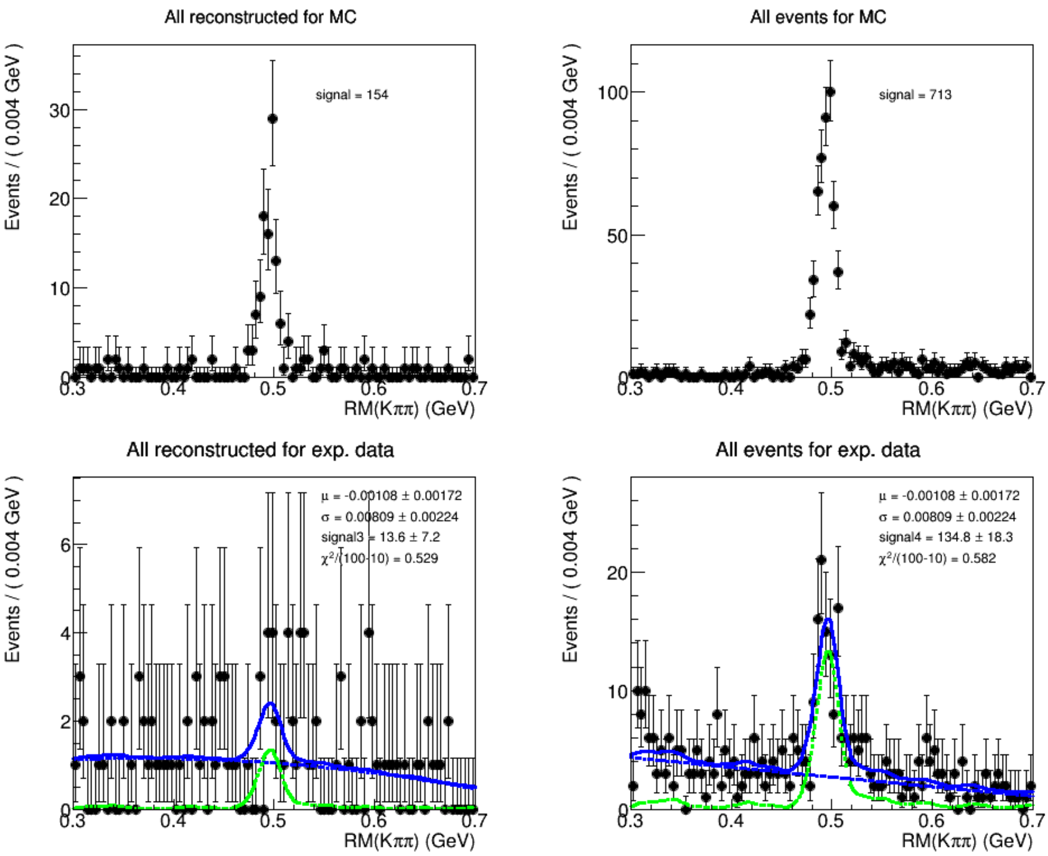

(a) 0.0-0.1 GeV

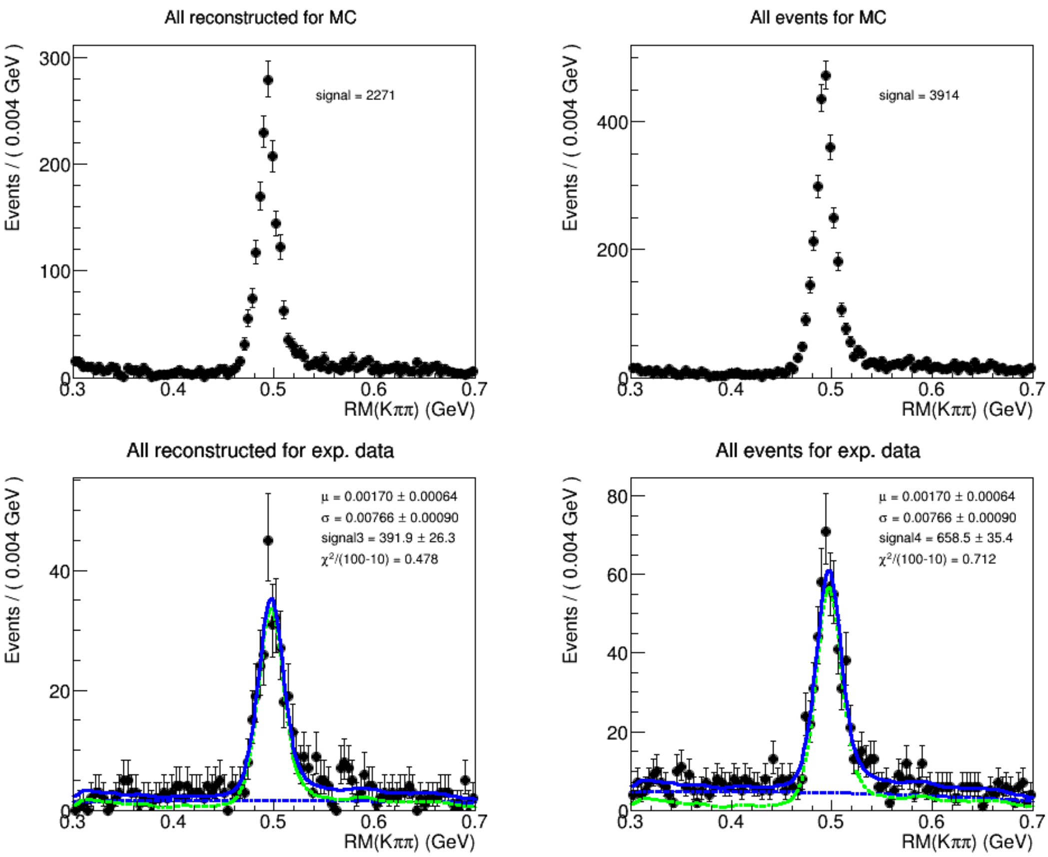

(b) 0.1-0.2 GeV

Figure 22: Recoiling mass spectrum of $\pi^+\pi^-K^-$.

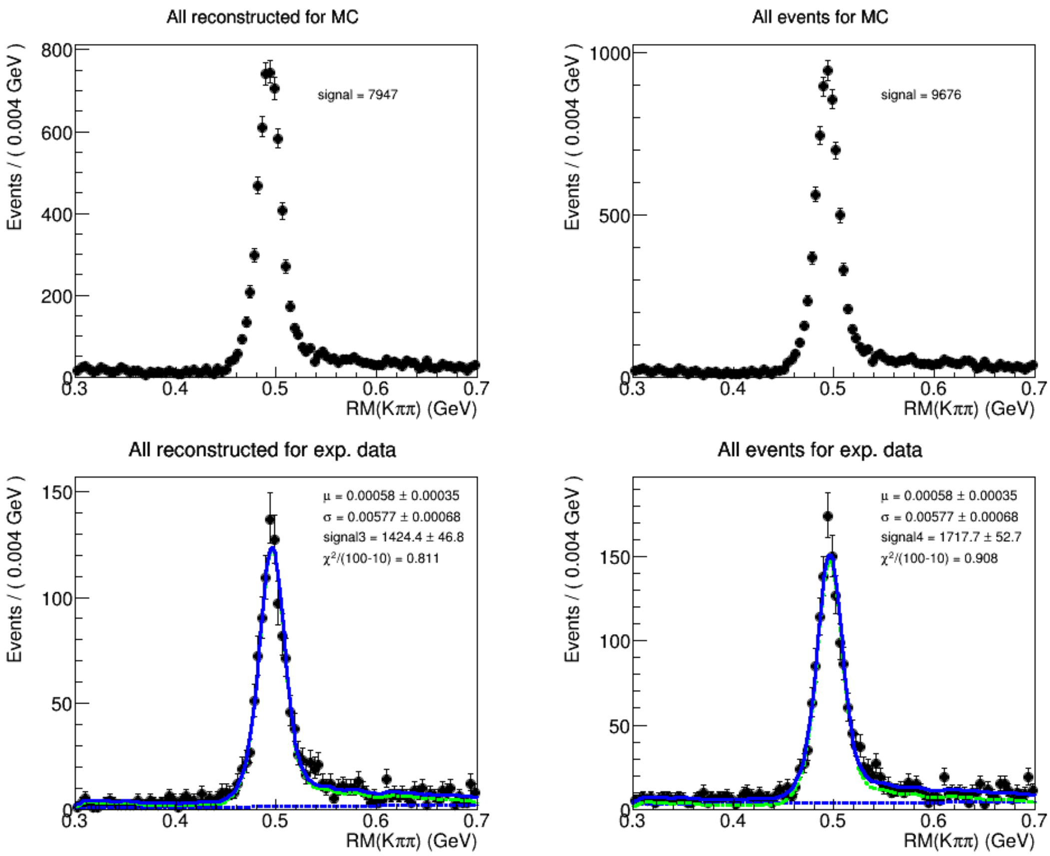

(a) 0.2-0.3 GeV

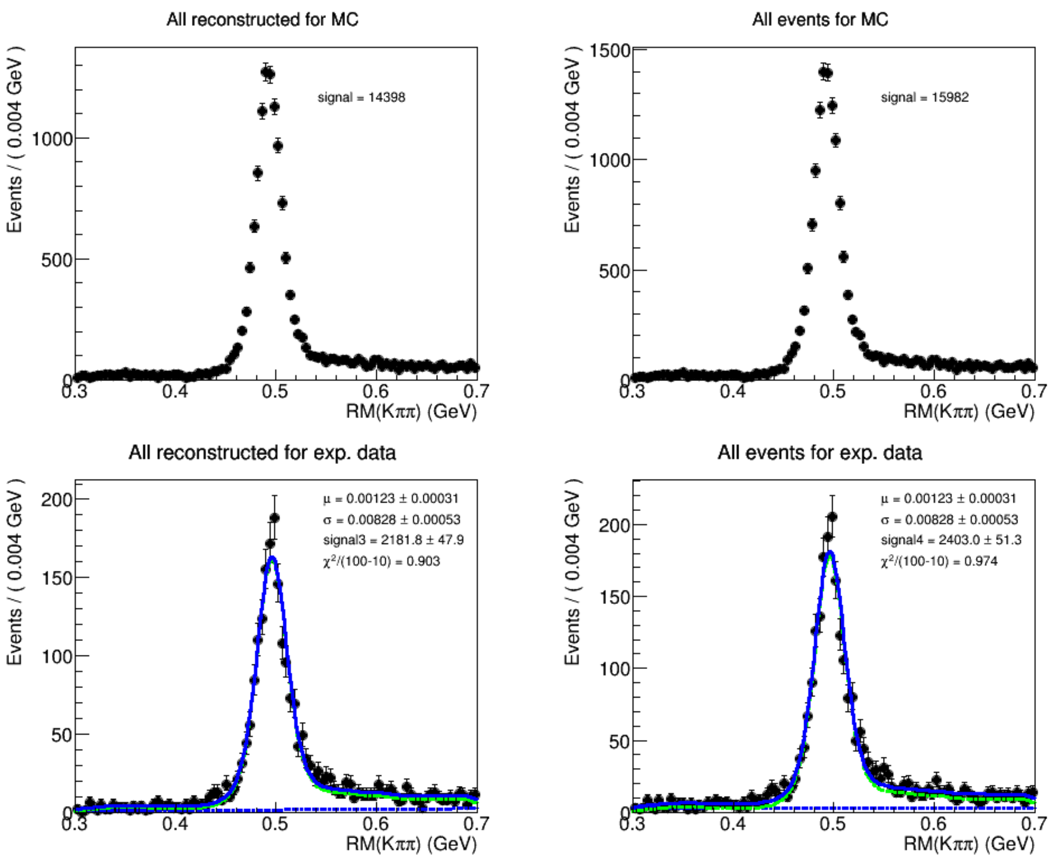

(b) 0.3-0.4 GeV

Continuation of Figure 22

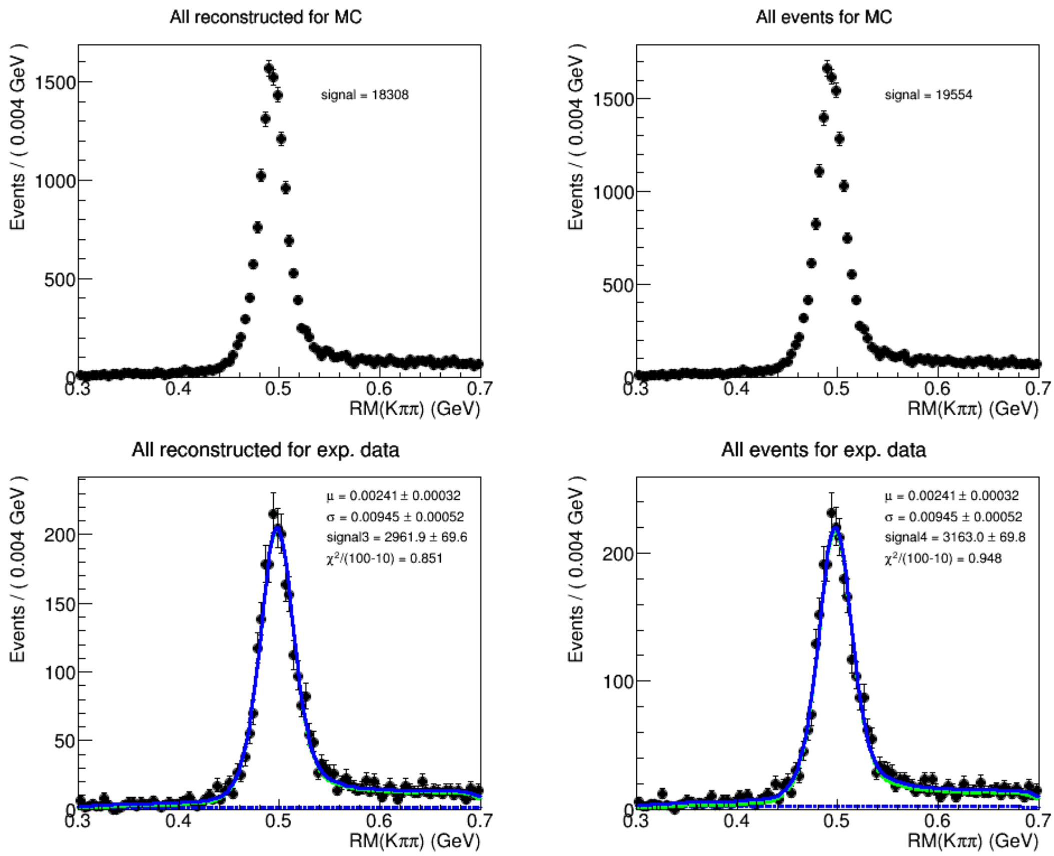

(a) 0.4-0.5 GeV

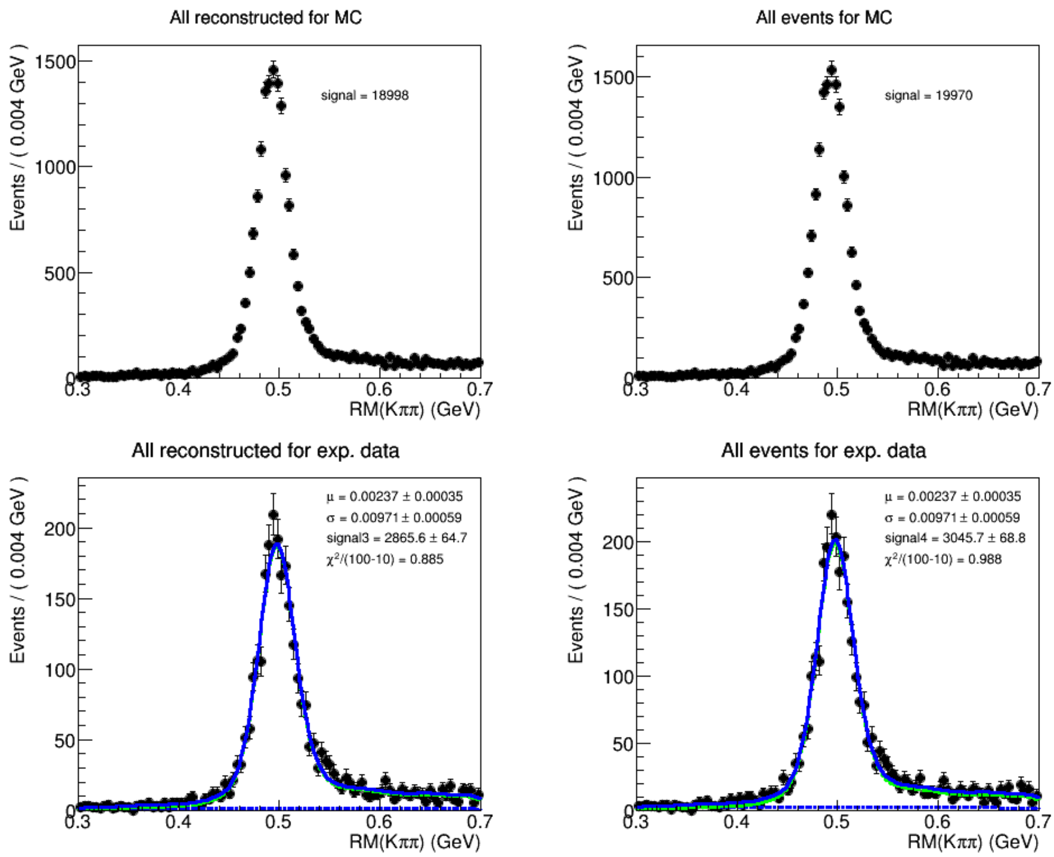

(b) 0.5-0.6 GeV

Continuation of Figure 22

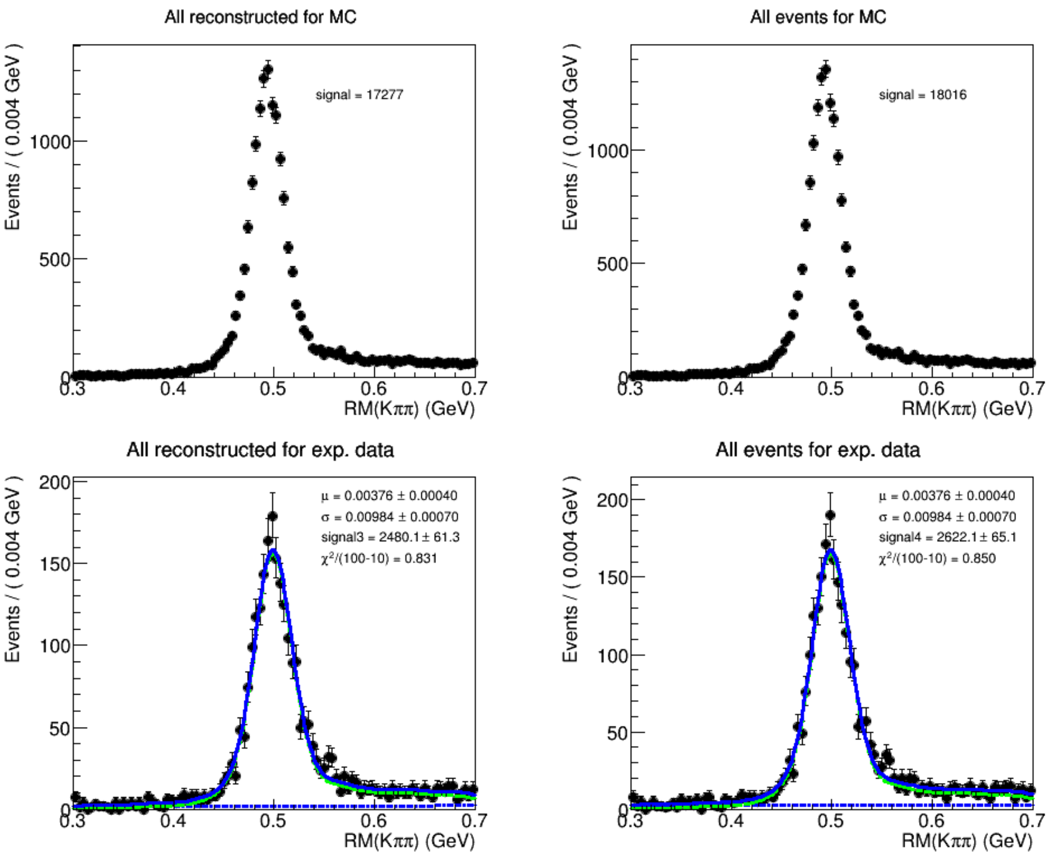

(a) 0.6-0.7 GeV

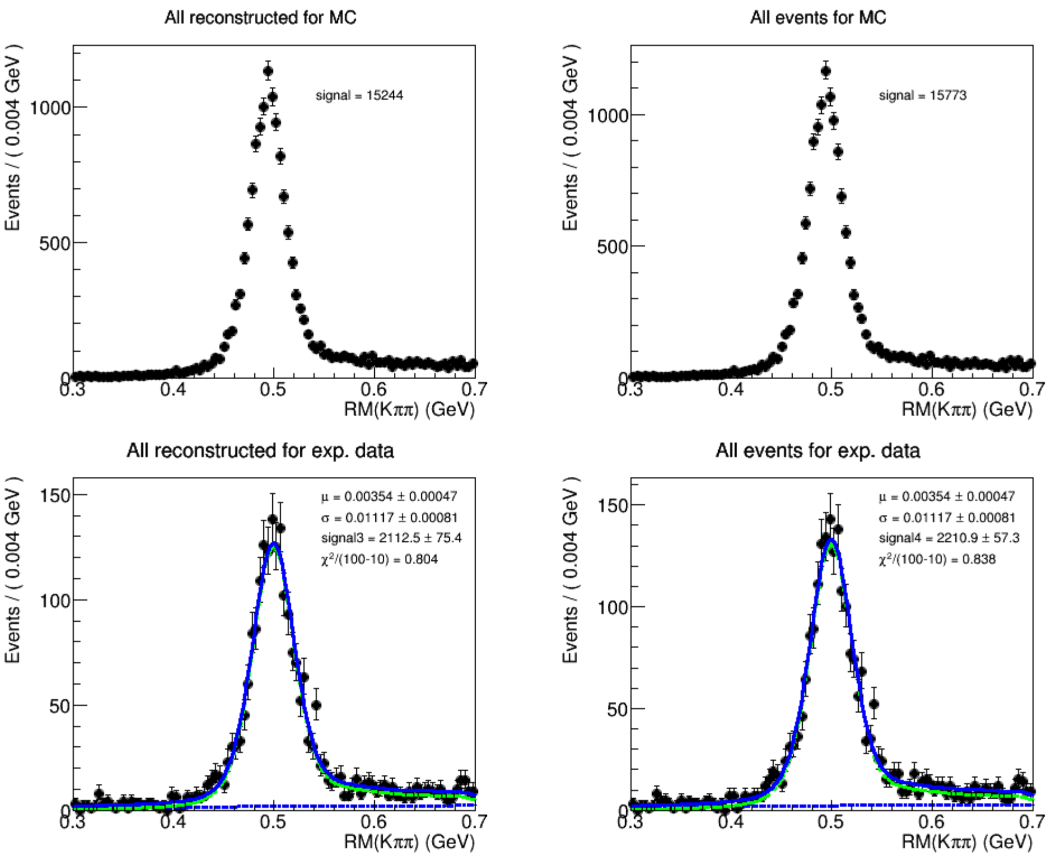

(b) 0.7-0.8 GeV

Continuation of Figure 22

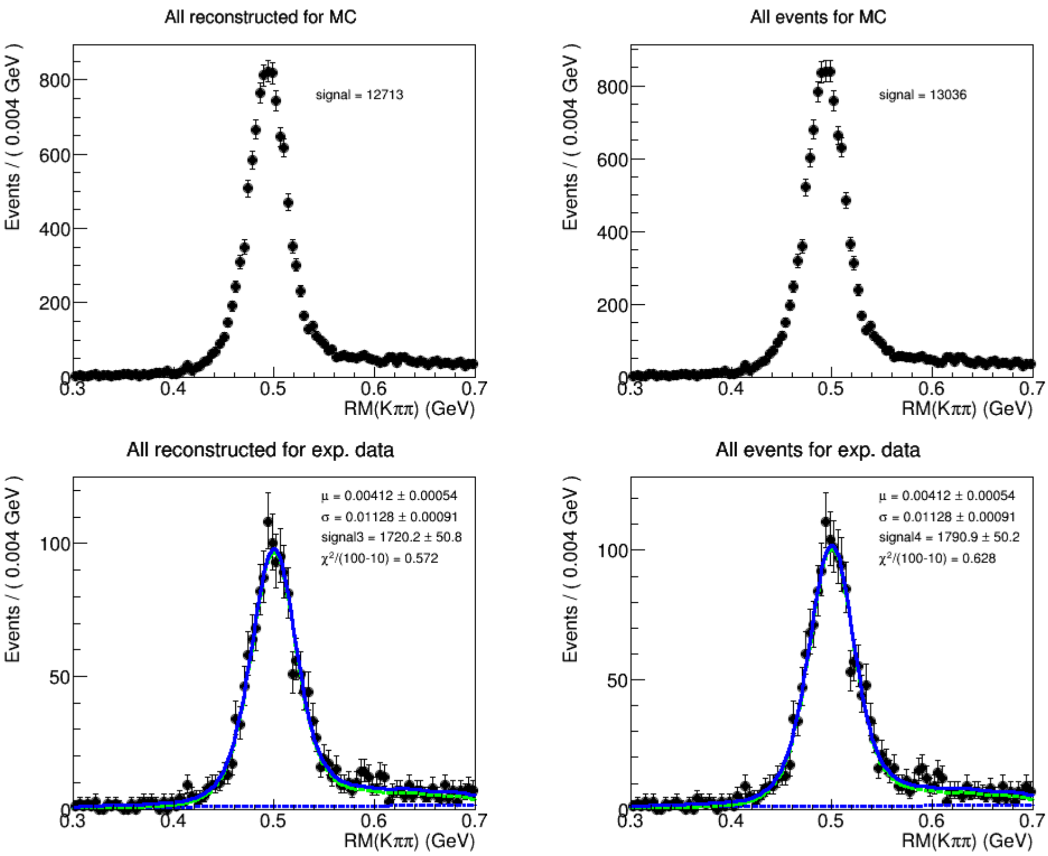

(a) 0.8-0.9 GeV

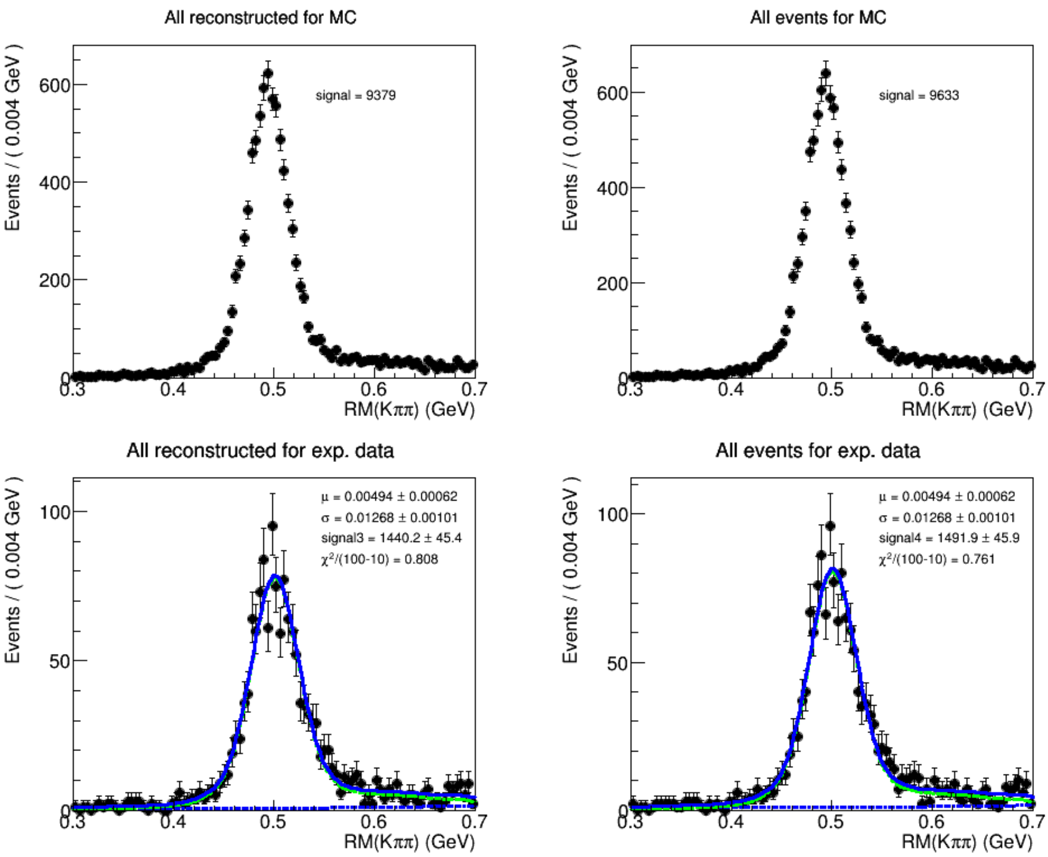

(b) 0.9-1.0 GeV

Continuation of Figure 22

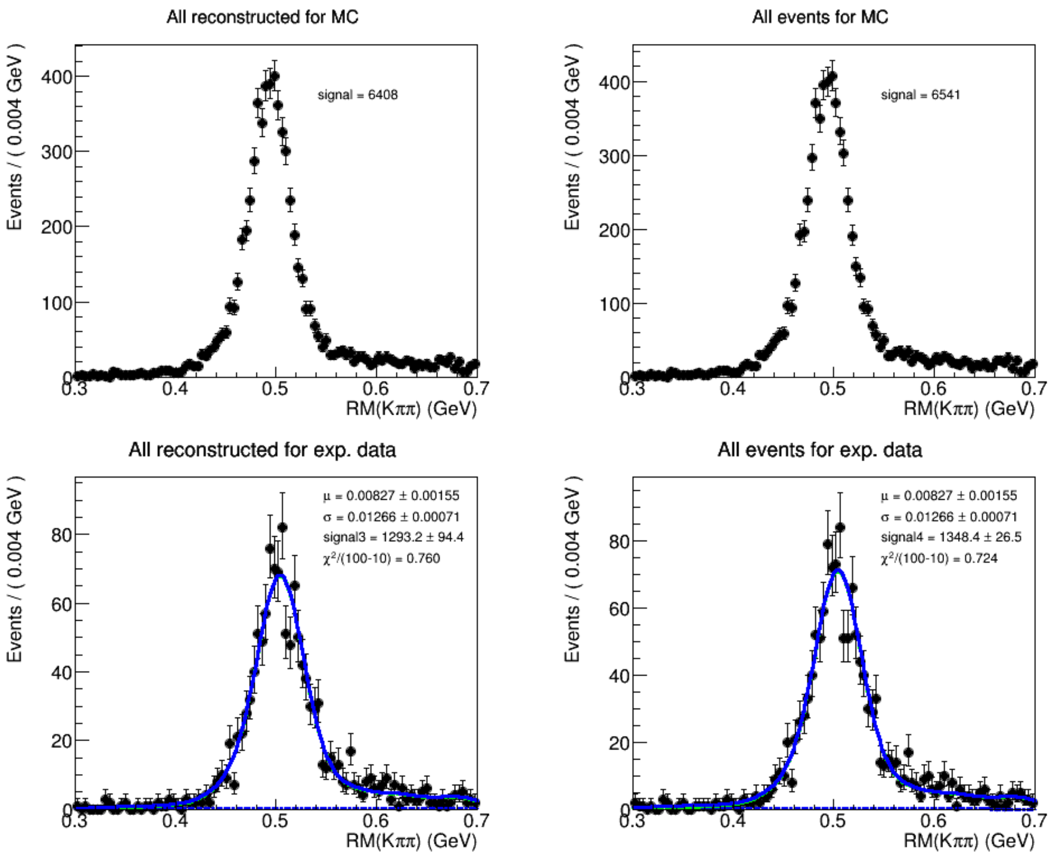

(a) 1.0-1.1 GeV

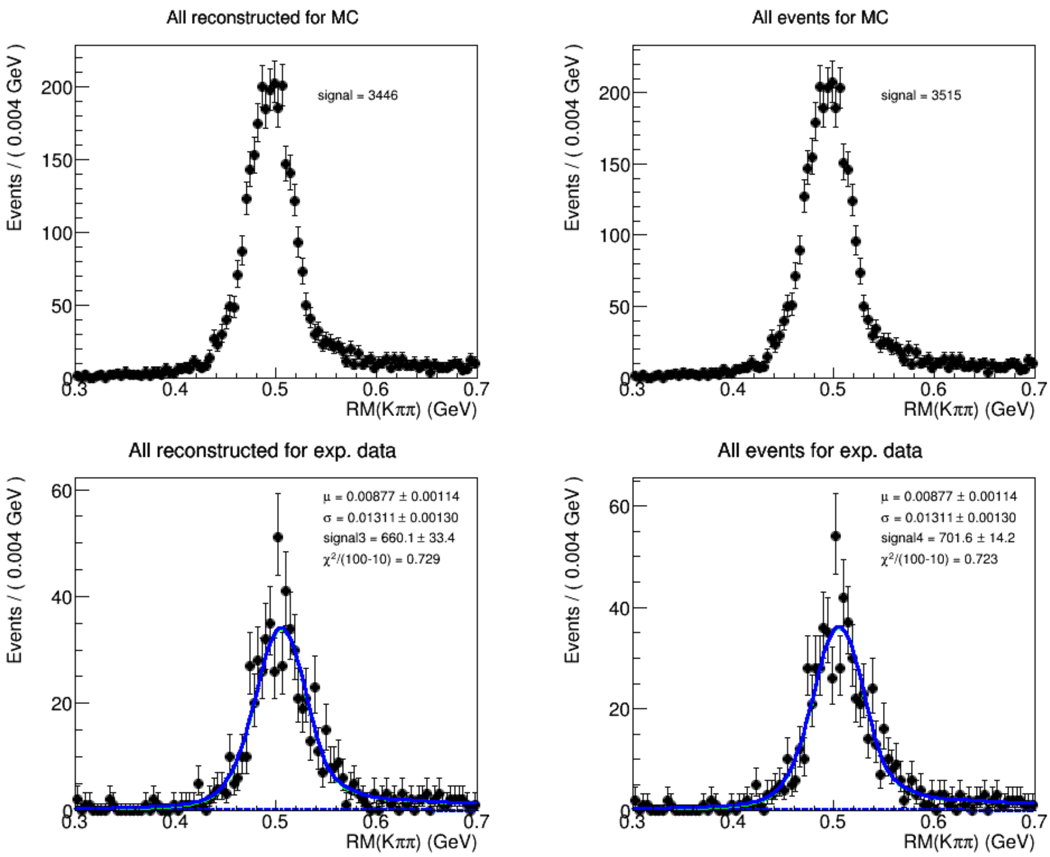

(b) 1.1-1.2 GeV

Continuation of Figure 22

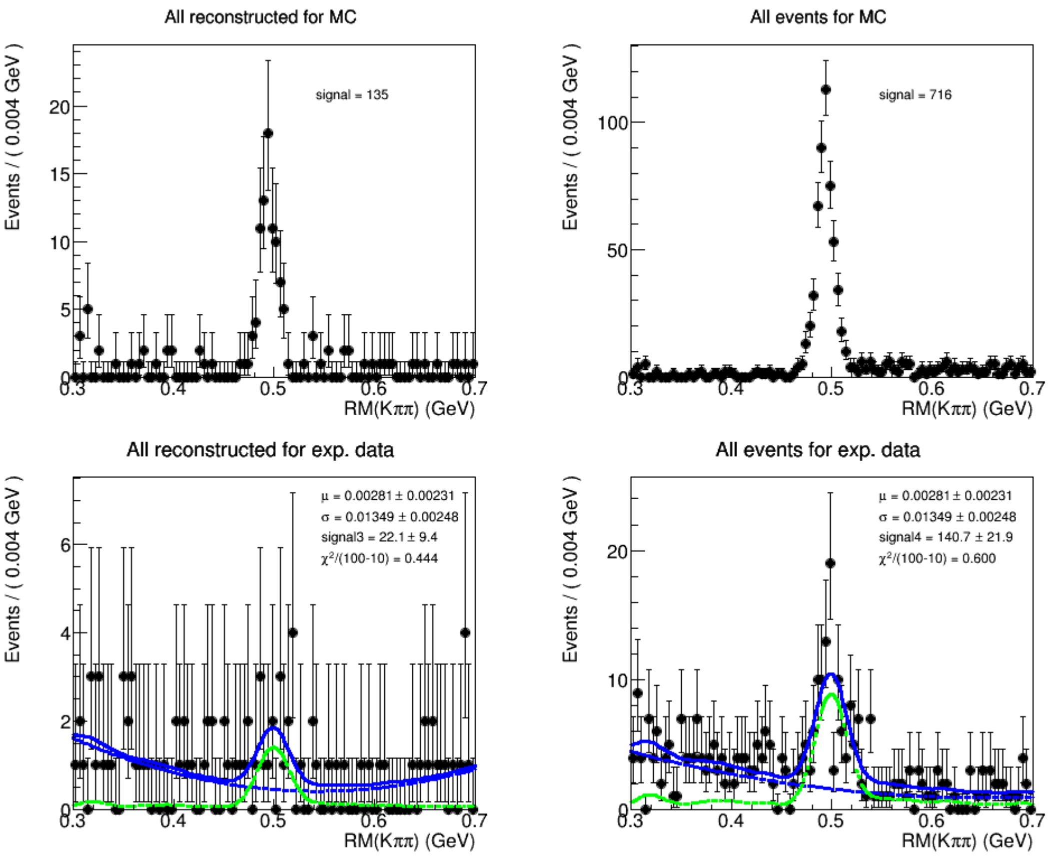

(a) 0.0-0.1 GeV

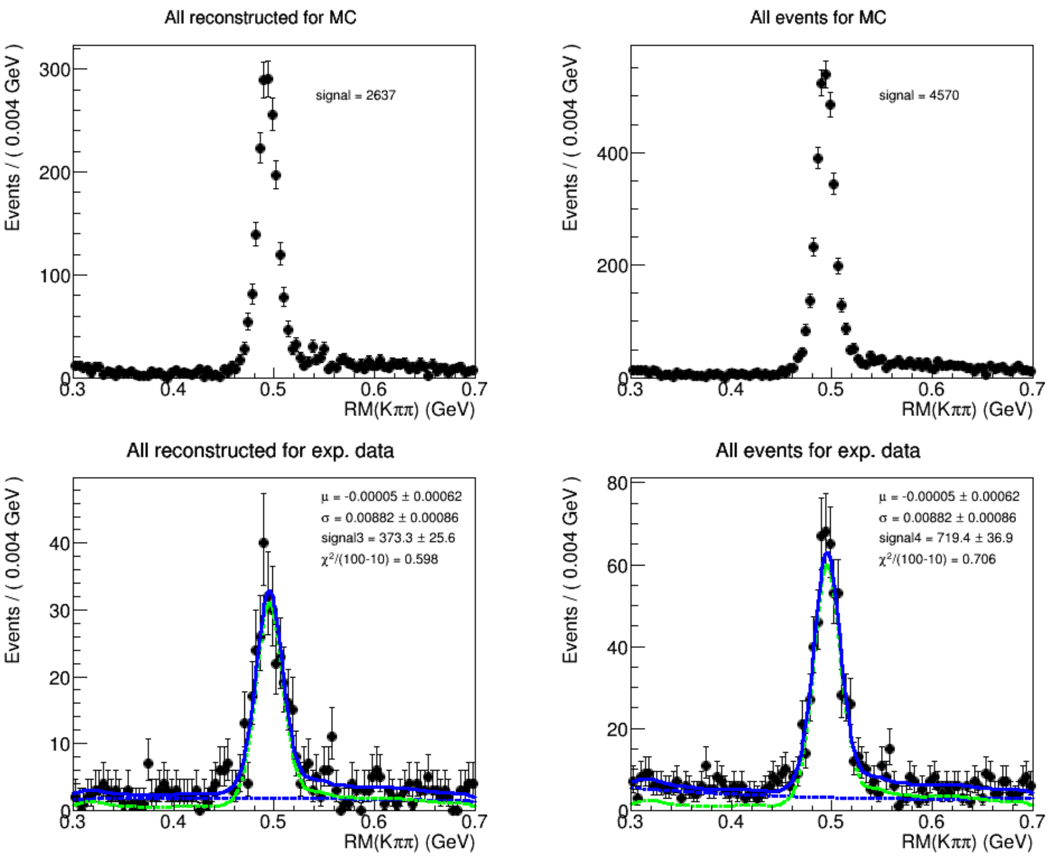

(b) 0.1-0.2 GeV

Figure 23: Recoiling mass spectrum of $\pi^+\pi^-K^+$.

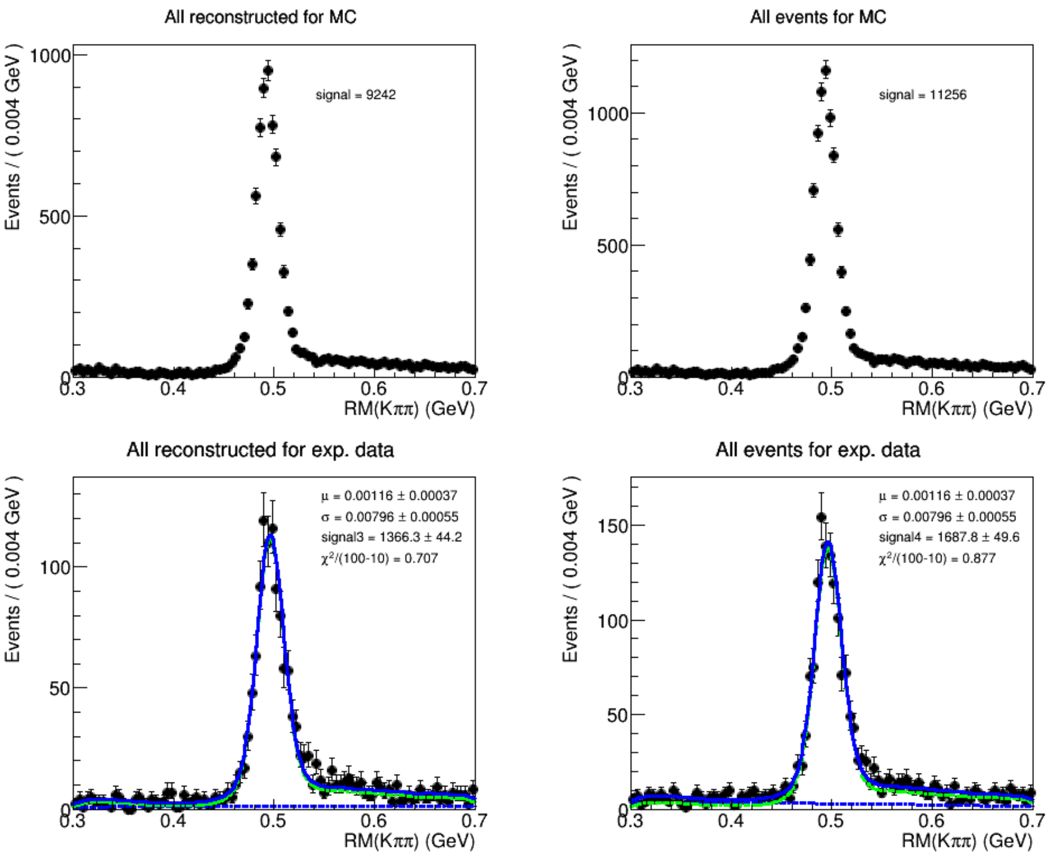

(a) 0.2-0.3 GeV

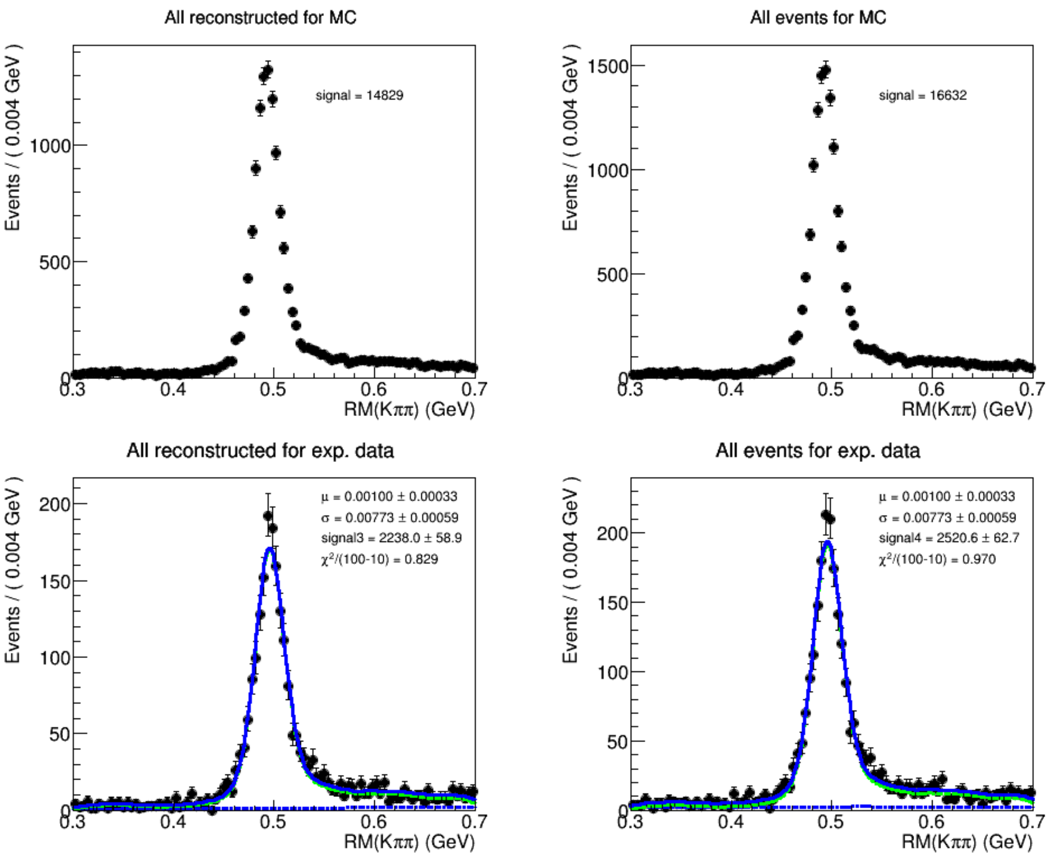

(b) 0.3-0.4 GeV

Continuation of Figure 23

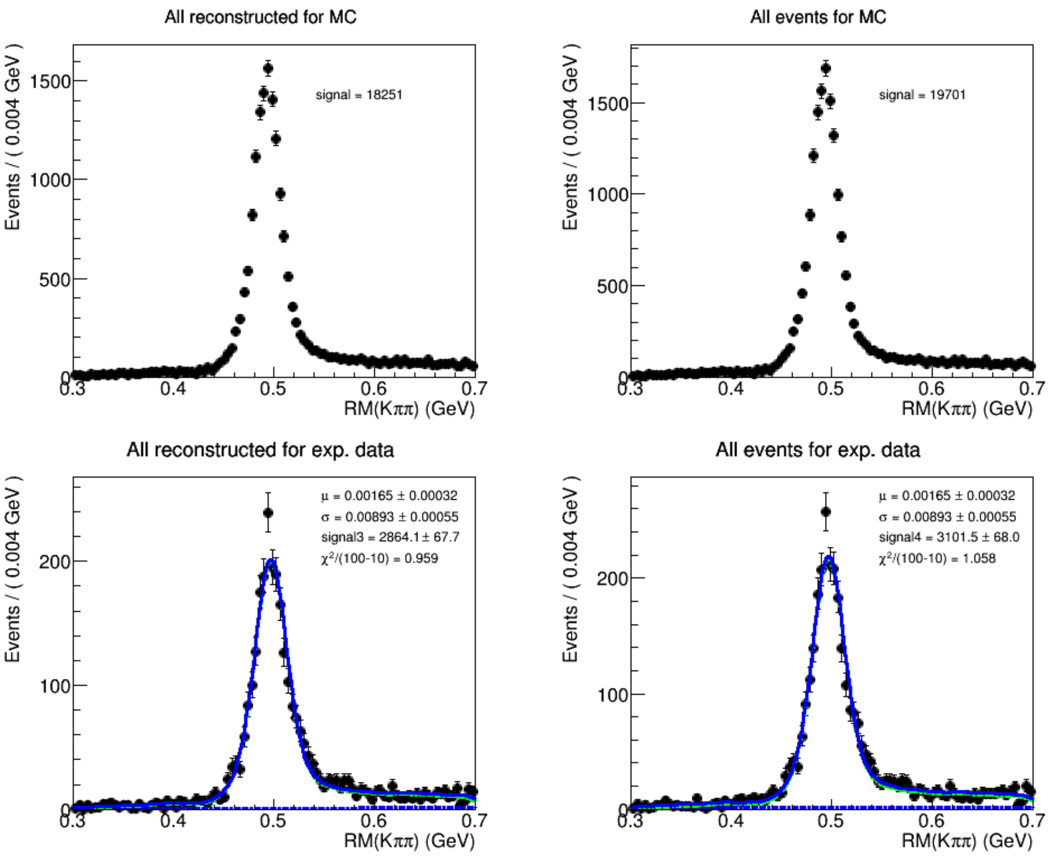

(a) 0.4-0.5 GeV

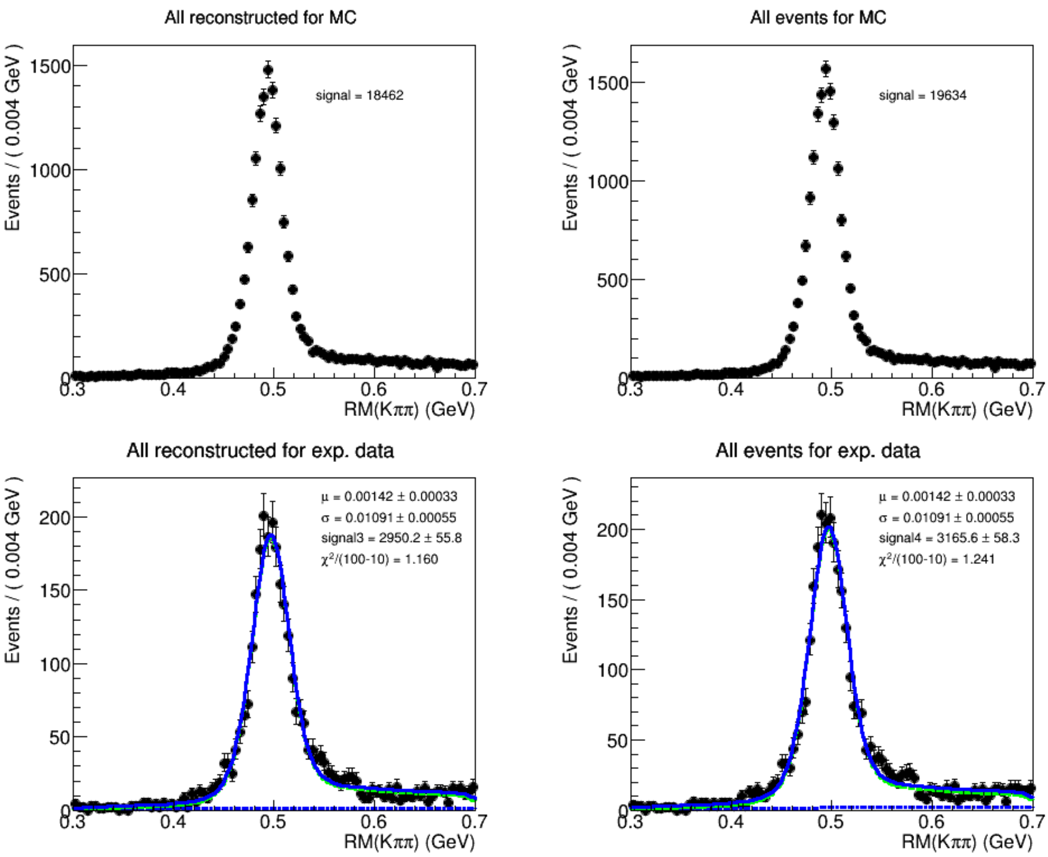

(b) 0.5-0.6 GeV

Continuation of Figure 23

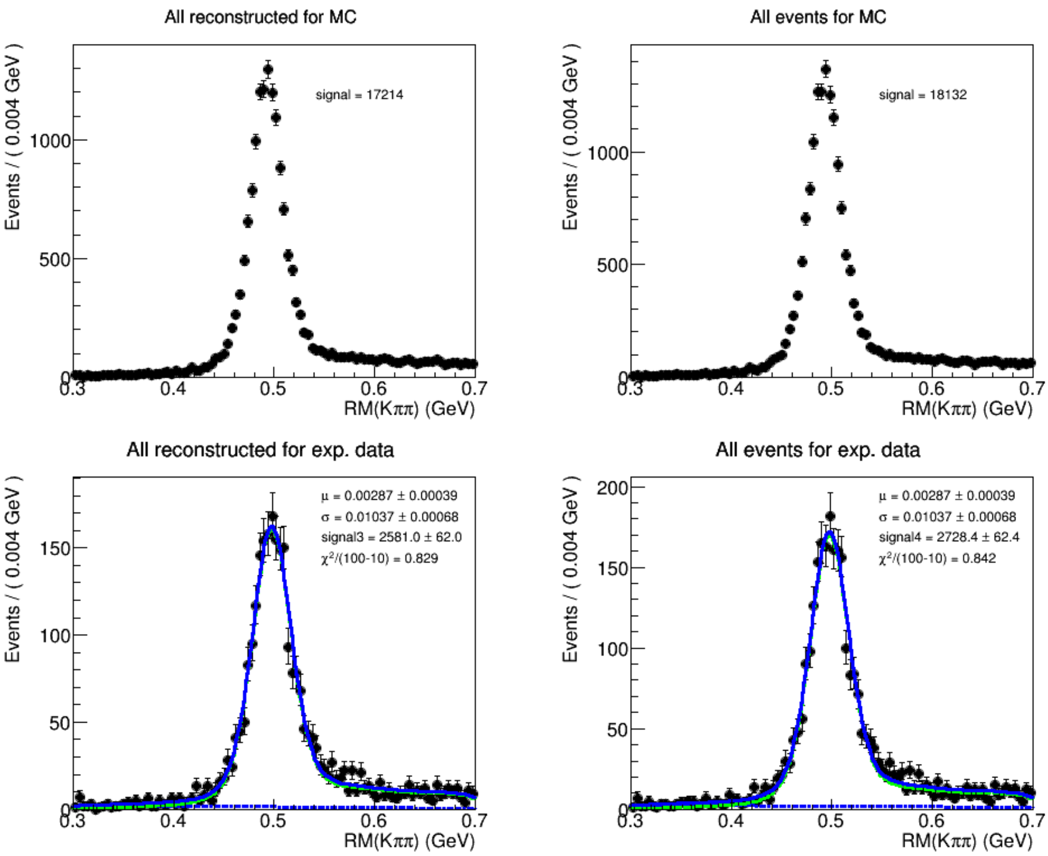

(a) 0.6-0.7 GeV

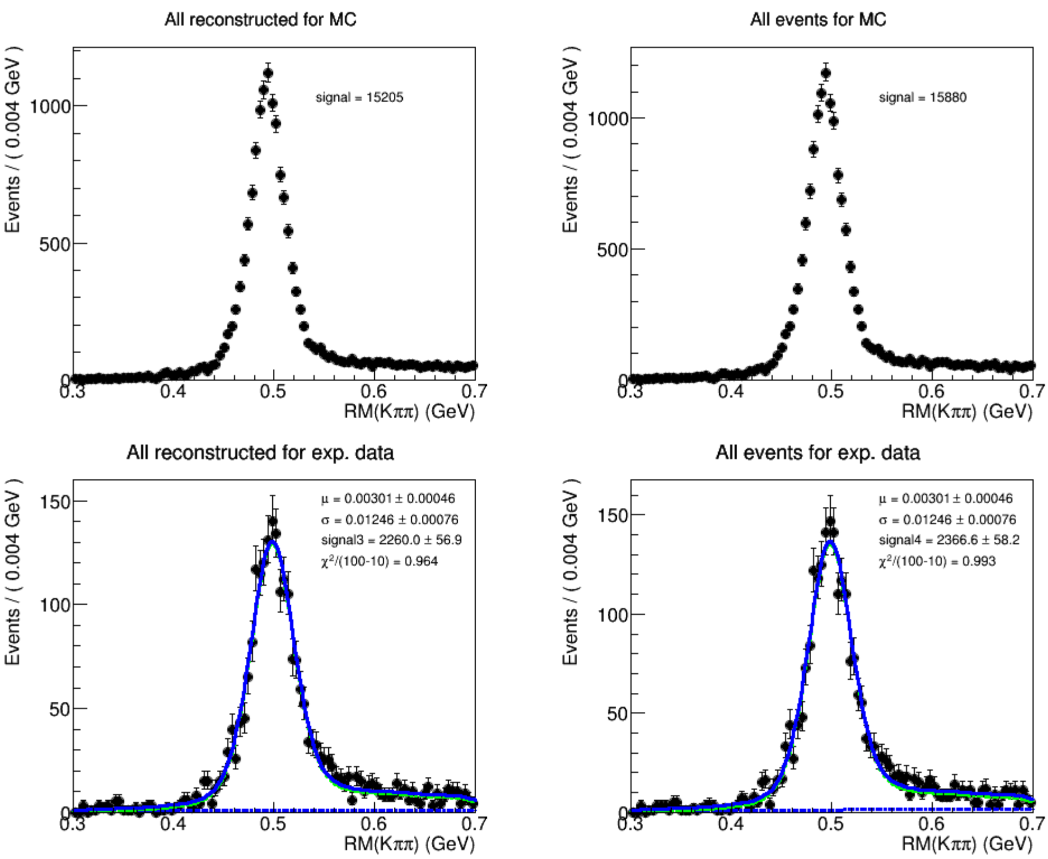

(b) 0.7-0.8 GeV

Continuation of Figure 23

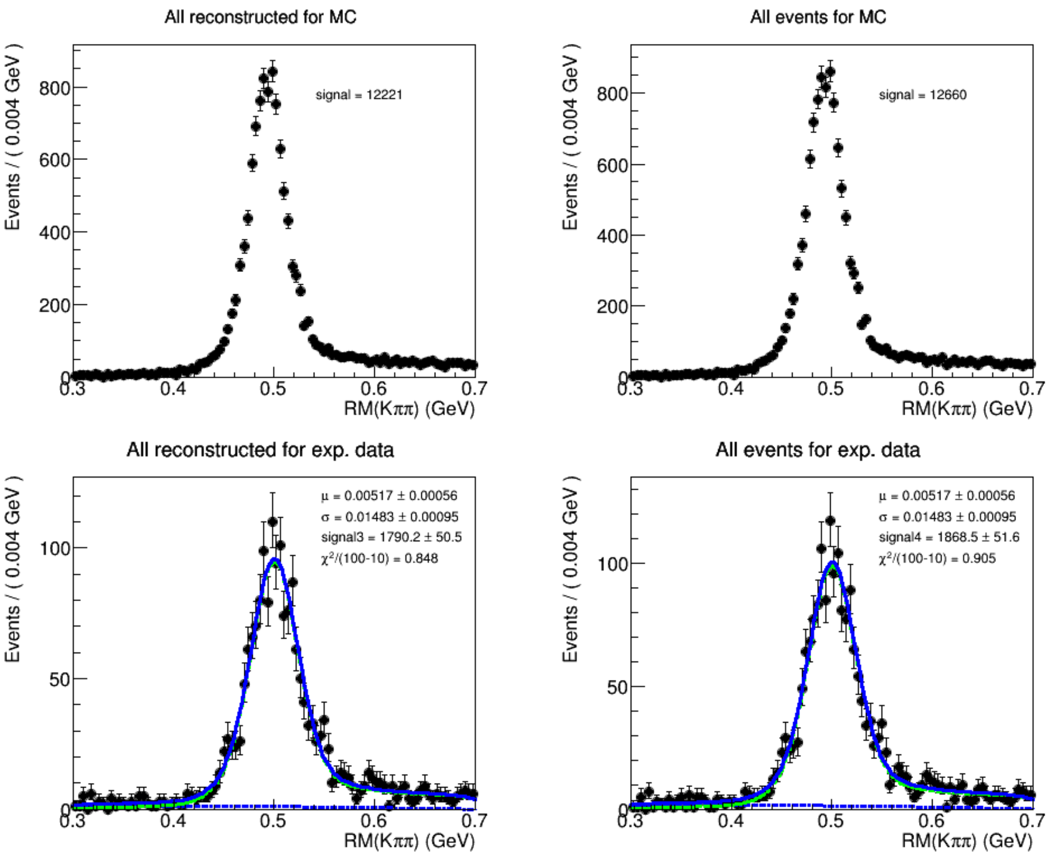

(a) 0.8-0.9 GeV

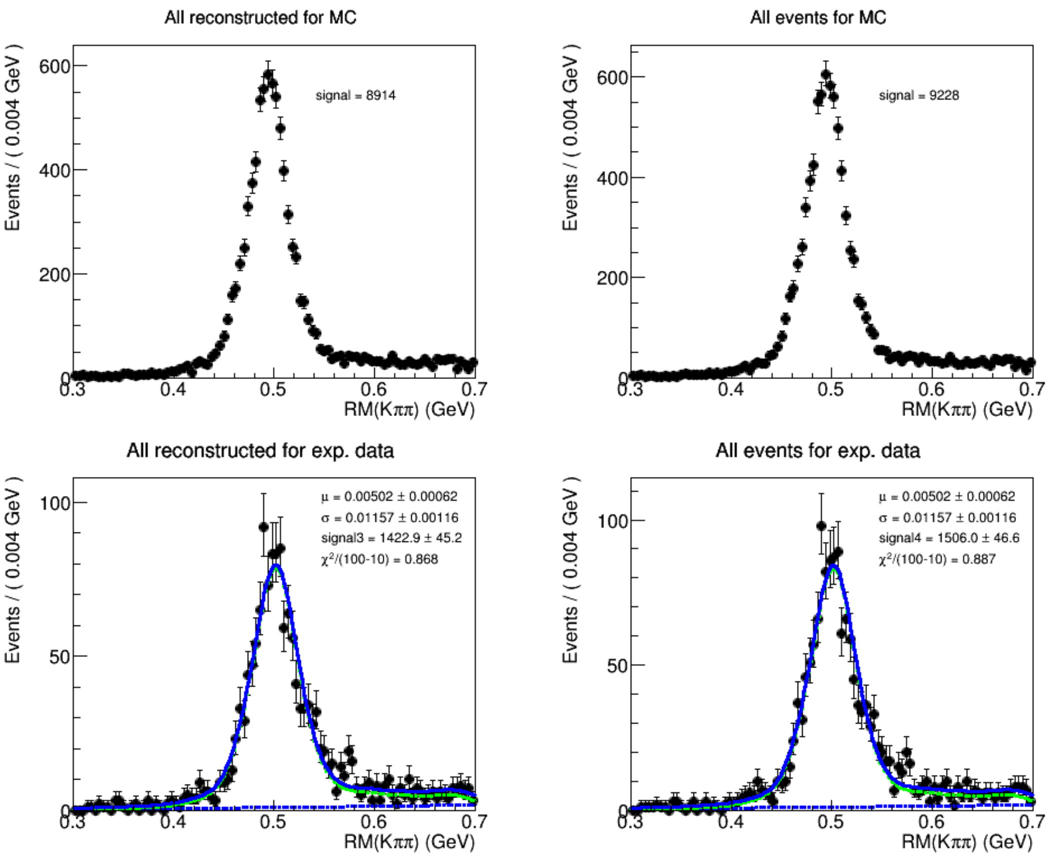

(b) 0.9-1.0 GeV

Continuation of Figure 23

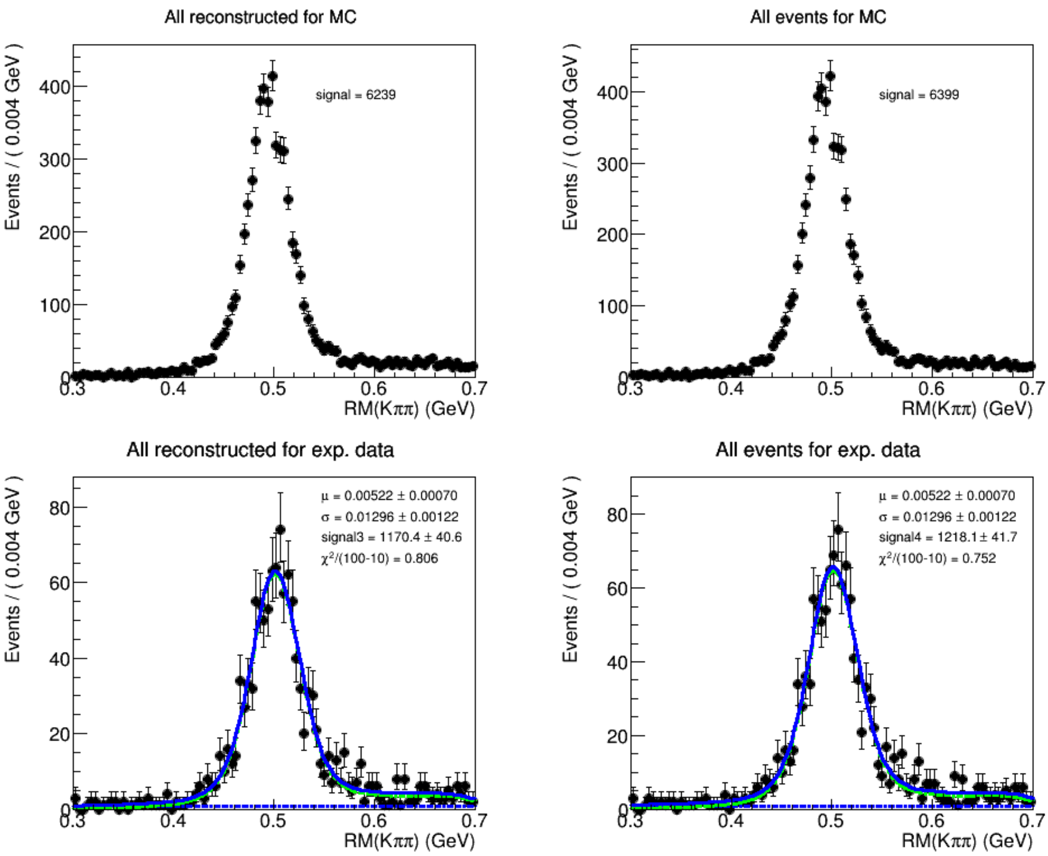

(a) 1.0-1.1 GeV

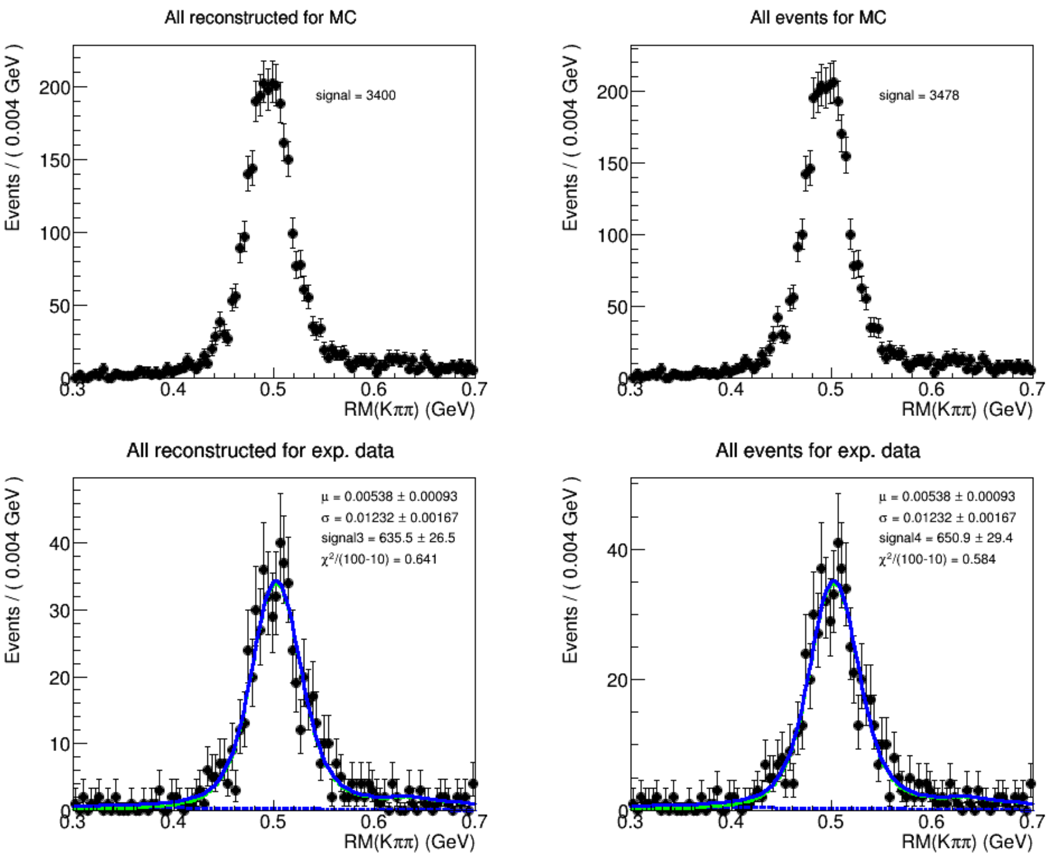

(b) 1.1-1.2 GeV

Continuation of Figure 23

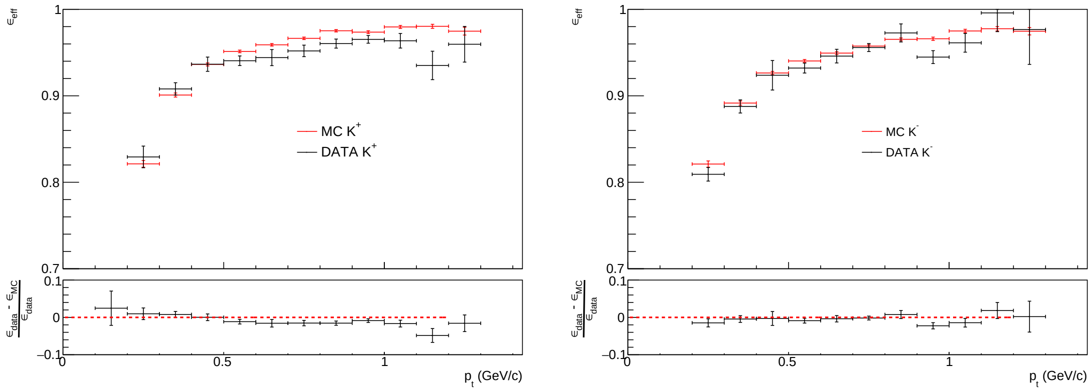

(a) (b)

Figure 24: Comparason of tracking efficiency of data and MC Vs p_T. Left plot is for K^+, right plot for K^-.

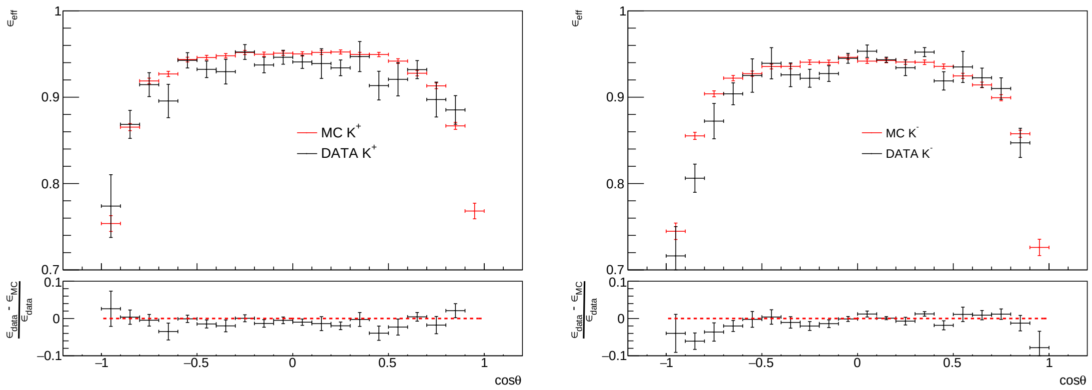

(a) (b)

Figure 25: Comparason of tracking efficiency of data and MC Vs polar angle. Left plot is for K^+, right plot for K^-.

C Check with method using PID

In our work, we avoid to use particle identification(PID) to avoid further uncertainty from PID. Acturally, PID can also be used in the event selection to suppress background, especially for background from μ which can not well suppressed with the method currently used. A further study is done to check the method with PID and the method without PID which currently used.

The method with PID is similar with current method but adding a requirement that the 2 reconstructed charged tracks should be identified as Kaon: $Prob(K) > Prob(\pi)$ and $Prob(K) > Prob(p)$. With this requirement, the cross section can be measured with the same procedure as used in the work. The result is listed in Tab. 9 and compared with method without PID. They are consistent within statistical uncertainty.

Table 9: summary of cross section of K^+K^-.

E_{cm} (GeV)	ϵ	$(1+\delta)$	ϵ_{PID}	σ (nb)	σ_{PID} (nb)
2	0.1888	2.7130	0.1843	0.3546 ± 0.0073 ± 0.0106	0.3483 ± 0.0083
2.05	0.1810	2.8670	0.1774	0.3020 ± 0.0132 ± 0.0107	0.2927 ± 0.0132
2.1	0.1565	3.3810	0.1519	0.2203 ± 0.0059 ± 0.0080	0.2139 ± 0.0051
2.15	0.1305	4.0118	0.1259	0.1769 ± 0.0110 ± 0.0044	0.1696 ± 0.0110
2.175	0.1476	3.5351	0.1415	0.1857 ± 0.0061 ± 0.0051	0.1833 ± 0.0059
2.2	0.1773	2.9787	0.1704	0.2346 ± 0.0057 ± 0.0081	0.2304 ± 0.0058
2.2324	0.1975	2.6937	0.1865	0.2558 ± 0.0064 ± 0.0072	0.2540 ± 0.0065
2.3094	0.1671	3.2601	0.1555	0.1811 ± 0.0041 ± 0.0067	0.1821 ± 0.0048
2.3864	0.1177	4.5809	0.1090	0.1044 ± 0.0030 ± 0.0040	0.1014 ± 0.0030
2.396	0.1137	4.7256	0.1060	0.1069 ± 0.0020 ± 0.0041	0.1026 ± 0.0018
2.5	0.0985	5.6227	0.0870	0.0878 ± 0.0123 ± 0.0048	0.0912 ± 0.0130
2.6444	0.0892	6.2873	0.0751	0.0585 ± 0.0021 ± 0.0026	0.0568 ± 0.0019
2.6464	0.0884	6.2972	0.0738	0.0605 ± 0.0023 ± 0.0027	0.0581 ± 0.0020
2.7	0.0855	6.5641	0.0705	0.0381 ± 0.0088 ± 0.0044	0.0371 ± 0.0088
2.8	0.0797	7.1355	0.0628	0.0488 ± 0.0113 ± 0.0076	0.0377 ± 0.0091
2.9	0.0738	7.8308	0.0554	0.0328 ± 0.0010 ± 0.0017	0.0328 ± 0.0008
2.95	0.0697	8.1982	0.0513	0.0291 ± 0.0024 ± 0.0011	0.0272 ± 0.0020
2.981	0.0676	8.4299	0.0500	0.0314 ± 0.0023 ± 0.0020	0.0302 ± 0.0031
3	0.0667	8.5760	0.0496	0.0246 ± 0.0021 ± 0.0008	0.0263 ± 0.0020
3.02	0.0658	8.7326	0.0474	0.0266 ± 0.0023 ± 0.0015	0.0244 ± 0.0018
3.08	0.0570	9.2017	0.0406	0.0214 ± 0.0011 ± 0.0007	0.0214 ± 0.0007

ϵ is the selection efficiency in the method without PID.
ϵ_{PID} is the selection efficiency in method with PID.
$(1+\delta)$ is the correction factor, a combination of ISR and VP correction.
σ is the cross section. 1st uncertainty is statistical uncertainty and 2nd one is systematic uncertainty.
σ_{PID} is the cross section in method with PID.

D Cross check using polar angle fit

Fig. 26 shows the polar angle of 2 charged tracks for data, K^+K^- MC and di-mu MC. Events are selected with criteria in Sec. 4 of the memo with additional requirement that momentum of tracks should be within 3 sigma of that of kaon. The spectra of K^+K^- MC are scaled to data according to the numbers of events and di-mu MC scaled to data according luminosities. From the figure, it is not easy to separate kaons from muons on the basis of the polar angle distribution.

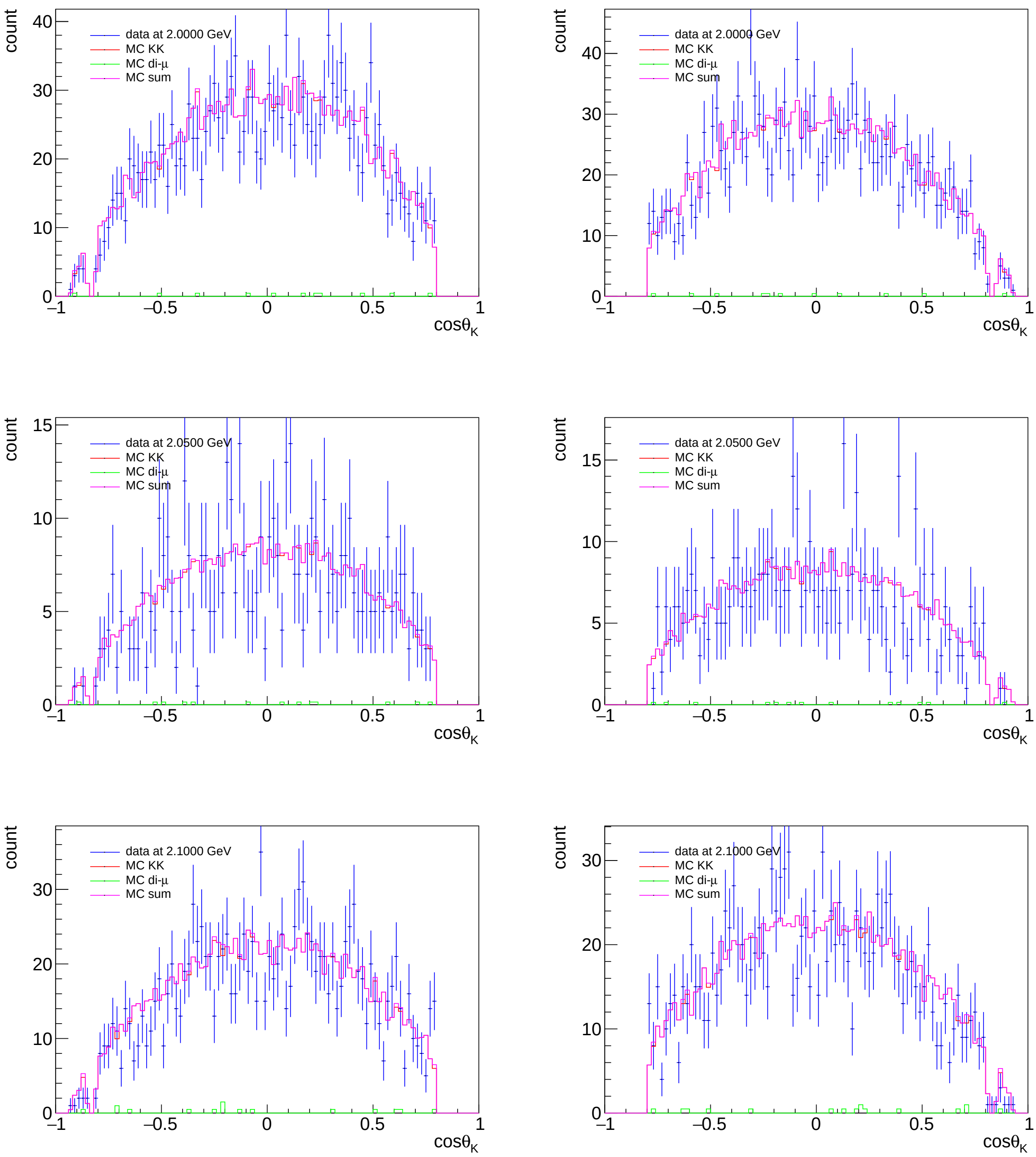

Figure 26: Polar angle of 2 charged tracks at 21 R scan energy points. Left ones are for positive tracks and right for negative tracks.

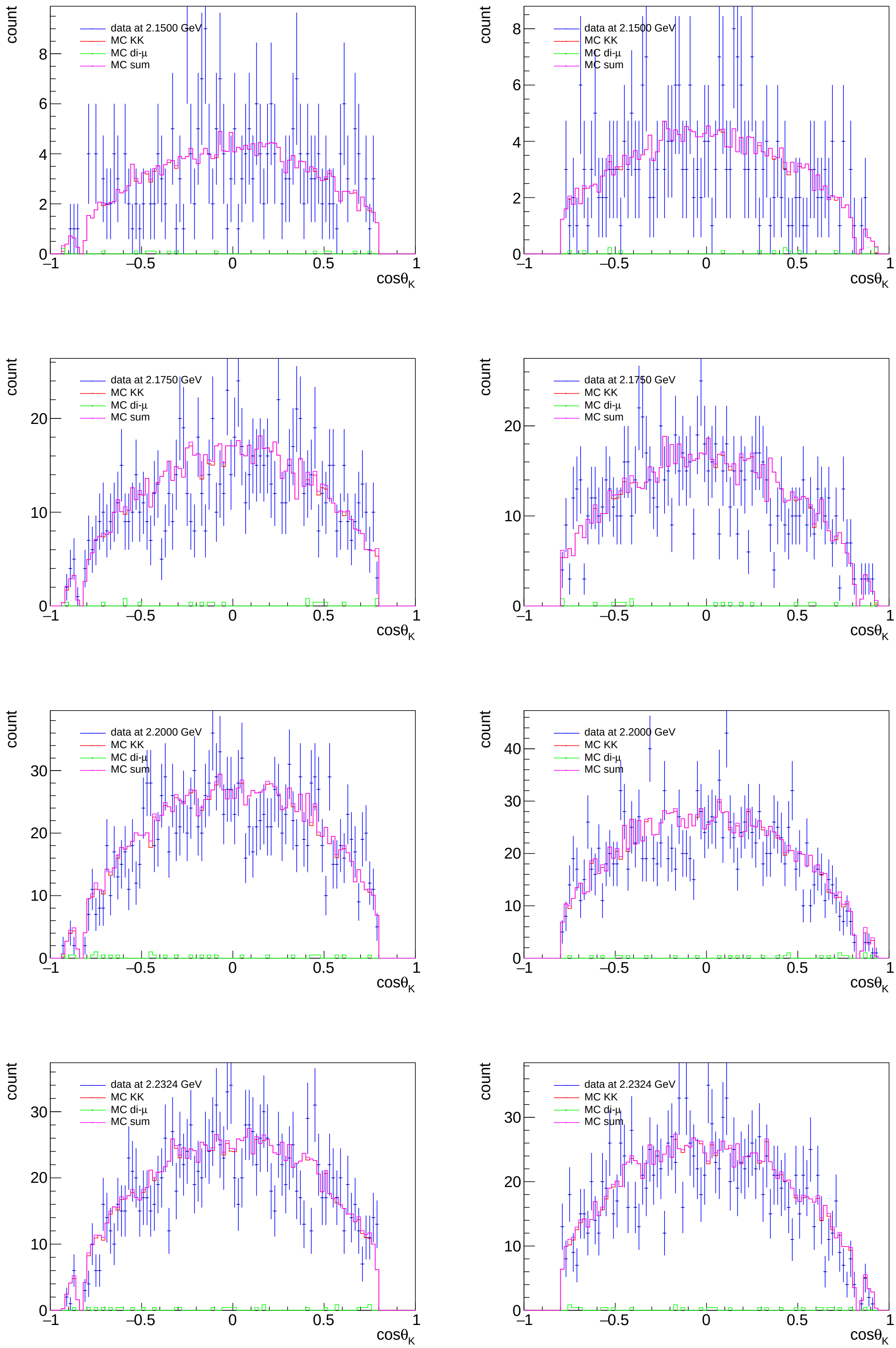

Continuation of Figure 26.

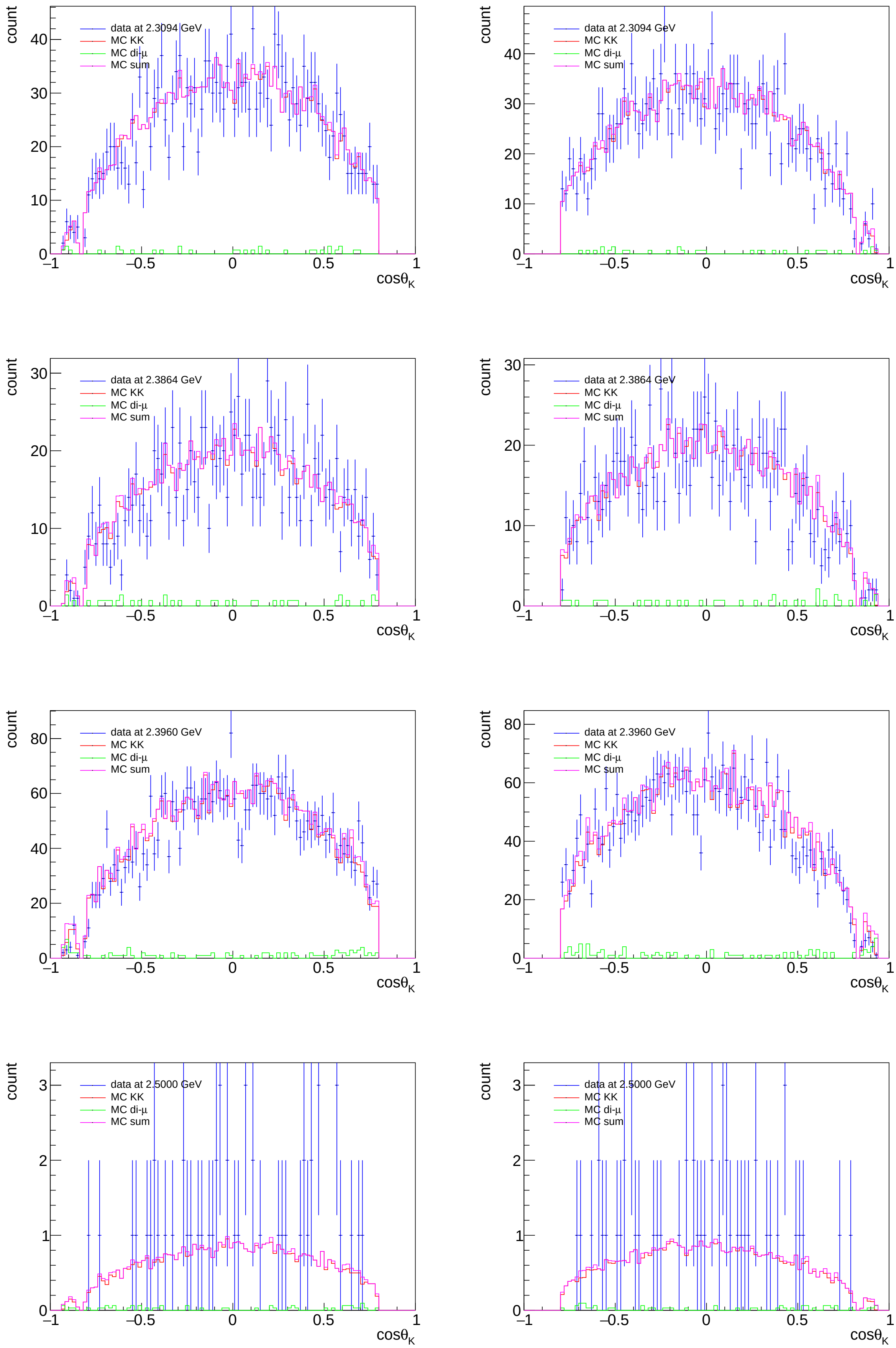

Continuation of Figure 26.

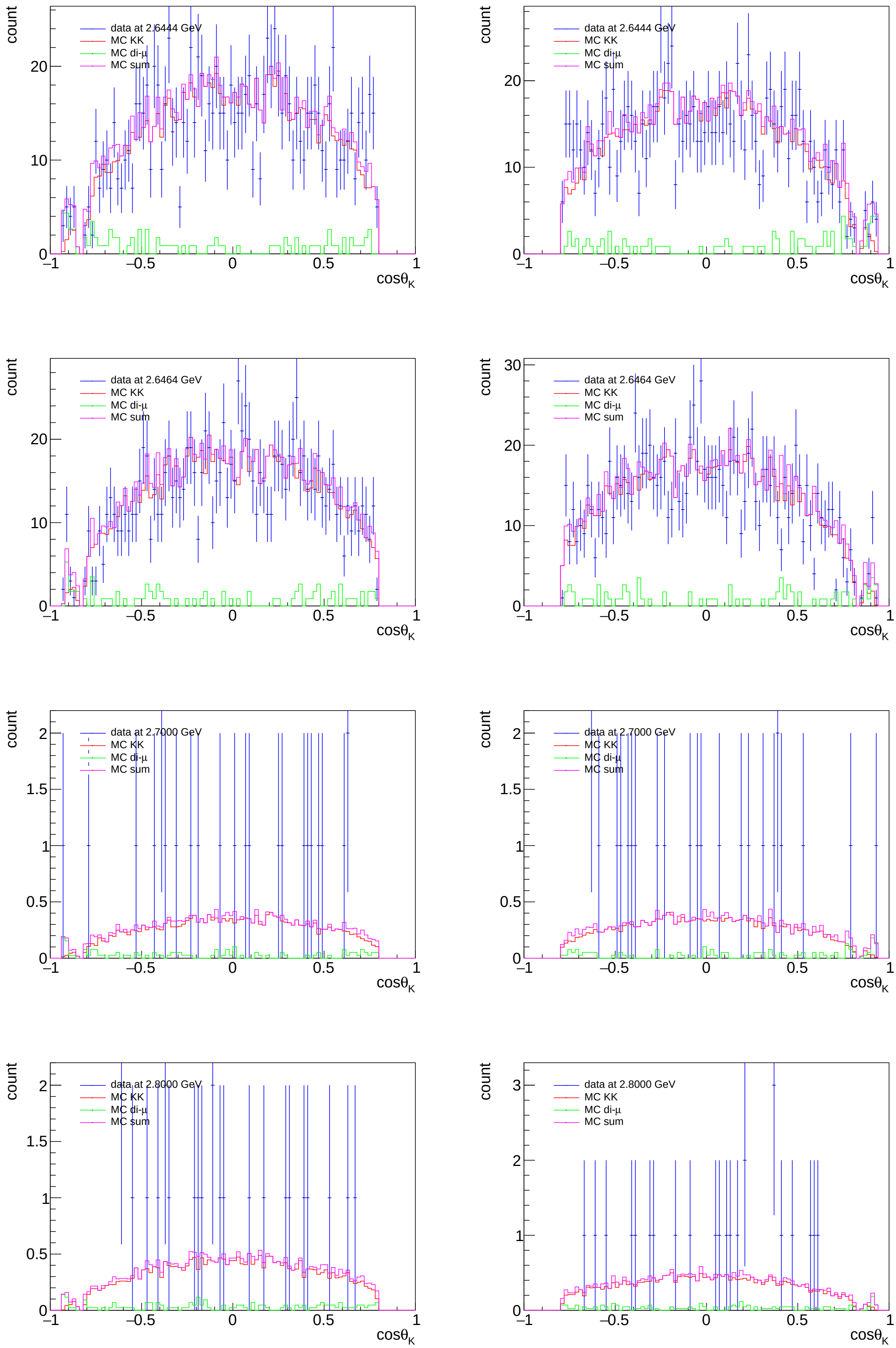

Continuation of Figure 26.

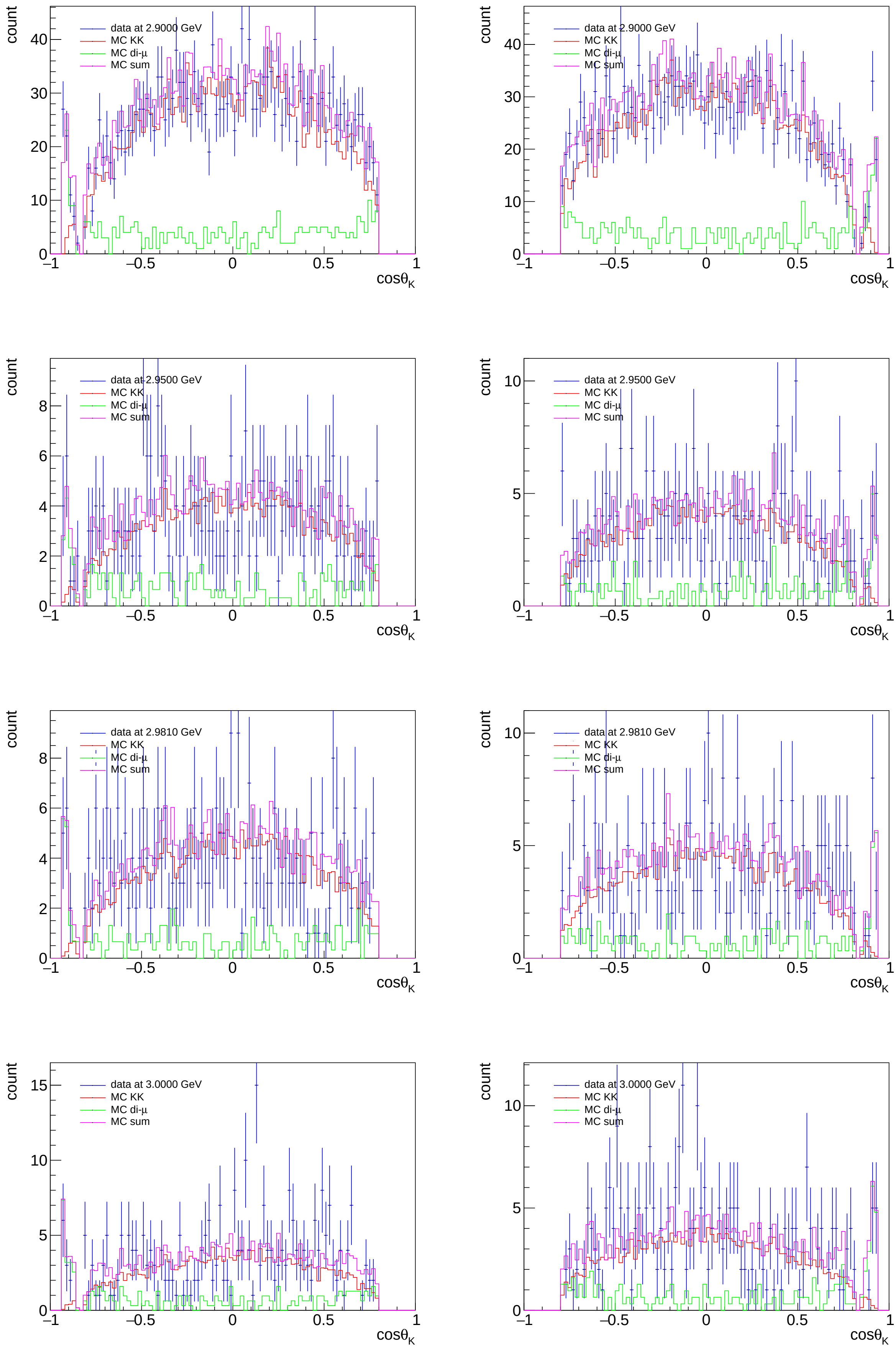

Continuation of Figure 26.

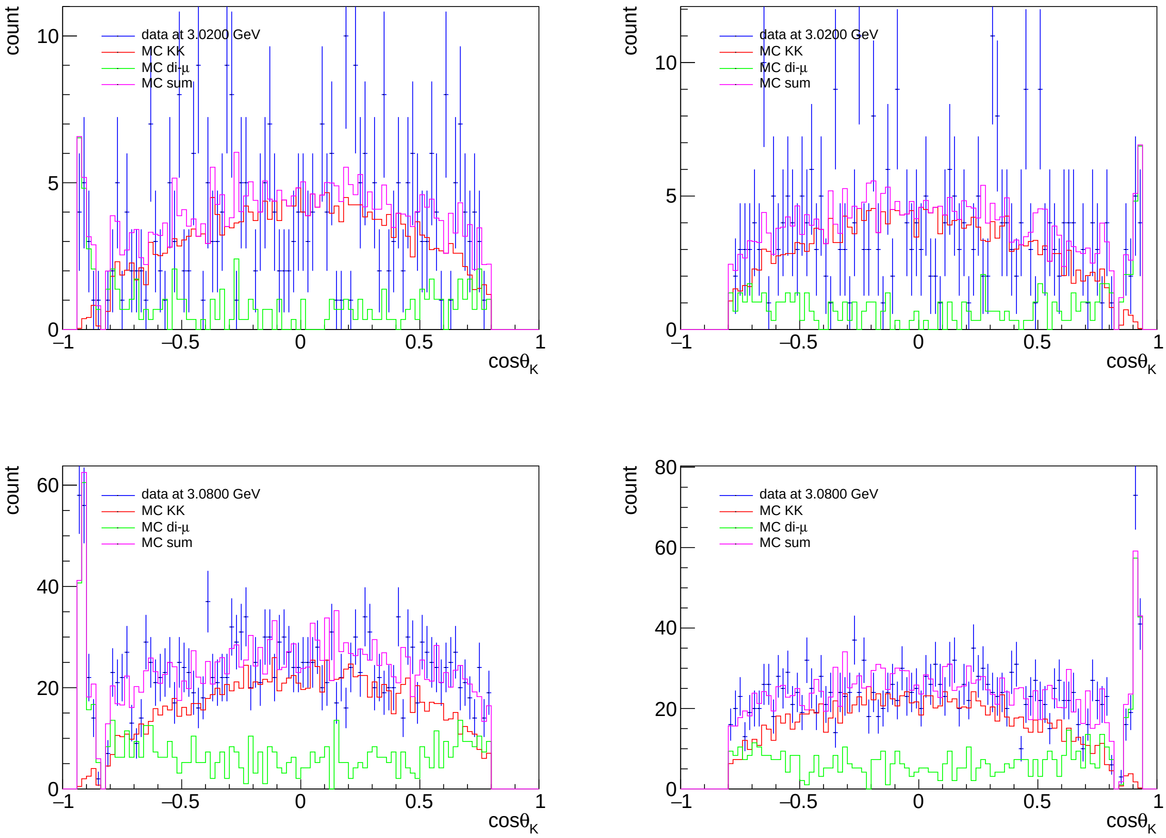

Continuation of Figure 26.

Table 10 and Fig. 27 shows the comparison of the number of kaon obtained from polar angle fitting and momentum fitting. From the comparison, they are consistent. The details of fitting results of the polar angle fitting are shown in Fig. 28.

Table 10: The number of kaon obtianed from polar angle fitting and from momentum fitting.

E_{cm} (GeV)	$N_{K,p}$	$N_{K,cos\theta}$	Δ (%)	E_{cm} (GeV)	$N_{K,p}$	$N_{K,cos\theta}$	Δ (%)
2	1821.2	1806.0	-0.8	2.6444	1075.6	1064.8	-1.0
2.05	512.6	512.9	0.1	2.6464	1079.7	1075.6	-0.4
2.1	1402.6	1408.1	0.4	2.7	21.6	19.5	-9.9
2.15	258.2	259.0	-0.1	2.8	22.0	27.0	22.7
2.175	1030.4	1018.3	-1.2	2.9	1840.0	1959.9	6.5
2.2	1677.1	1664.1	-0.8	2.95	227.4	256.0	12.6
2.2324	1605.7	1599.5	-0.2	2.981	260.7	254.6	-2.3
2.3094	2100.7	2014.5	-4.1	3	215.8	269.5	24.9
2.3864	1257.0	1273.5	1.3	3.02	240.0	266.0	10.8
2.396	3760.1	3859.6	2.6	3.08	1355.1	1417.0	4.6
2.5	53.5	54.0	1.0				

E_{cm} is the center-of-mass energy.
$N_{K,p}$ is the number of kaon from momentum fitting.
$N_{K,cos\theta}$ is the number of kaon from polar angle fitting.
$\Delta = (N_{K,cos\theta} - N_{K,p})/N_{K,p} \cdot 100\%$

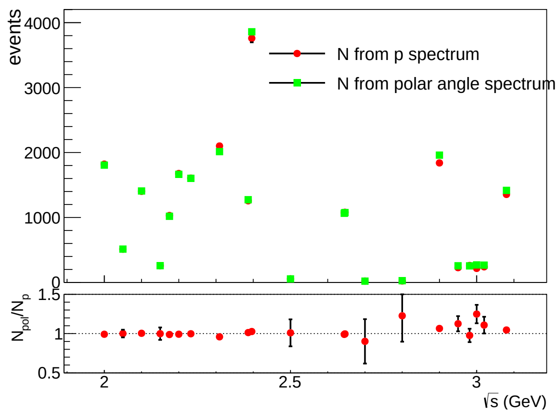

Figure 27: Comparison of results from polar angle fitting and momentum fitting. N_{pol}/N_p is the ratio of the number of signal obtained from polar angle spectra and from momentum spectra.

Fig. 28 shows the fitting result of polar angle distribution. Both positive tracks and negative tracks are filled in the plot. Thus, there are two entries for one event and the number shown in plots are the fitting results divided by 2. The shape used to describe the polar spectra are MC shape from K^+K^- MC from ConExc generator for signal and MC shape from di-μ MC from BABAYAGA generator for background.

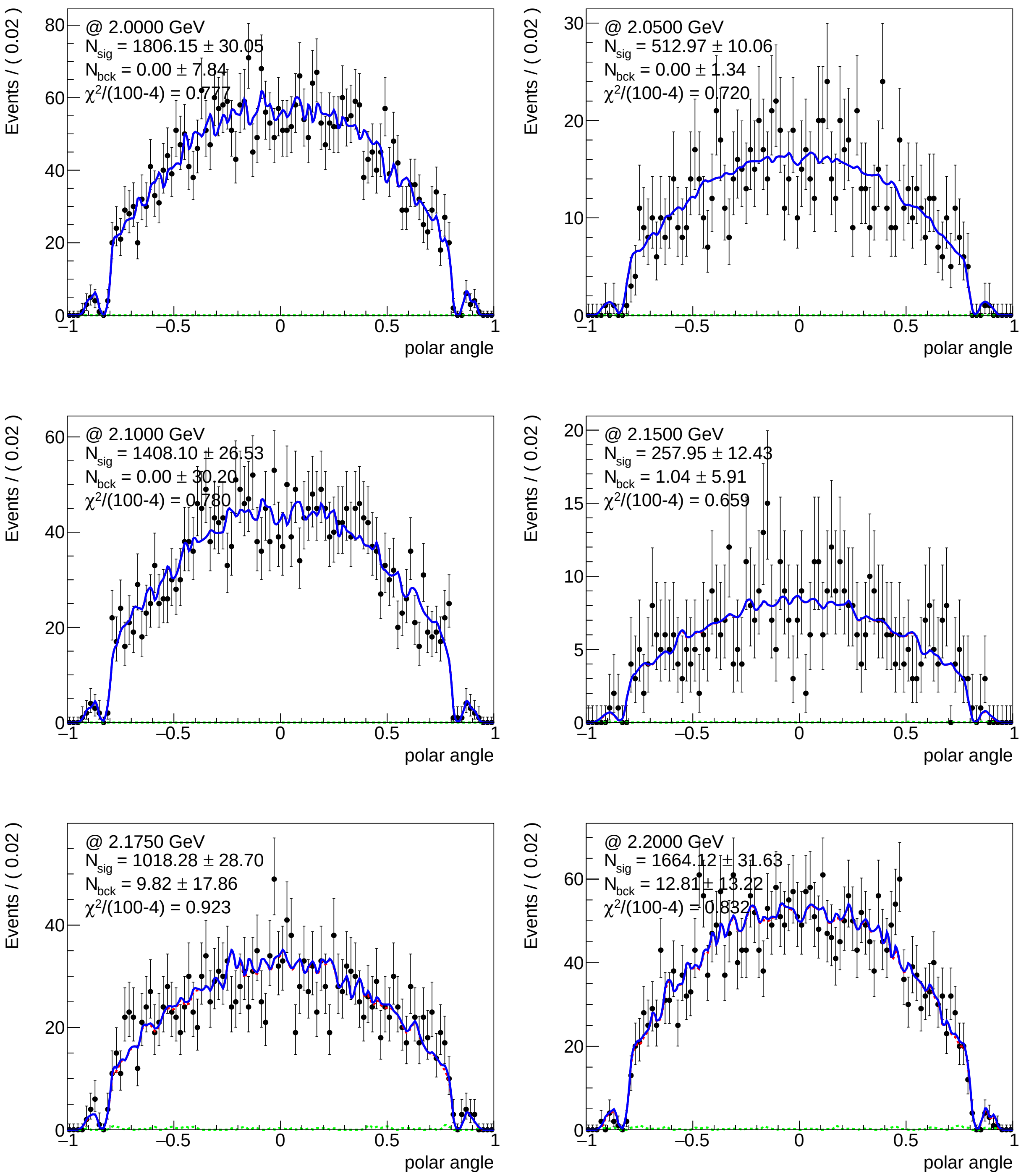

Figure 28: Polar angle of 2 charged tracks at 21 R scan energy points.

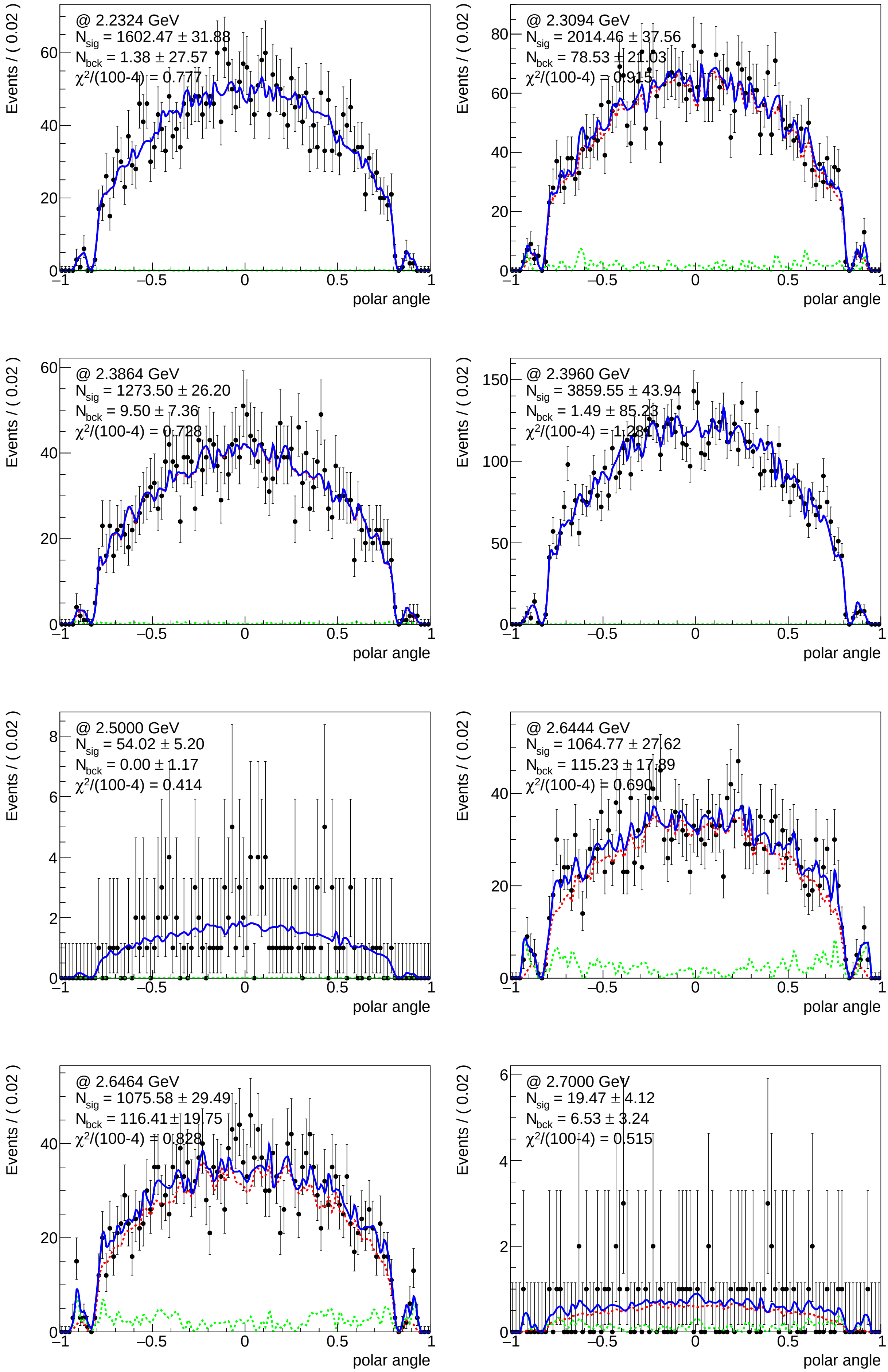

Continuation of Figure 28.

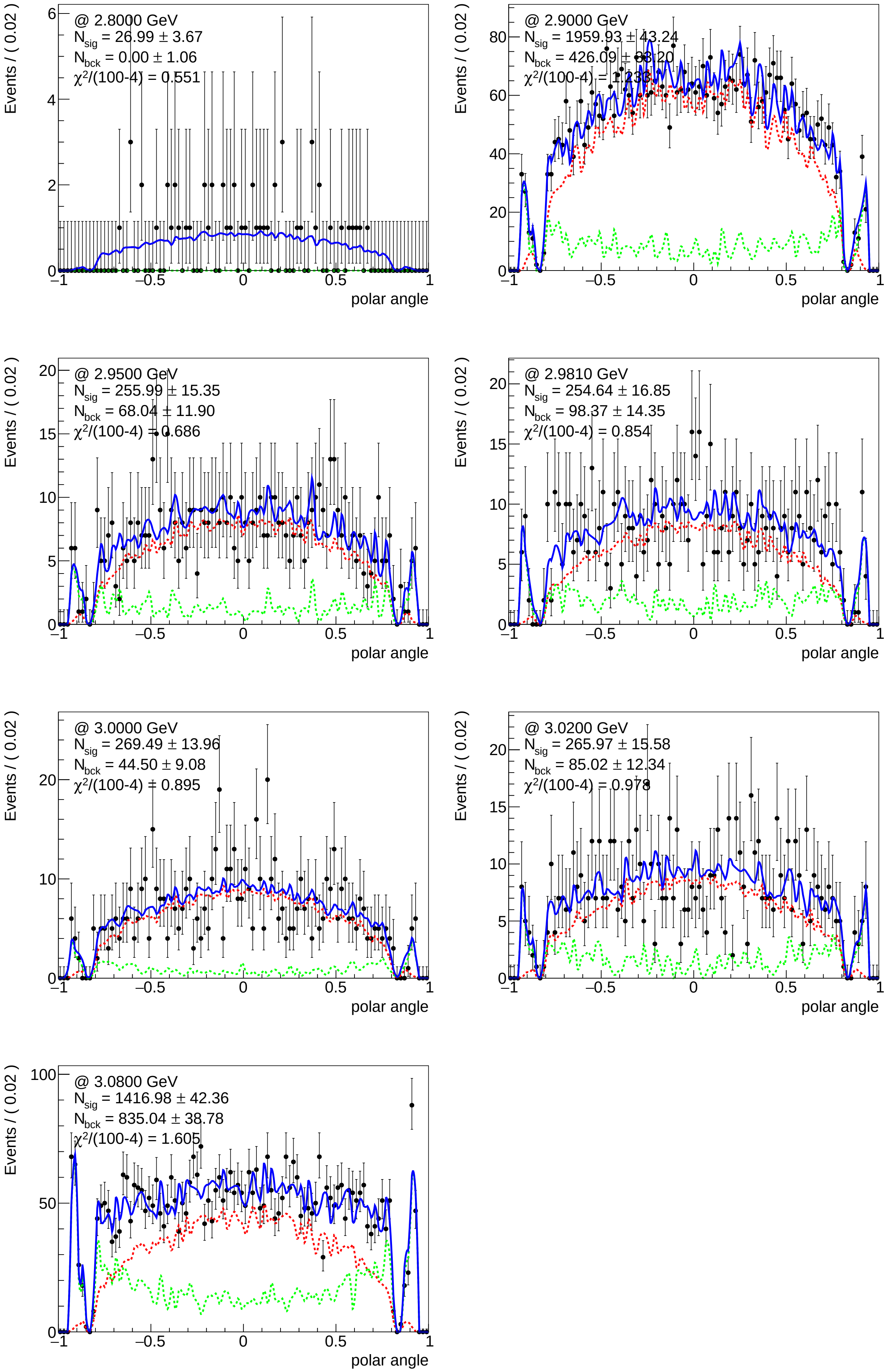

Continuation of Figure 28.

E Tranverse momentum of K^+K^-

Fig. 29 shows the tranverse momentum distribution for data and K^+K^- MC. Events are selected with criteria in Sec. 4 of the memo and require the momentum of both tracks within $p_{exp} \pm 3\sigma$. The spectra of MC are scaled to data according to the numbers of events.

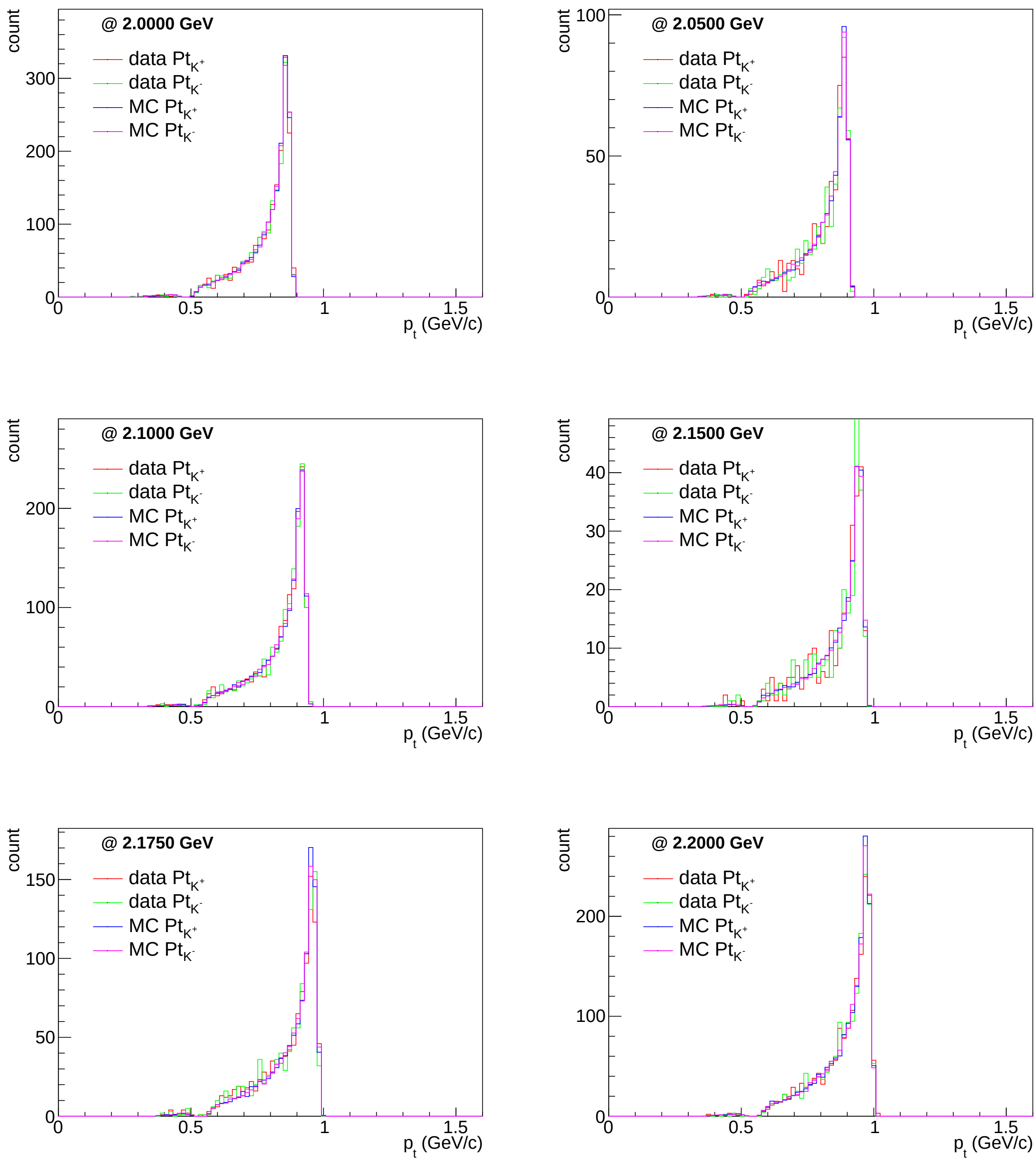

Figure 29: Pt distribution of data and MC at 21 R scan energy points.

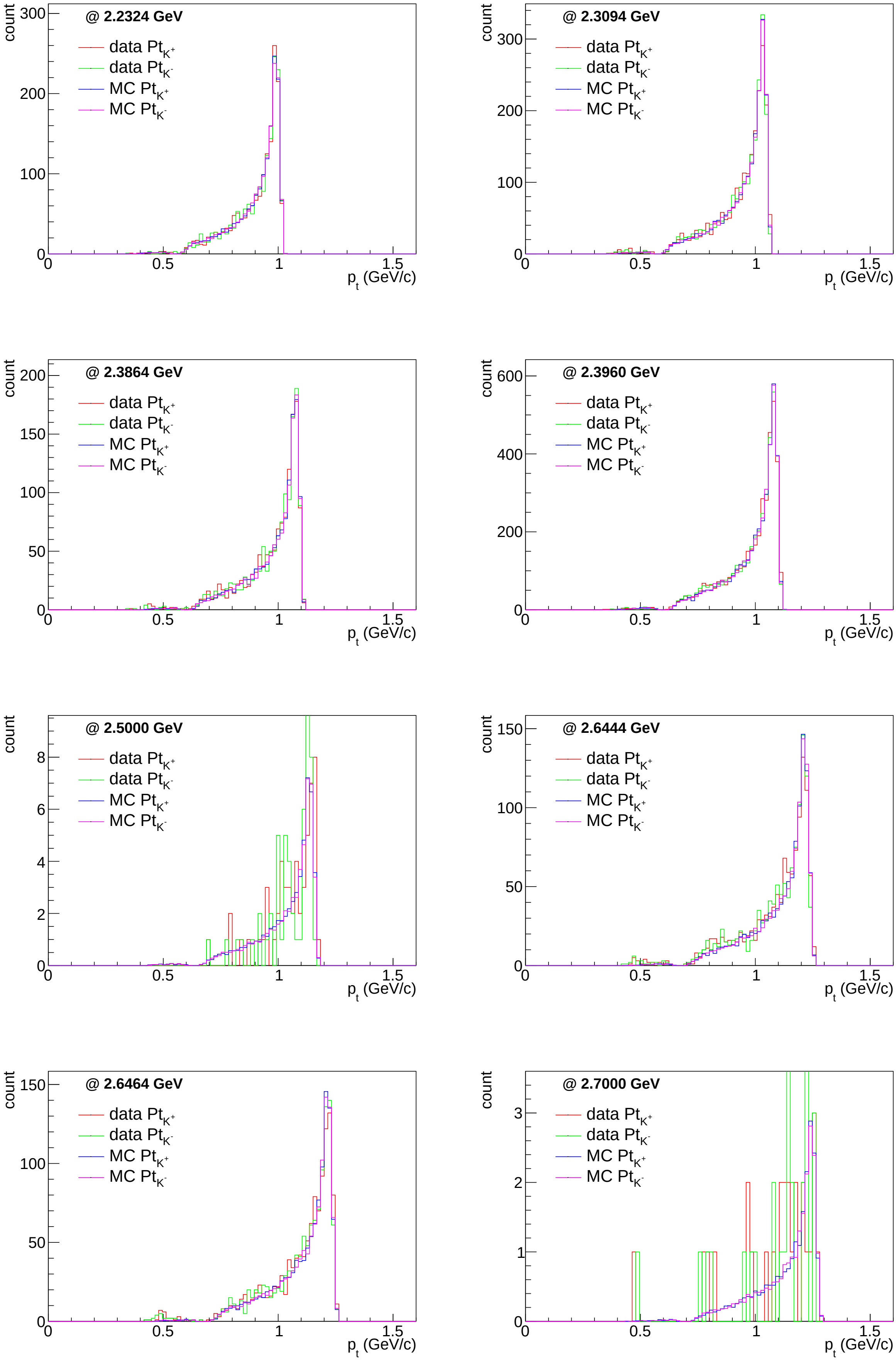

Continuation of Figure 29.

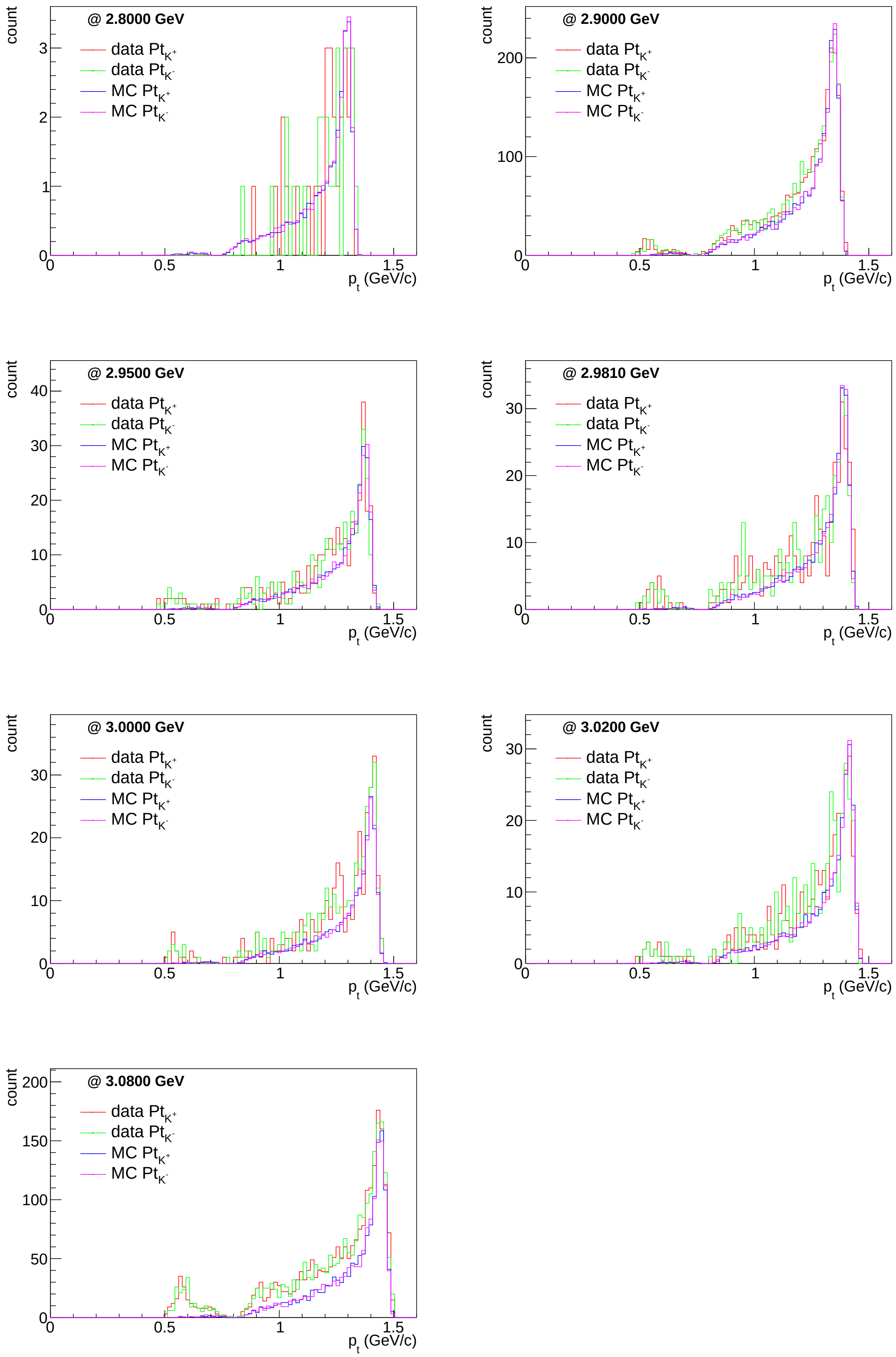

Continuation of Figure 29.

F Fit to the line shape of the cross sections

The nominal way of the fit to the line shape of cross section is described in Sec. 6.4. The line shape is described by Eq. 31

$$\sigma = |A_K|^2 \tag{31}$$

$$\begin{aligned} A_K = \;& c_\phi BW_\phi + c_{\phi'} BW_{\phi'} + c_{R1} BW_{R1} \\ & + c_\rho BW_\rho + c_{\rho'} BW_{\rho'} + c_{\rho''} BW_{\rho''} + c_{R2} BW_{R2} \\ & + c_\omega BW_\omega + c_{\omega'} BW_{\omega'} + c_{\omega''} BW_{\omega''} + c_{R3} BW_{R3} \\ & + c_{con} \cdot s^{-\alpha} \cdot e^{i\cdot\theta} \end{aligned} \tag{32}$$

where c's are coefficients; BW's are Breit-Wigner functions of resonances, including $\phi(\phi(1020))$, ϕ' ($\phi(1680)$), ρ ($\rho(770)$), ρ' ($\rho(1450)$), ρ'' ($\rho(1700)$), ω ($\omega(782)$), ω' ($\omega(1420)$), ω'' ($\omega(1650)$) and other resonances whose parameters are to be determined. $R1$ (denoted as ϕ'' in Sec. 6.4) denotes the resonance in energy region between 2.2 and 2.4 GeV, while $R2$ (ρ''' in Sec. 6.4) and$R3$ (ω''' in Sec. 6.4) are used to compensate possible contribution outside the region. The BW's take the form

$$BW(s, m, \Gamma(s)) = \frac{1}{m^2 - s - i\sqrt{s}\Gamma(s)}. \tag{33}$$

In the fit, masses and widths of resonances quoted from PDG, i.e. $\phi(1020)$, $\phi(1680)$, $\rho(770)$, $\rho(1450)$, $\rho(1700)$, $\omega(782)$, $\omega(1420)$, $\omega(1650)$, are fixed to values in PDG. Other parameters are free, including the masses and widths of $R1$, $R2$ and $R3$.

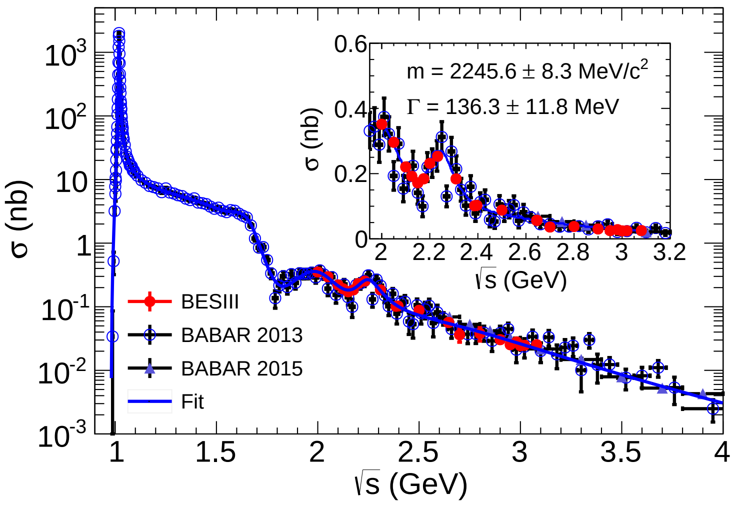

Figure 30: Line shape of cross section of $e^+e^- \to K^+K^-$.

Here, the coefficient, corresponding the product of Γ_{ee} and $Br_{R1\to KK}$, is not provided because it's hard to get a reliable value. Some efforts have been made to clarify the problem. We scanned the value of the coefficient $c_{R1'}$ while other parameters are treated as the same in the nominal fit. The result shows there are several minimum χ^2 values at different coefficients, which is shown in Fig. 31.

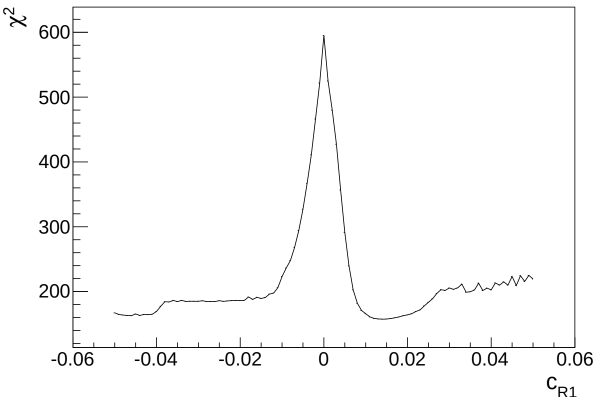

Figure 31: χ^2 value versus the coefficient of $R1$.

Two fit results are shown in Fig. 32, which are at $c_{R1} = -0.046$ and $c_{R1} = 0.014$. The results fit quite well to the spectra, while the interference between components is very different. Since there are several components contribute to the cross section in region 2.2 to 2.4 GeV, it's hard to judge which one is the physical one.

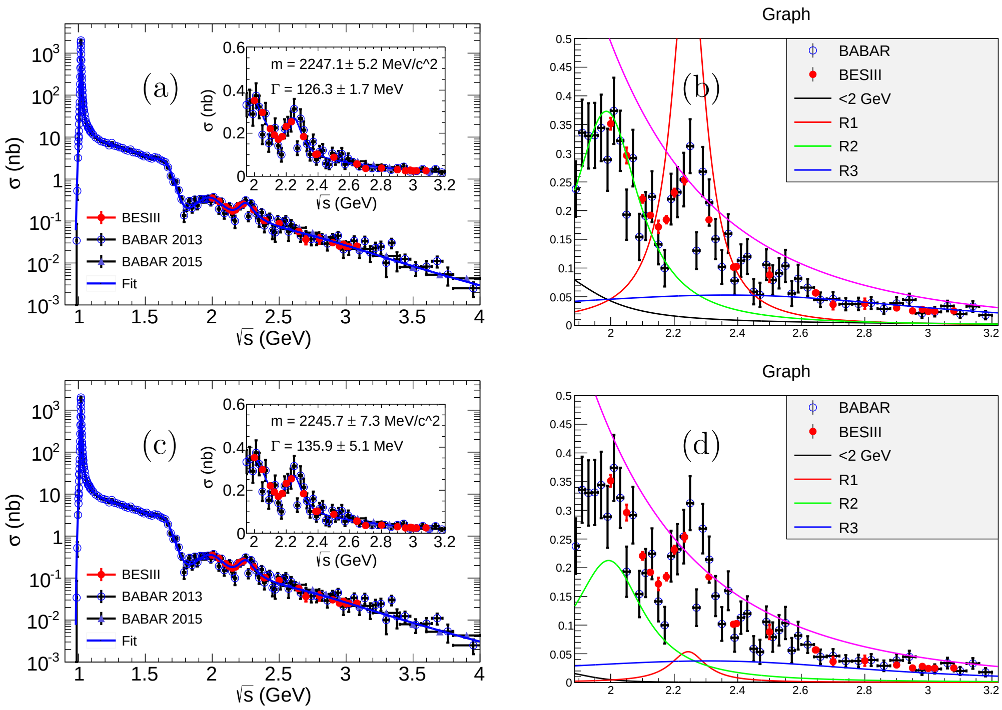

Figure 32: Two solutions of the fit to the cross sections. (a) and (c) are the total fit result with different c_{R1}, corresponding to $c_{R1} = -0.046$ and $c_{R1} = 0.014$. (b) and (d) are the components in (a) and (c), respectively. Red line represents the interest state $R1$.

The product of Γ_{ee} and $Br_{R1\to KK}$ is implicated in the coefficient. If the Breit-Wigner function is described with the product explicitly, there is no need for the coefficient. The Breit-Wigner function can be parameterized as

$$BW = \frac{M_{R1}}{\sqrt{s}} \cdot \frac{\sqrt{12\pi\Gamma_{ee}Br_{R1\to KK}\Gamma_{\rm tot}}}{s - M_{R1}^2 + iM_{R1}\Gamma_{\rm tot}} \cdot \sqrt{\frac{PS(s)}{PS(M_{R1}^2)}} \cdot e^{i\theta}, \tag{34}$$

where $PS(s) = \sqrt{1/4 - m_K^2/s}$. Using this Breit-Wigner function to do the fit, there are also several solutions for $\Gamma_{ee} \cdot Br_{R1 \to KK}$. Figure 33 shows two solutions. In this case, we do not tend to report the result of $\Gamma_{ee} \cdot Br_{R1 \to KK}$.

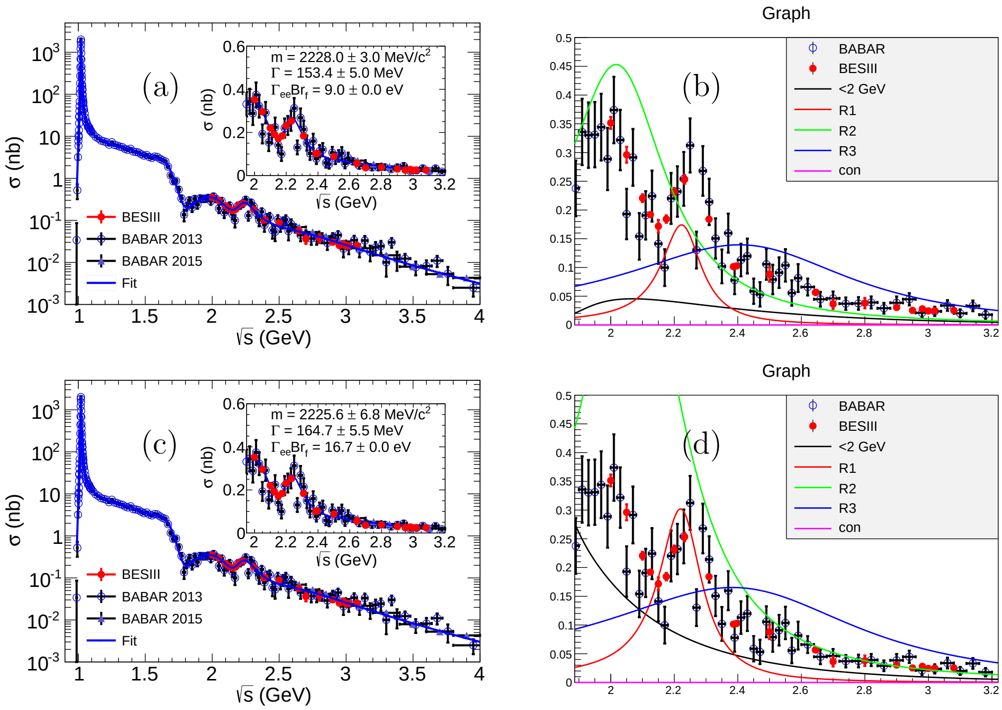

Figure 33: Two solutions of the fit to the cross sections. (a) and (c) are the total fit result with different $\Gamma_{ee} \cdot Br_{R1 \to KK}$, corresponding to $\Gamma_{ee} \cdot Br_{R1 \to KK} = 9$ eV and $\Gamma_{ee} \cdot Br_{R1 \to KK} = 16.7$ eV. (b) and (d) are the components in (a) and (c). Red line represents the interest state $R1$.